Studying the building's dynamic behaviour
Real data analysis and numerical modelling

Real data analysis

- Ambient vibration measurements
- Weak/strong motion measurements
- Forced vibrations measurements

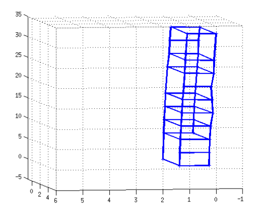
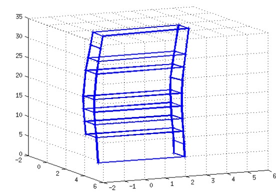

Fourier Transform

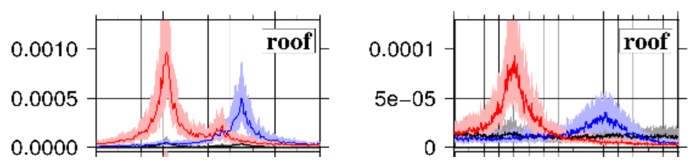

Modal Analysis
Frequency Domain Decomposition

Deconvolution approach

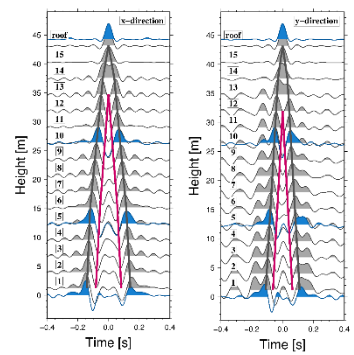

Studying the building's dynamic behaviour
Real data analysis and numerical modelling

Numerical modeling

- Finite Element Modeling (FEM)

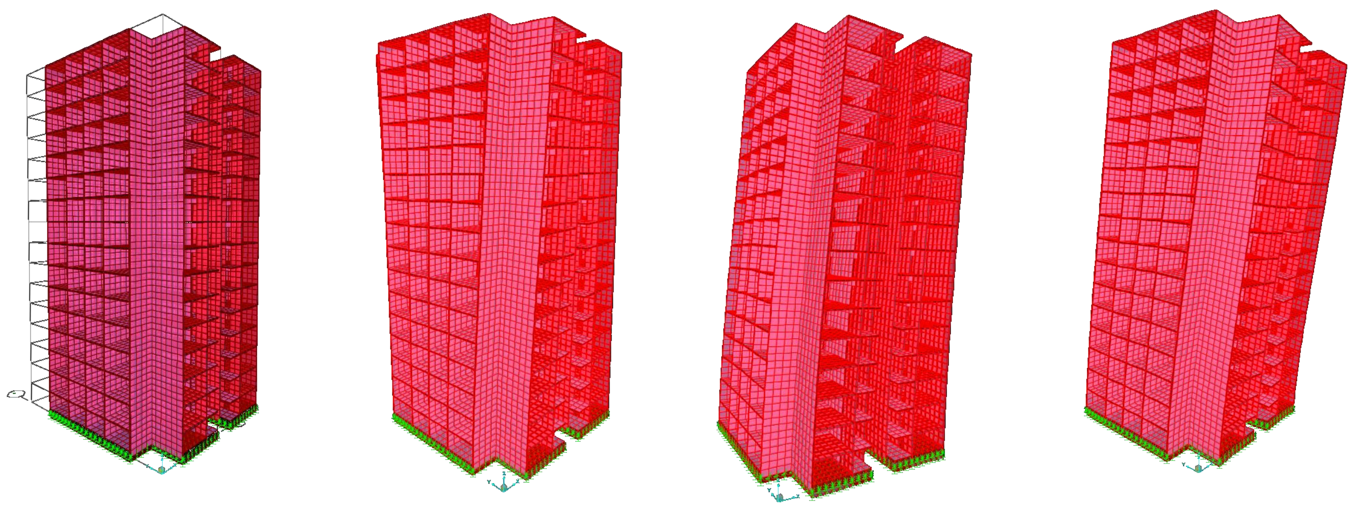

Instrumentation – Permanent installation

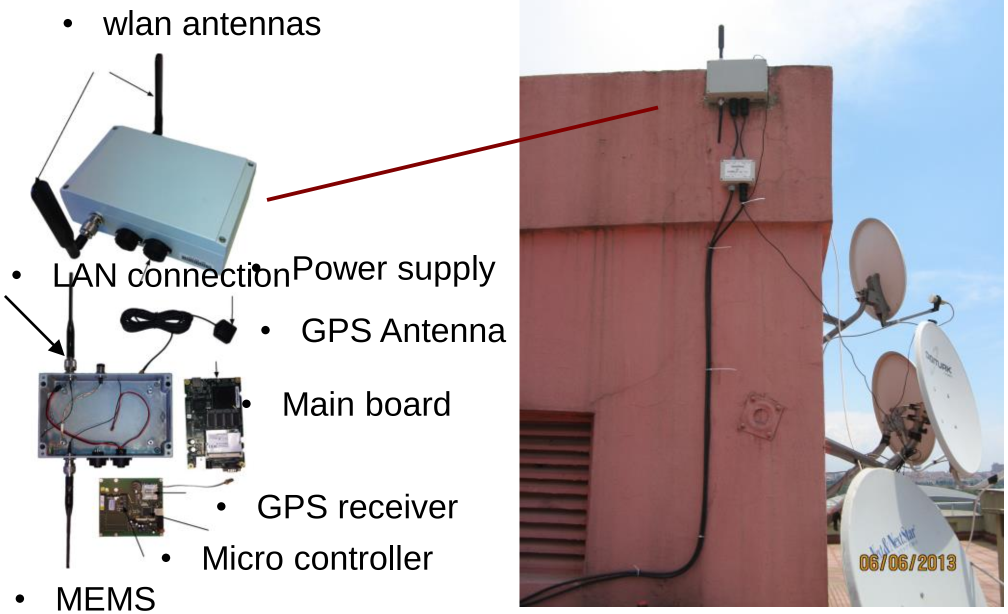

(1)

(2)

(3)

(1) SOSEWIN - node

(2) SOSEWIN + Güralp CMG-5tc

(3) SOSEWIN + 4.5Hz Geophone

Instrumentation – Permanent installation

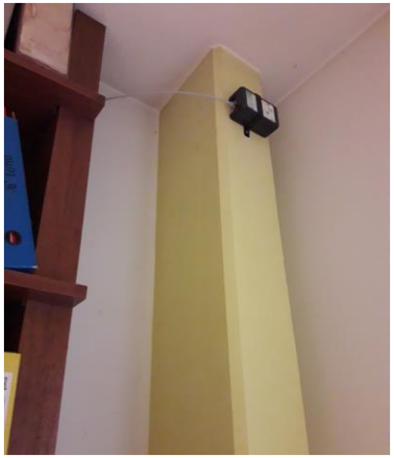

The accelerograph Suricat has following properties:
- three-axial accelerometers
- possible sampling rates: 128 Hz, 256 Hz, 512 Hz
- possibility to connect to the internet and to transmit the data in real time
- power and battery supply for the case of power breakdown
- possibility to connect external GPS antenna

Instrumentation – Temporary installation

EDL 24bit digitizer

with 1Hz Mark Sensor

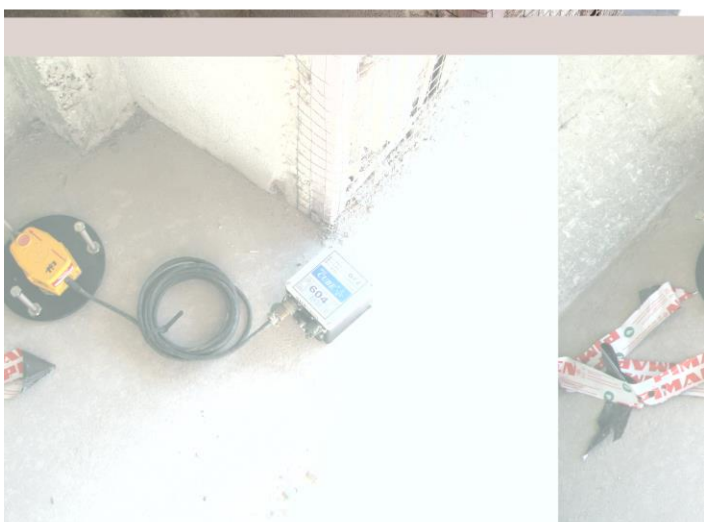

CUBE data loggers

with 4.5Hz geophones and GPS timing

Instrumentation – Temporary installation
Thumper truck experiment – Forced vibrations

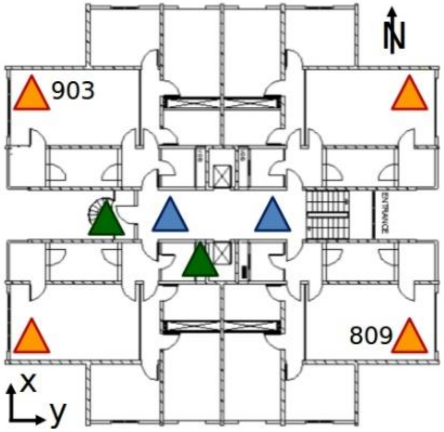

Instrumentation – Temporary installation
Thumper truck experiment – Forced vibrations

Fourier Spectrum

$$G(\omega) = \int_{-\infty}^{\infty} g(t)\exp(i\omega t)\,dt$$

- In what way are there two numbers at each frequency? From basic complex number theory:

$$e^{i\theta} = \cos\theta + i\sin\theta$$

- Using this, the definition can be rewritten as:

$$G(\omega) = \int_{-\infty}^{\infty} g(t)\left[\cos(\omega t) + i\sin(\omega t)\right]dt$$

- Thus, the definition can be rewritten as:
- The two numbers at each frequency are a(ω) and b(ω) (for g(t) real).

$$a(\omega) = \int_{-\infty}^{\infty} g(t)\cos(\omega t)\,dt$$

cos(ωt) even function

$$b(\omega) = \int_{-\infty}^{\infty} g(t)\sin(\omega t)\,dt$$

sin(ωt) odd function

$$G(\omega) = a(\omega) + ib(\omega)$$

Modified from D. Boore, 2004

Fourier Amplitude Spectra

16 story residential tunnel formwork building in Istanbul, Turkey

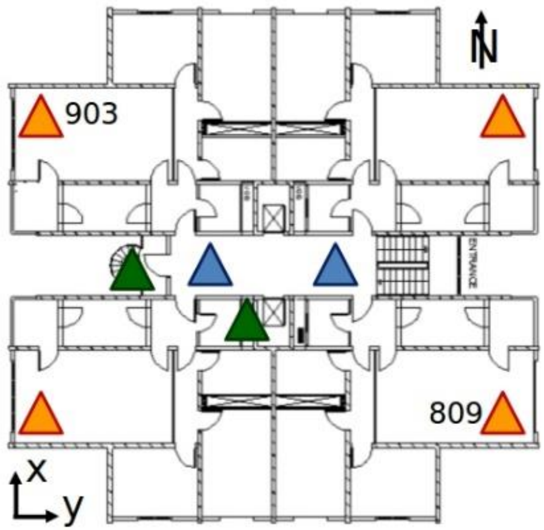

Ambient vibration measurements

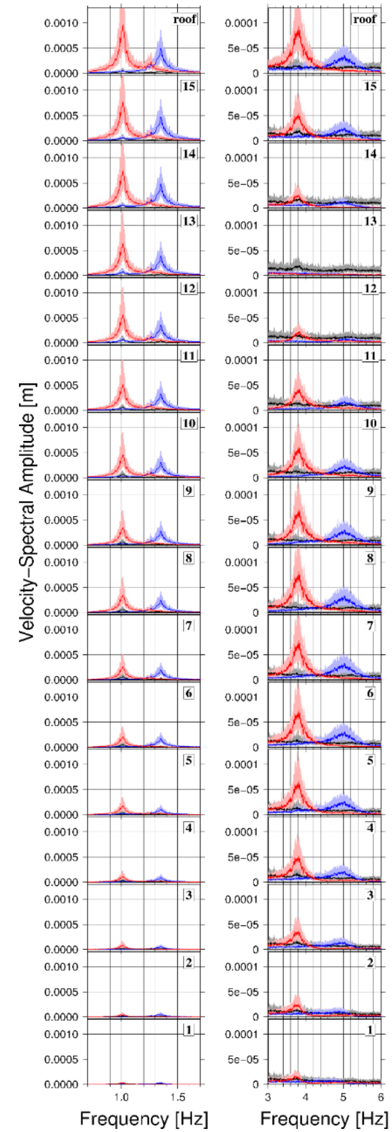

Fourier Amplitude Spectra

1. mode

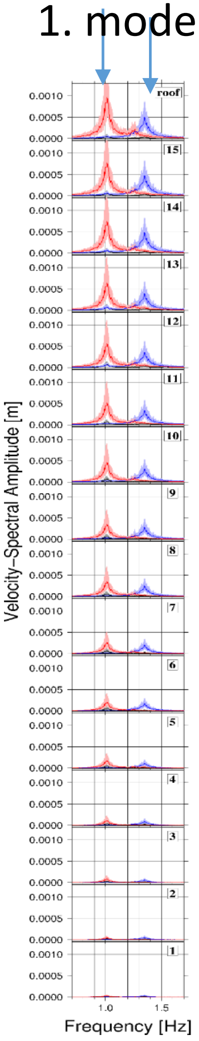

1. mode

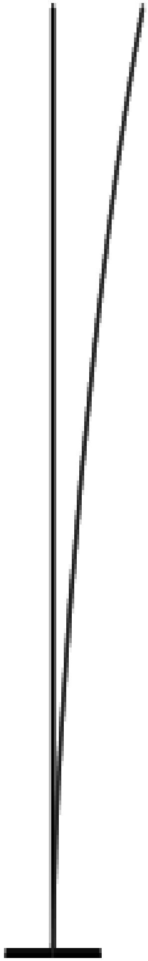

Fourier Amplitude Spectra

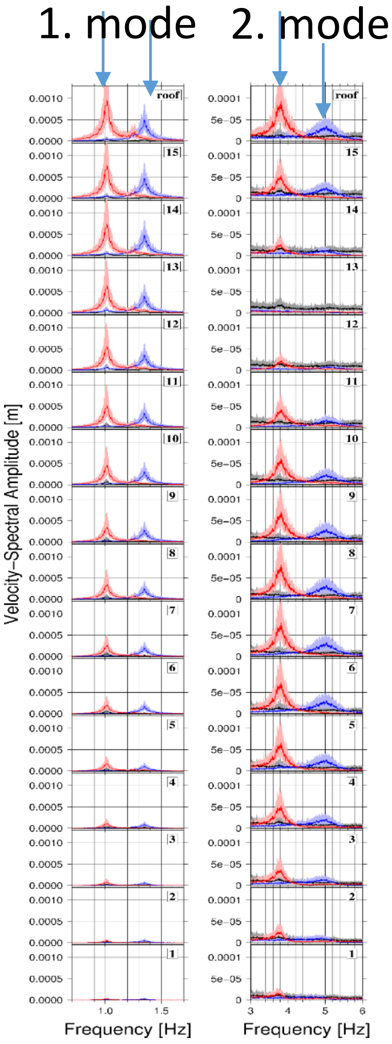

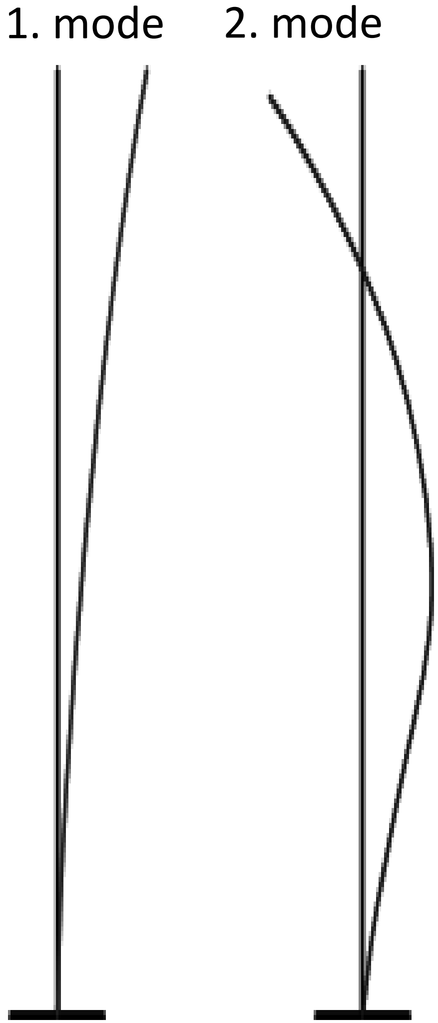

Fourier Amplitude Spectra

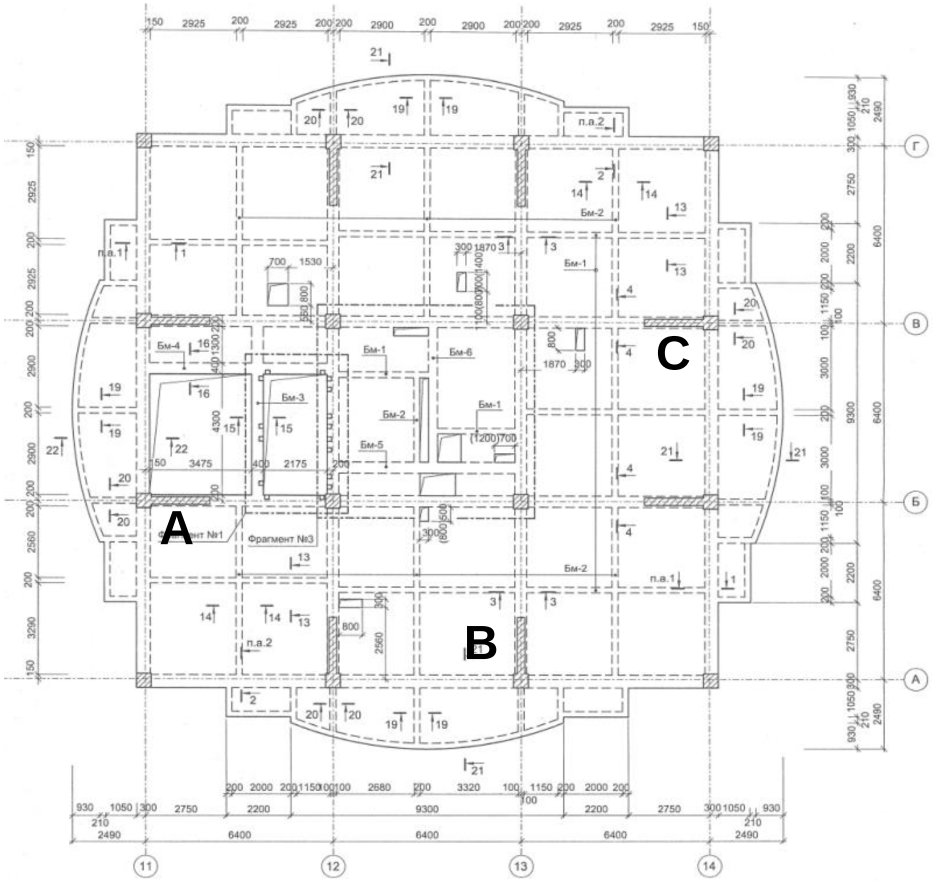

13 storey reinforced concrete building in Bishkek (Kyrgyzstan)
Ambient vibration measurements

Fourier Amplitude Spectra

13 storey reinforced concrete
building in Bishkek (Kyrgyzstan)
Ambient vibration measurements

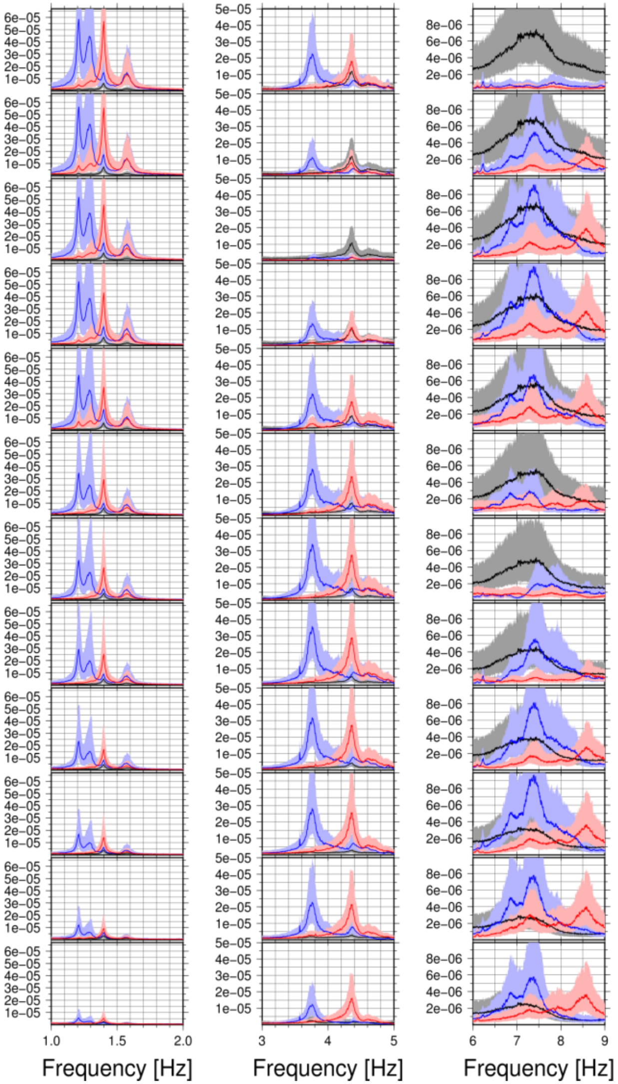

Fourier Amplitude Spectra

Dormitory in Gemona, Italy

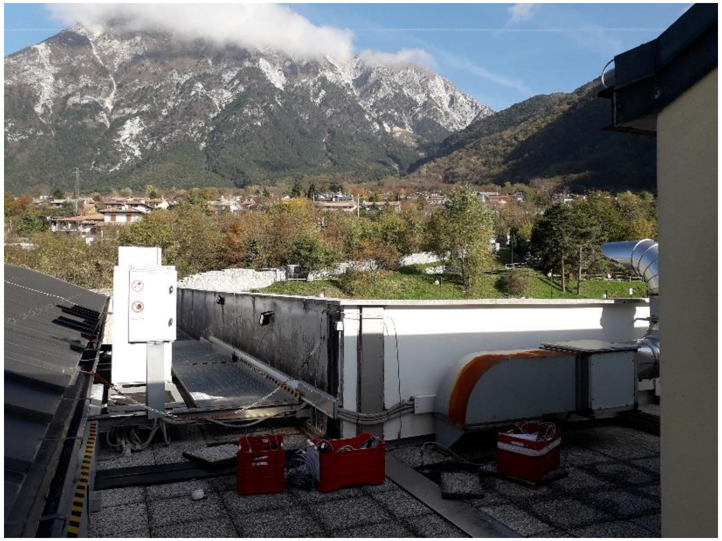

Fourier Amplitude Spectra

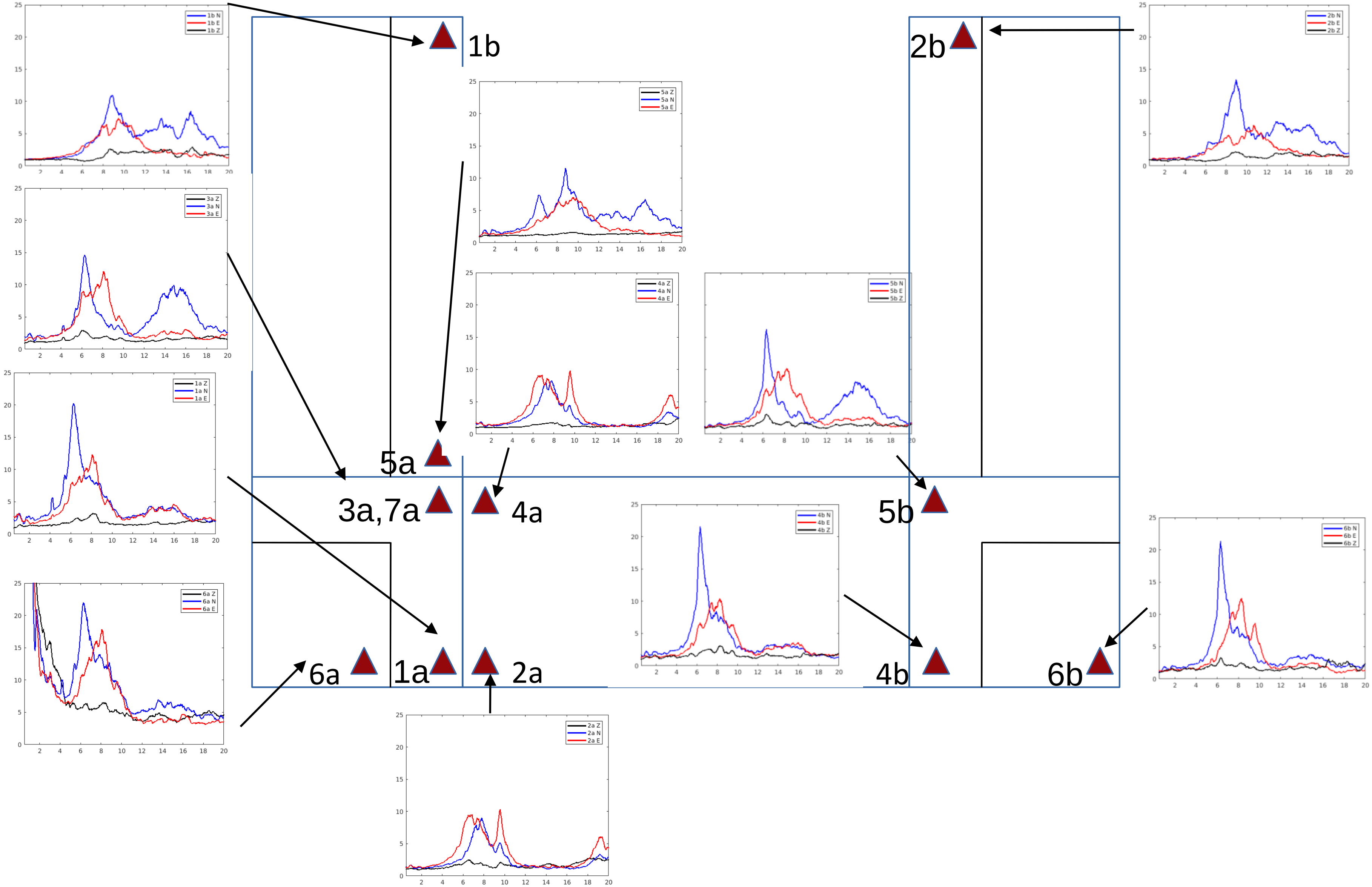

Fourier Amplitude Spectra

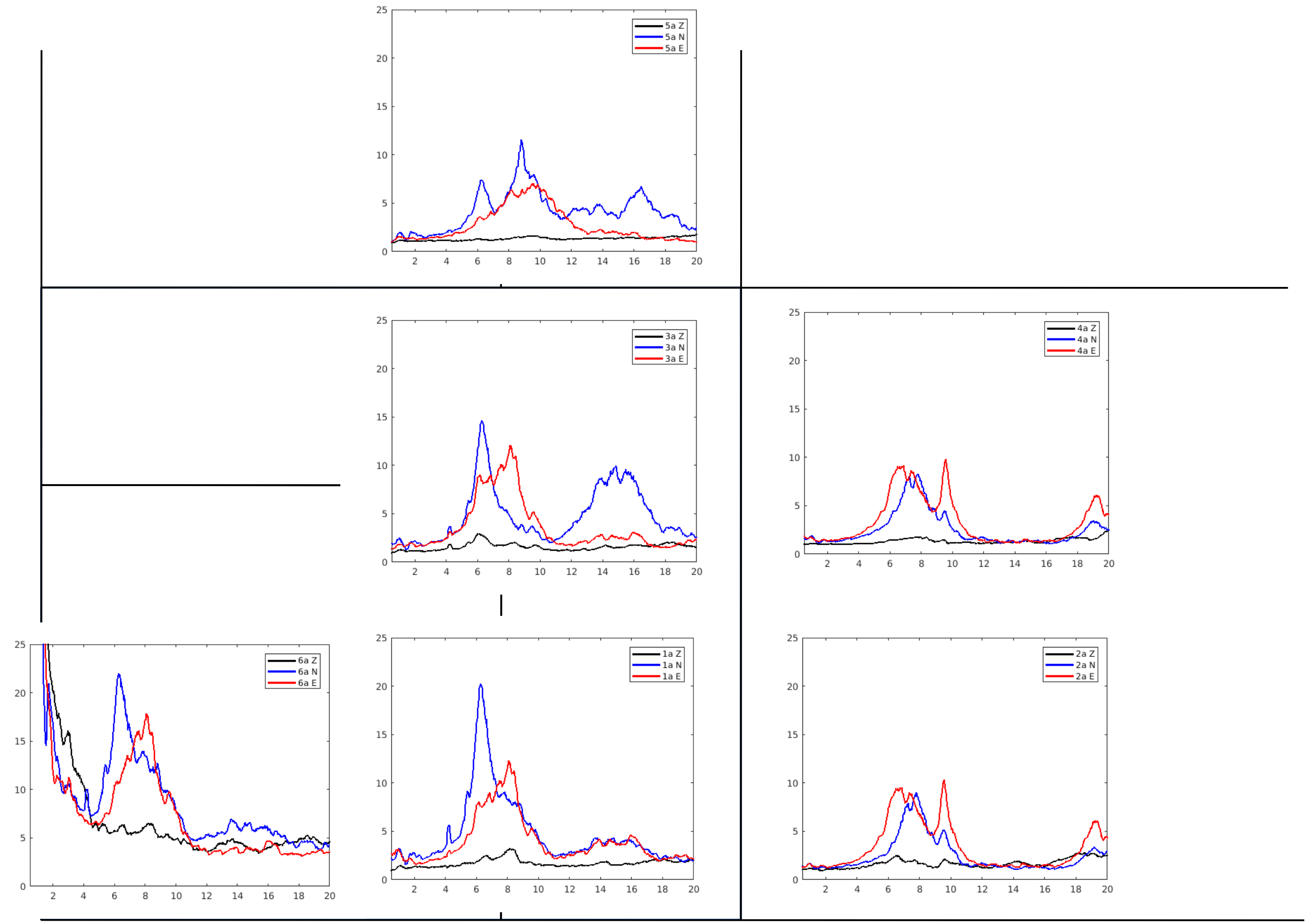

Fourier Amplitude Spectra

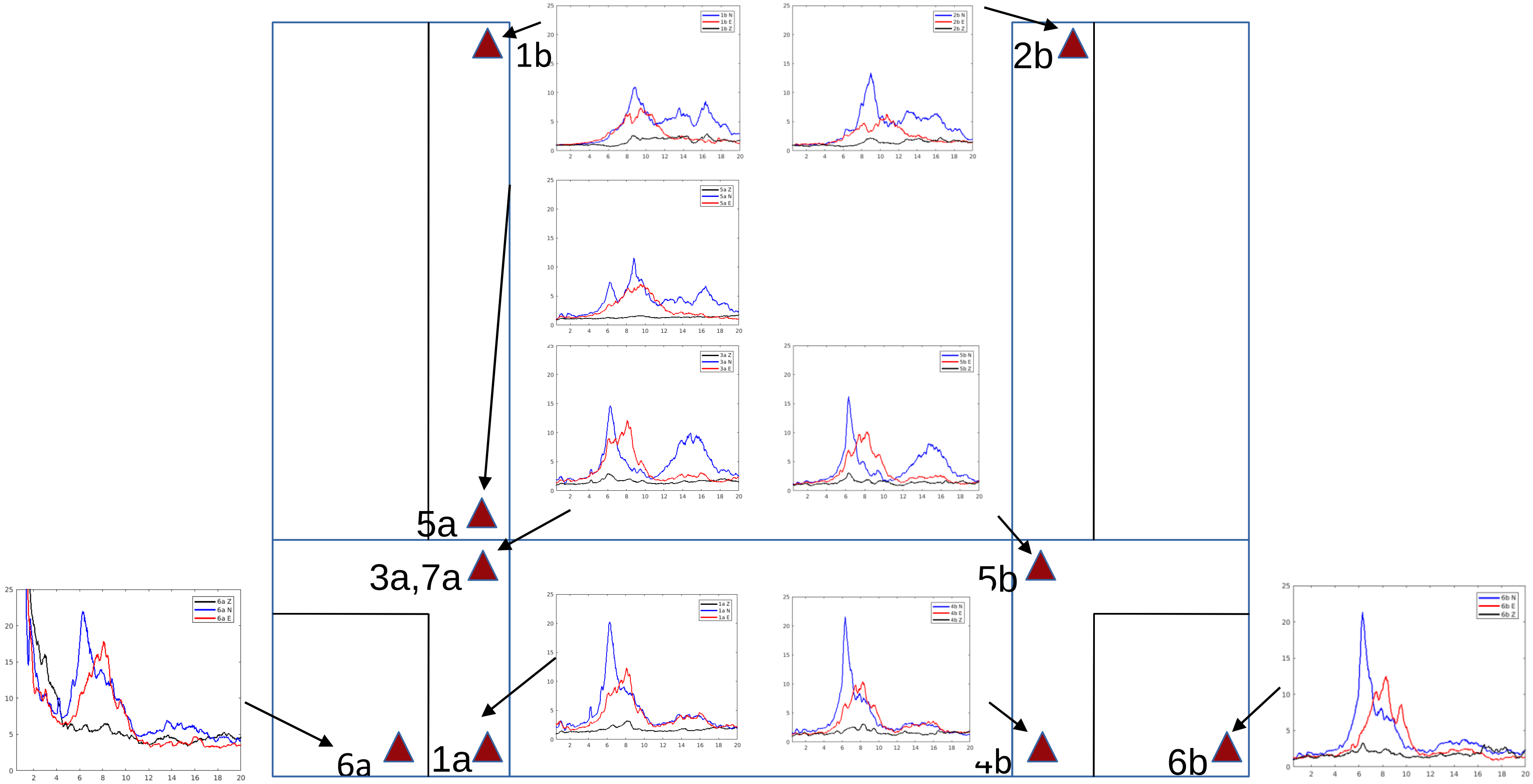

Studying the building's dynamic behaviour

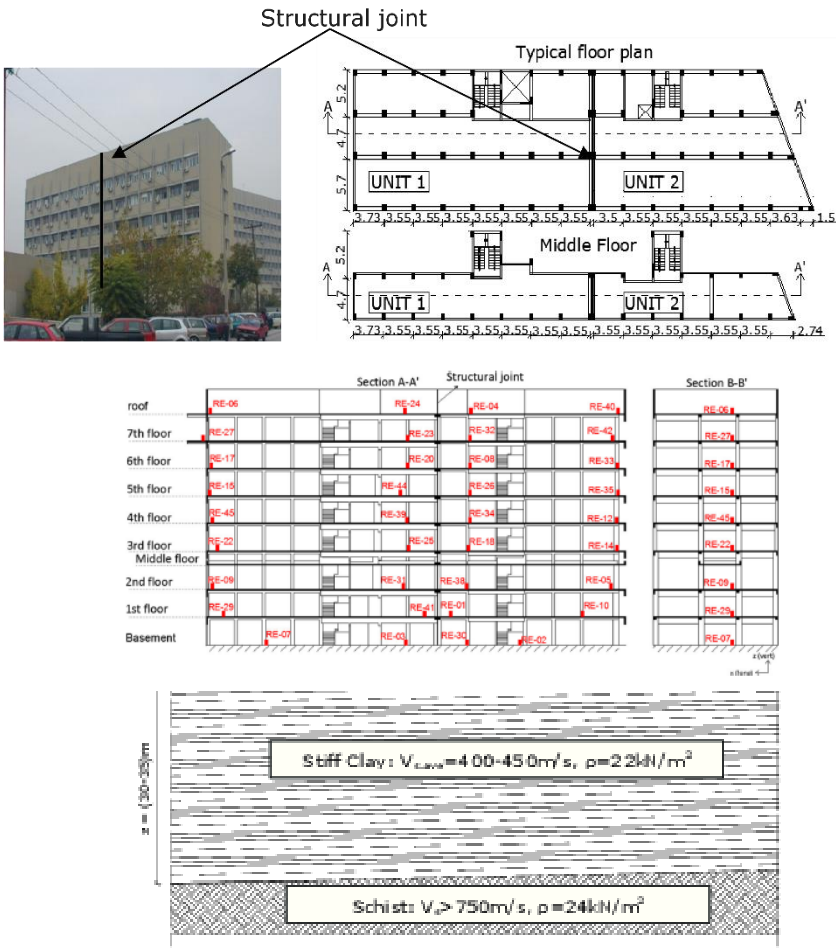

(b)

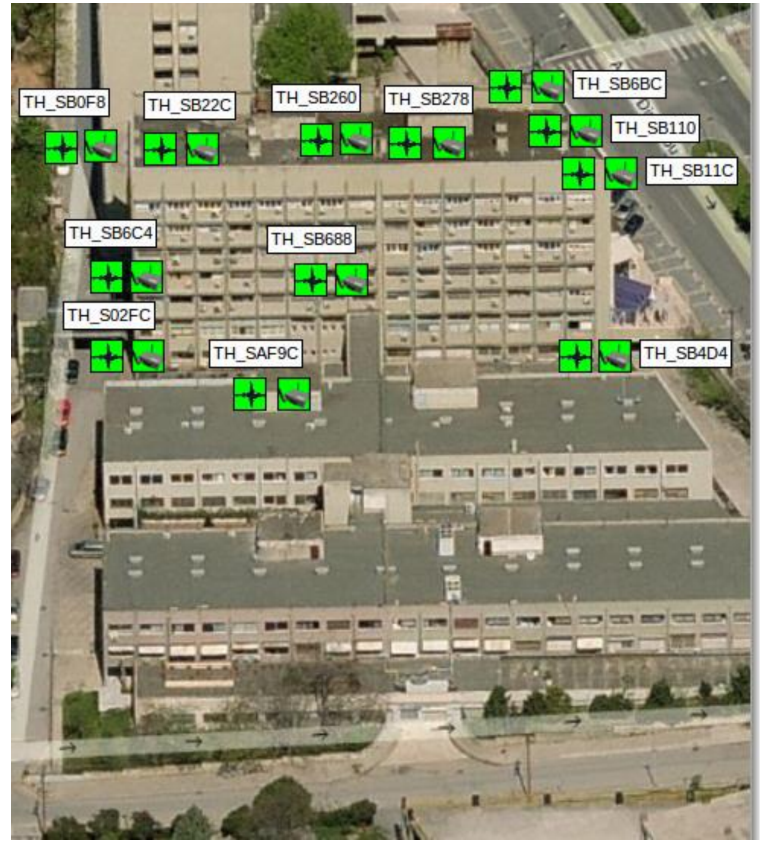

AHEPA hospital, Thessaloniki, Greece

[Bindi et al. 2015]

Daily variation of the fundamental frequency

Power spectral density

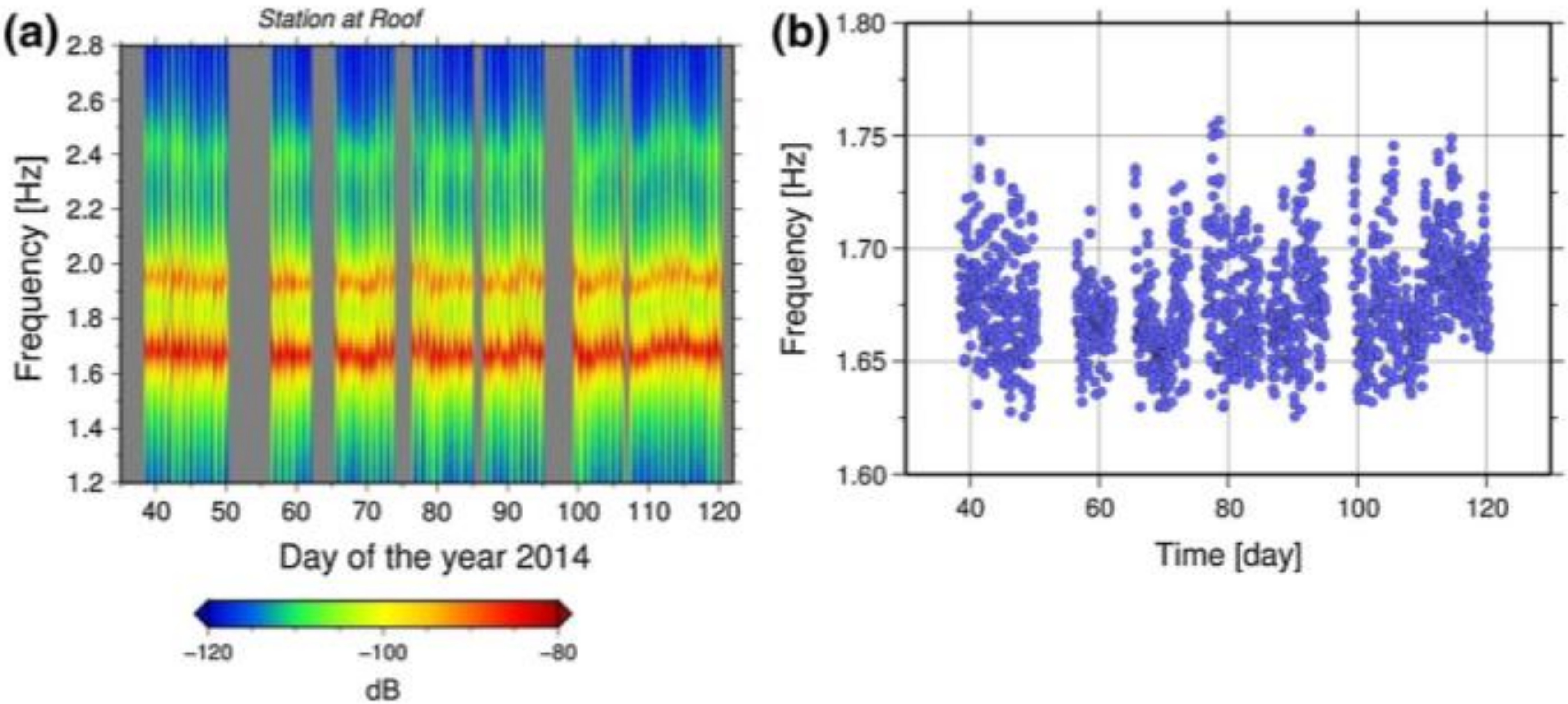

Seasonal variation of the fundamental frequency

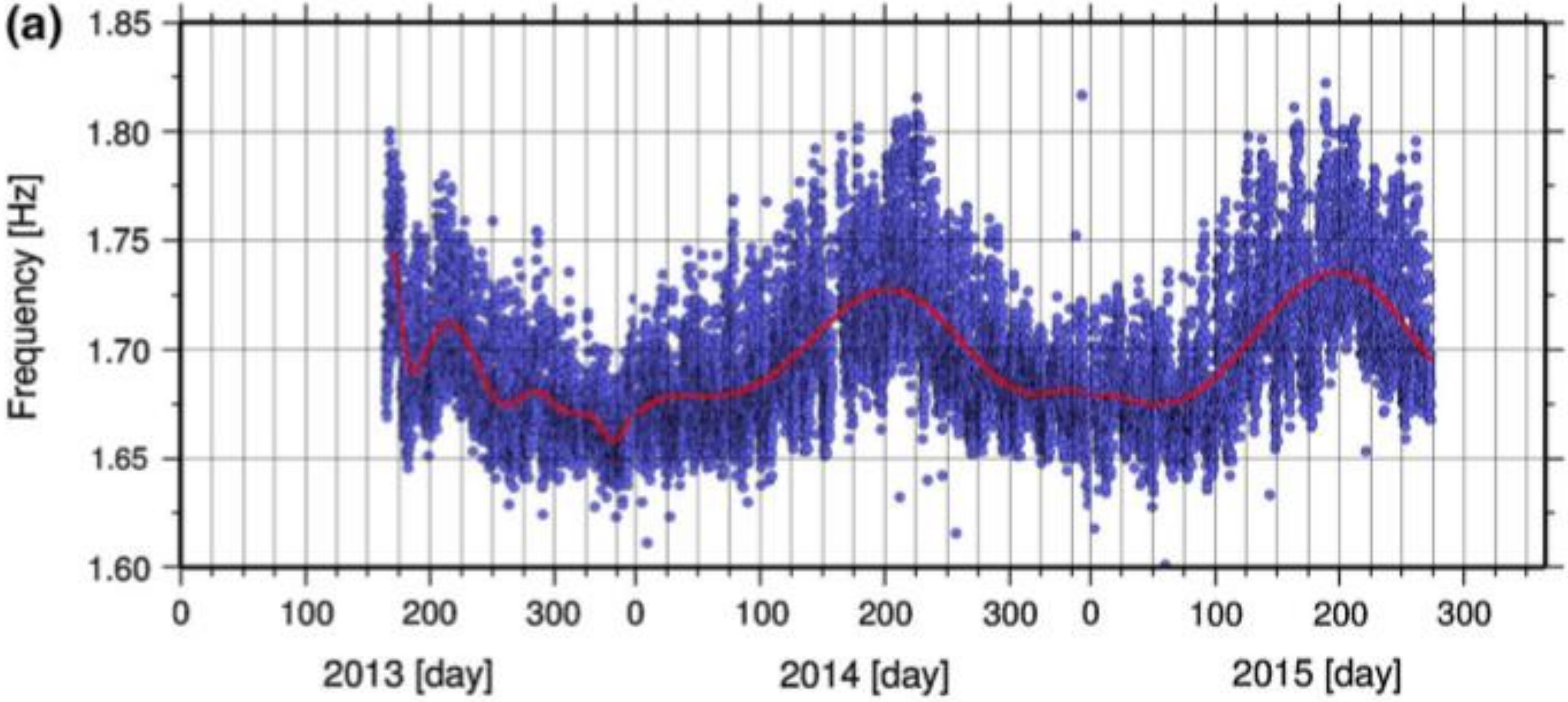

Mode shapes – translational modes

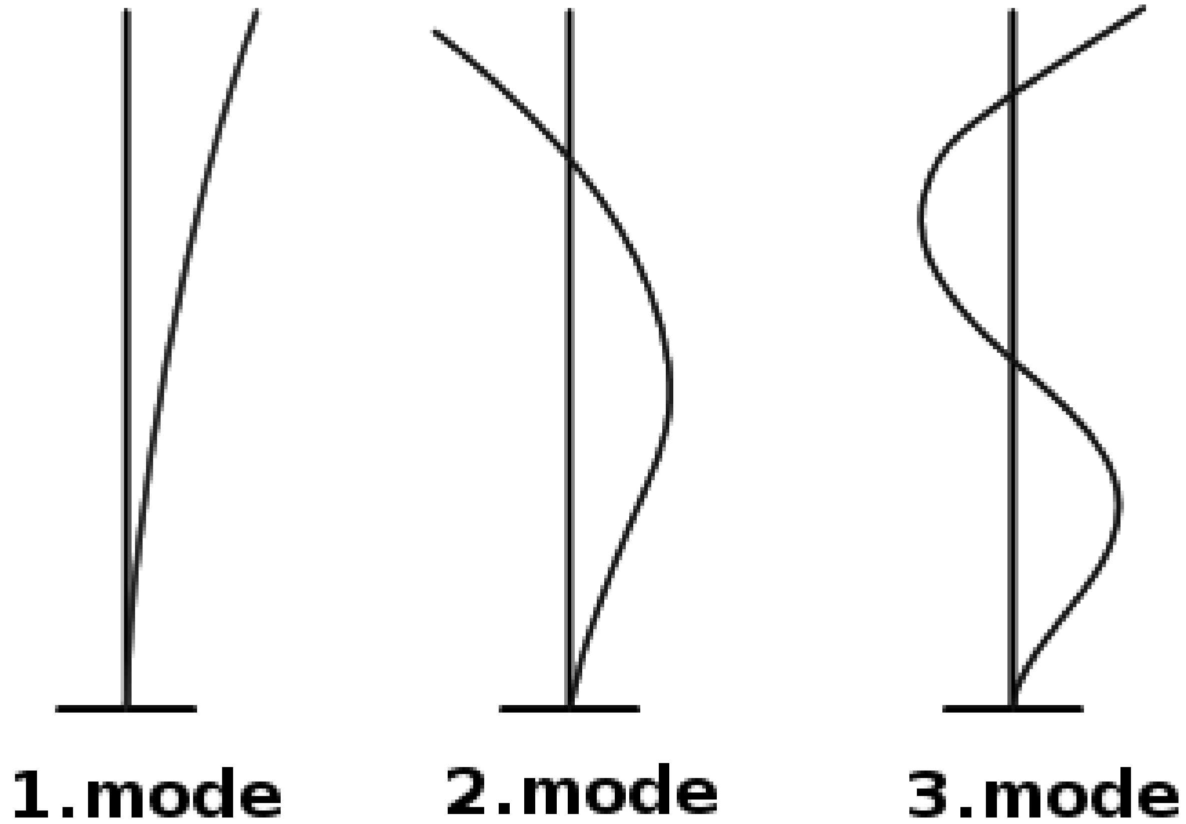

Mode shapes – translational modes

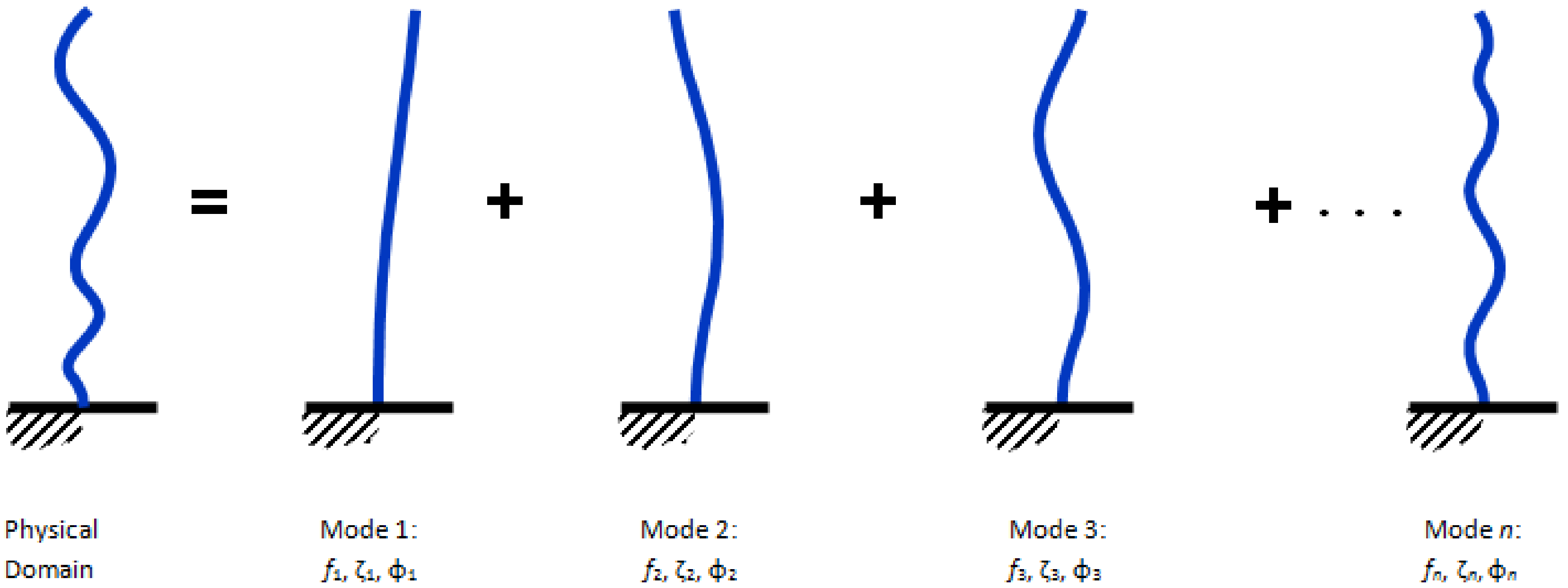

Mode shapes – Rotational modes

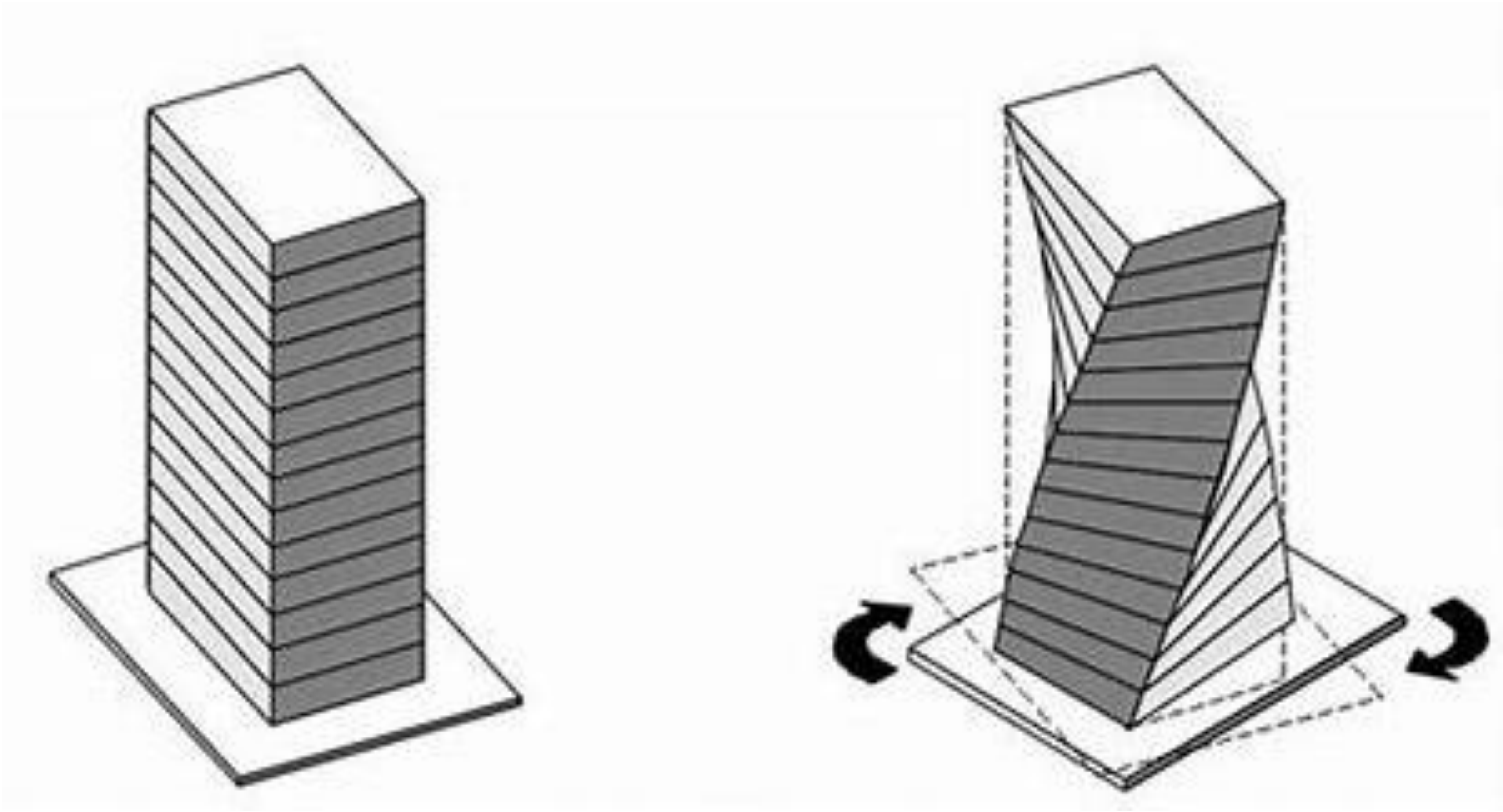

Estimating rotational modes

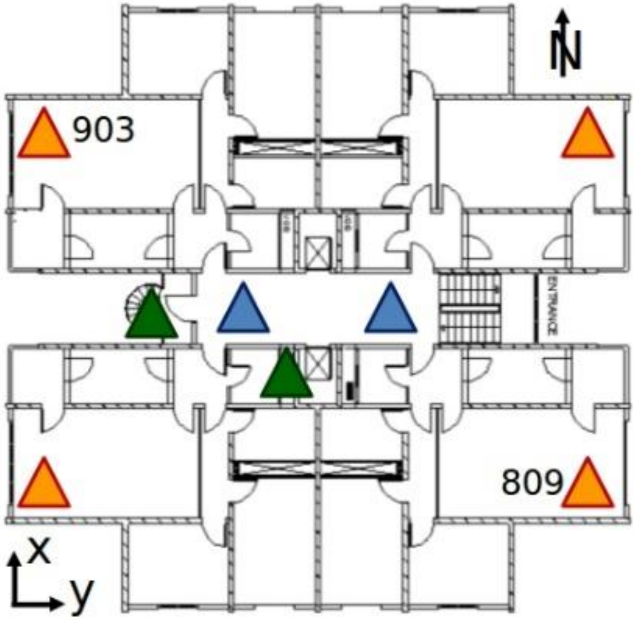

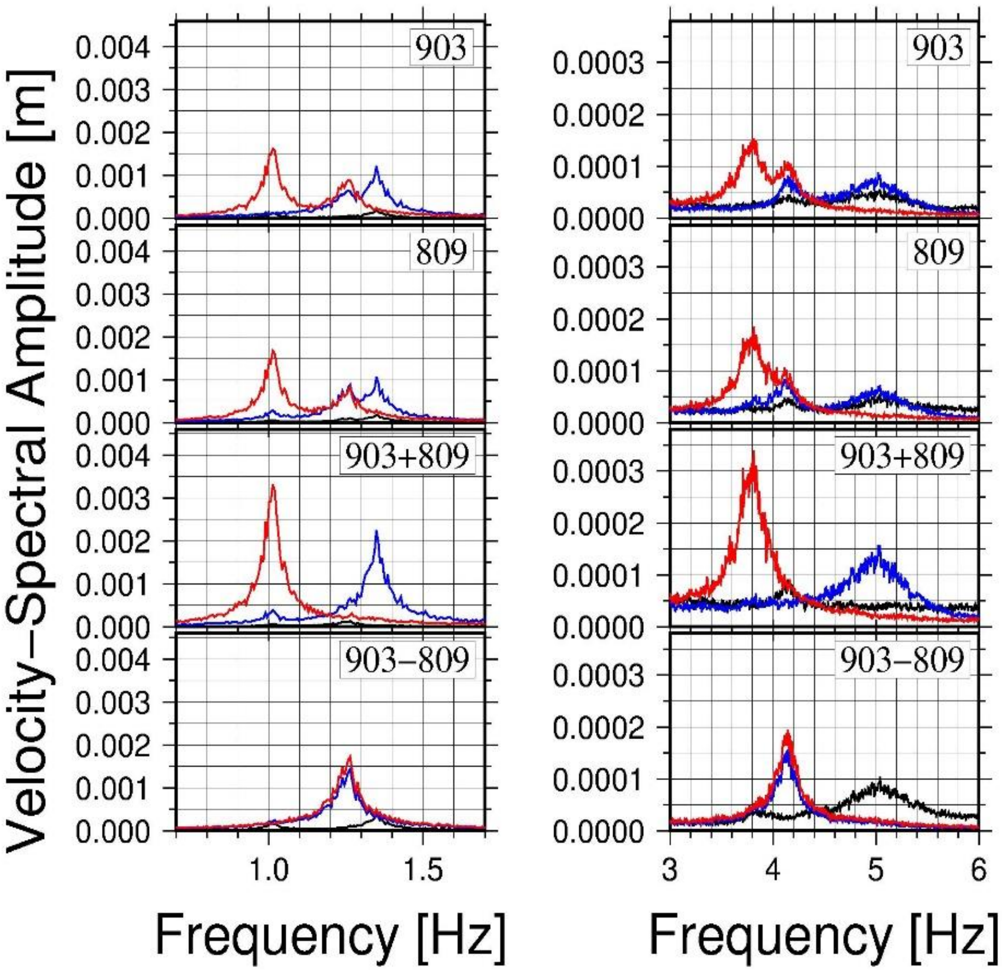

Estimating rotational modes

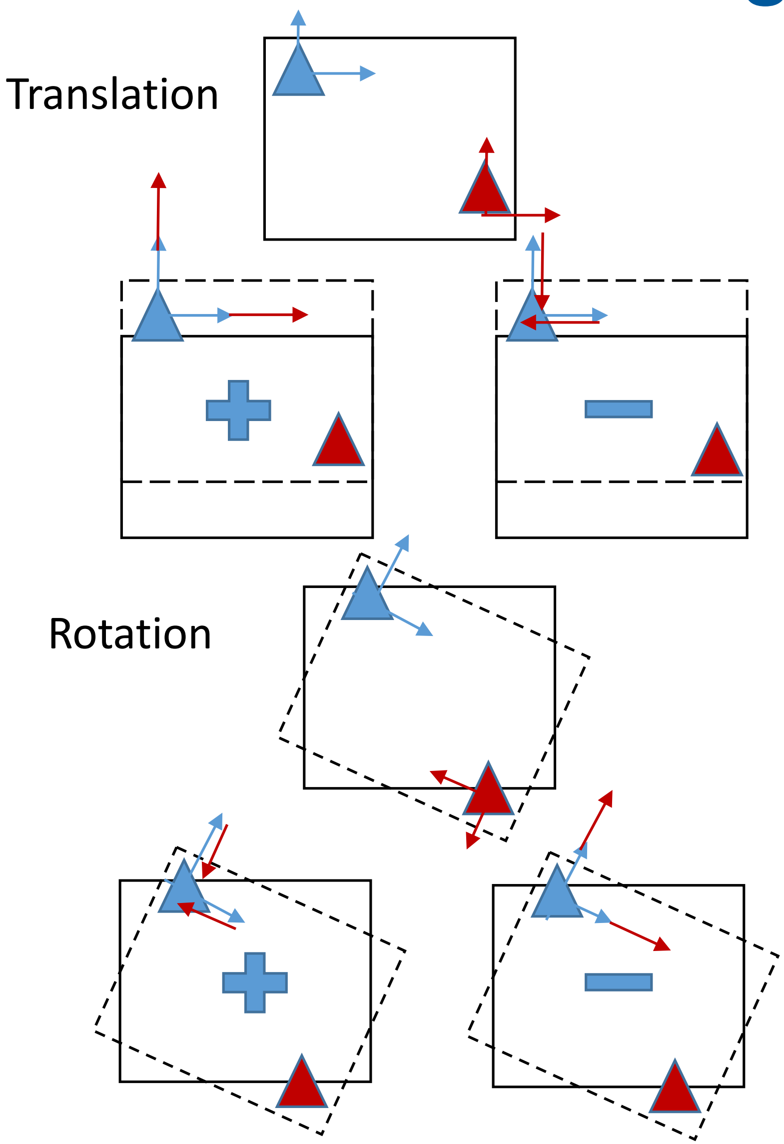

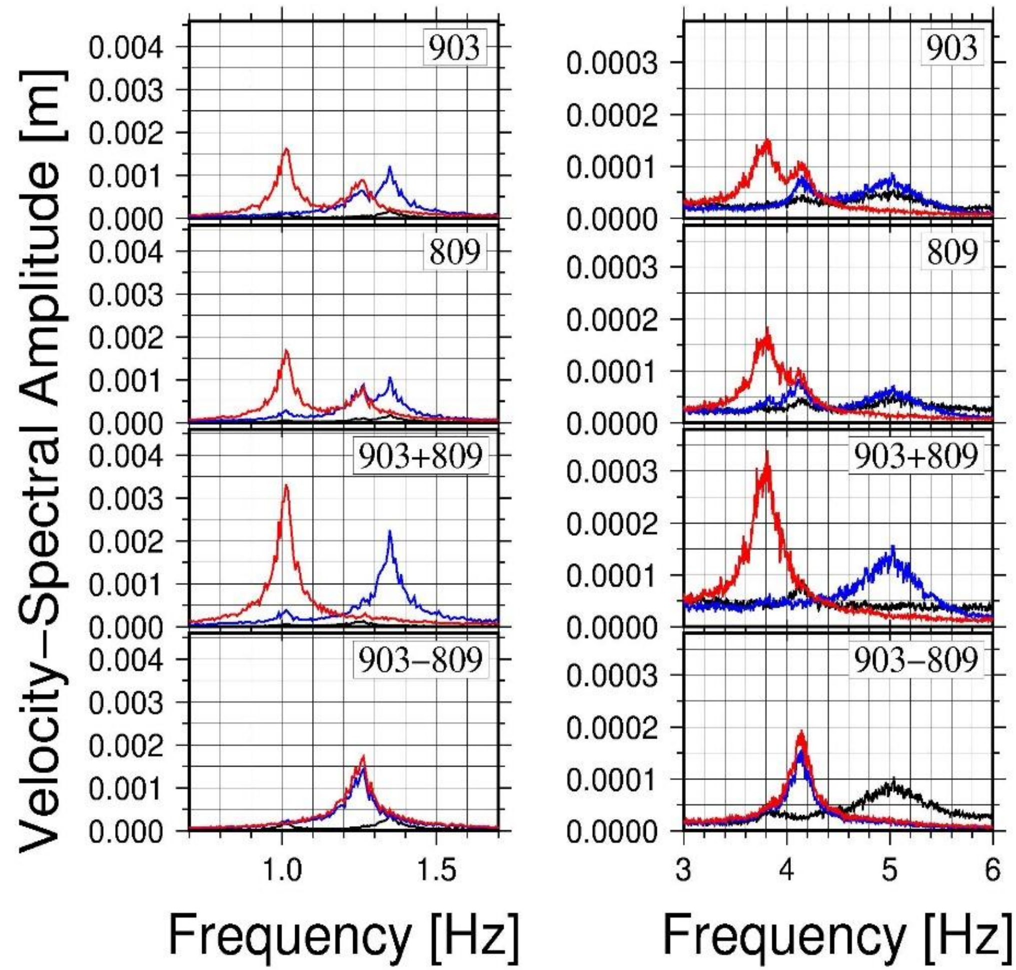

Operational Modal analysis
Frequency Domain Decomposition (FDD)

- developed by Brincker et al. 2001
- considered to be an improved version of the peak picking method
- consists of decomposing the systems cross power spectral density into its singular values (singular value decomposition, SVD)
- It is shown that taking the SVD of the spectral matrix, the latter is decomposed into a set of auto spectral density functions each corresponding to a single degree of freedom (SDOF) system

Operational Modal analysis
Frequency Domain Decomposition (FDD)

9 storey baseisolated panel building in Bishkek (Kyrgyzstan)

Data set: recordings of ambient vibrations

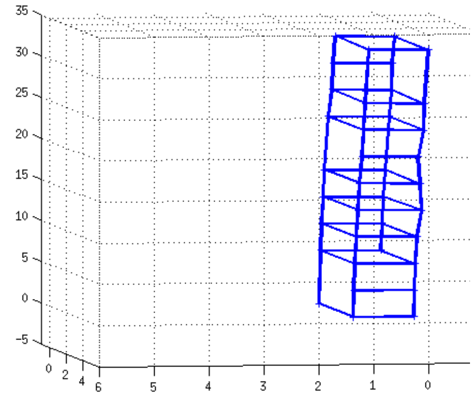

f=2.26 Hz

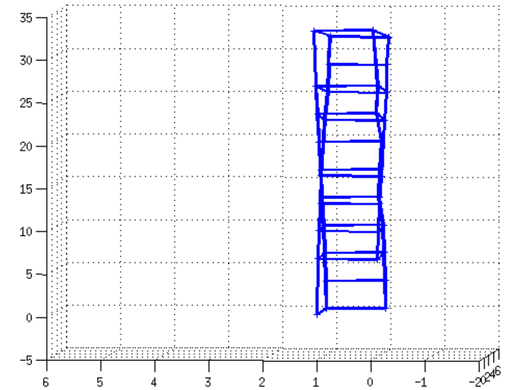

f=2.74 Hz

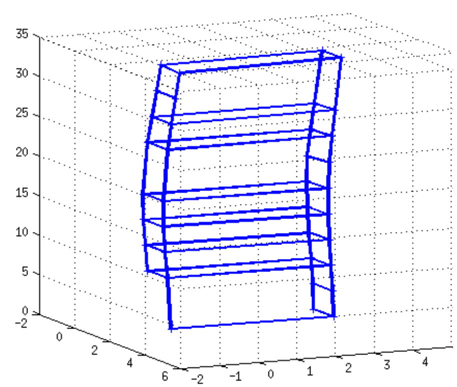

f=8.55 Hz

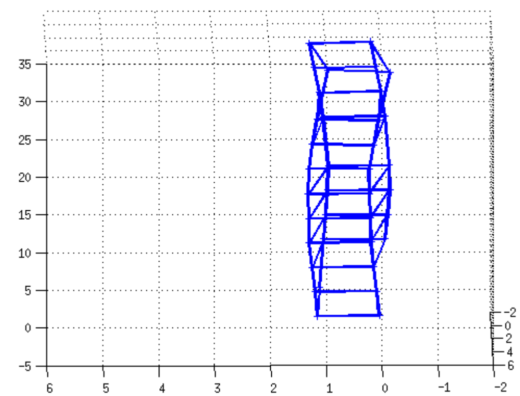

f=9.65 Hz

Operational Modal analysis
Frequency Domain Decomposition (FDD)

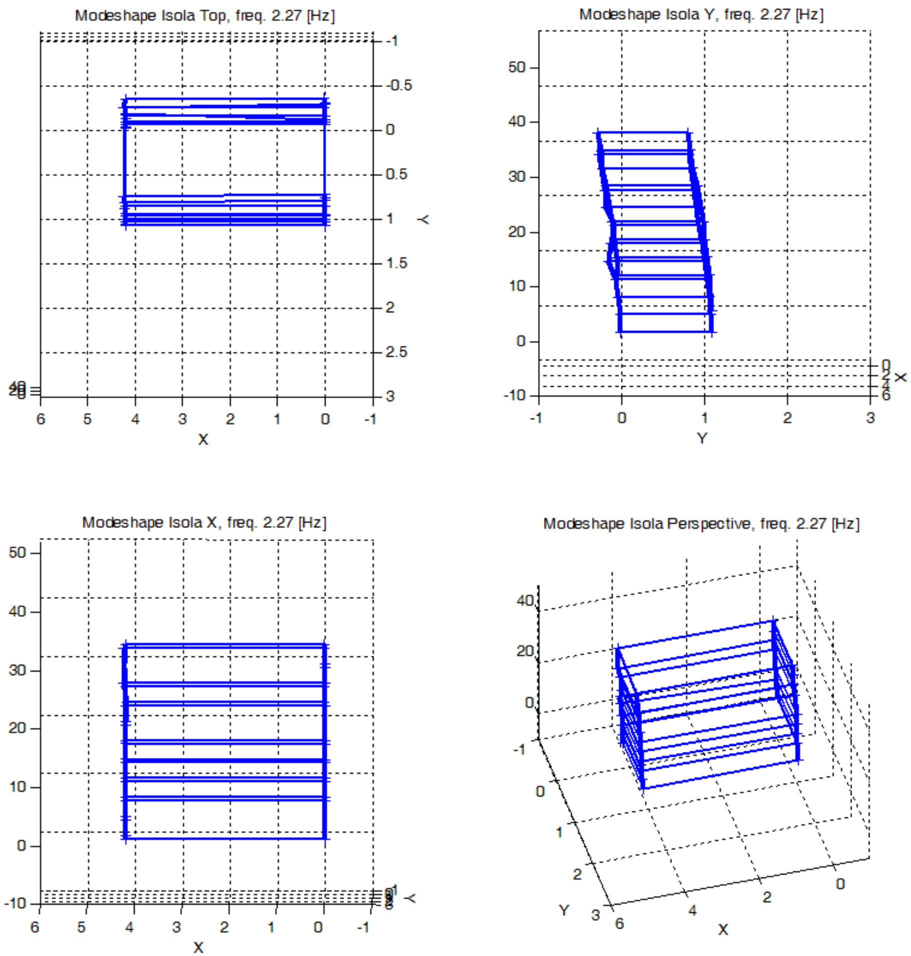

Operational Modal analysis
Frequency Domain Decomposition (FDD)

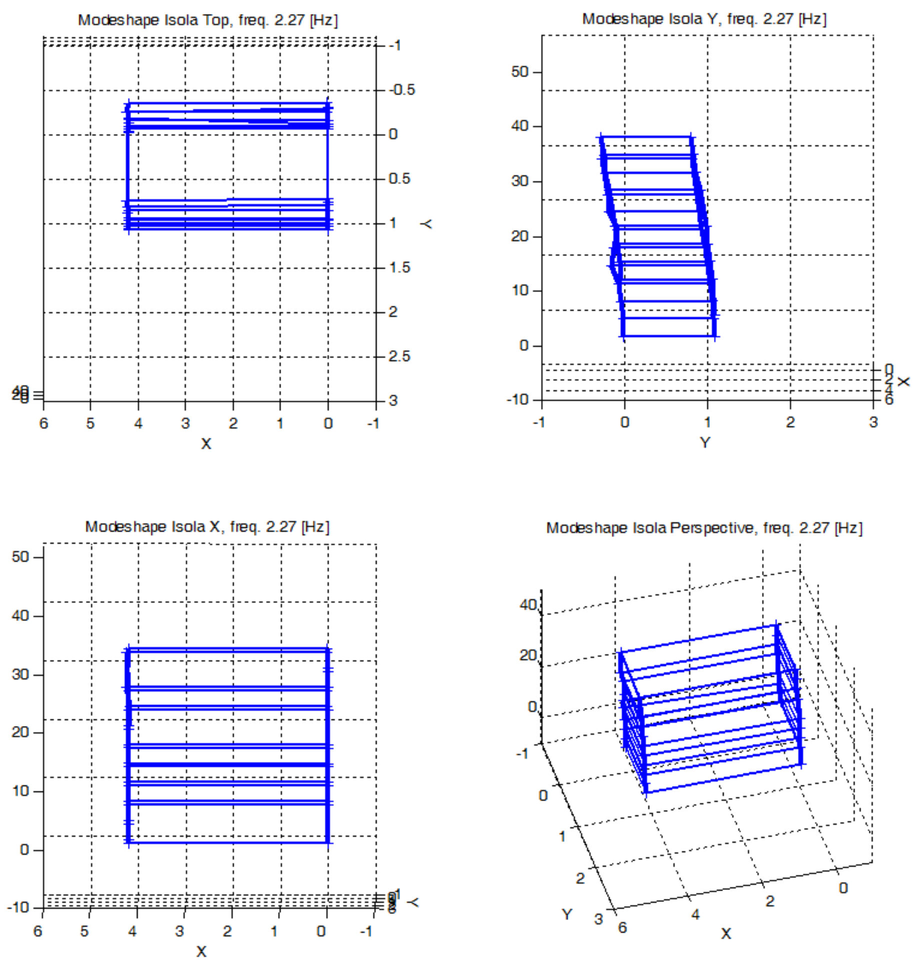

1. bending mode in logitudinal direction
f=2.26 Hz

Operational Modal analysis
Frequency Domain Decomposition (FDD)

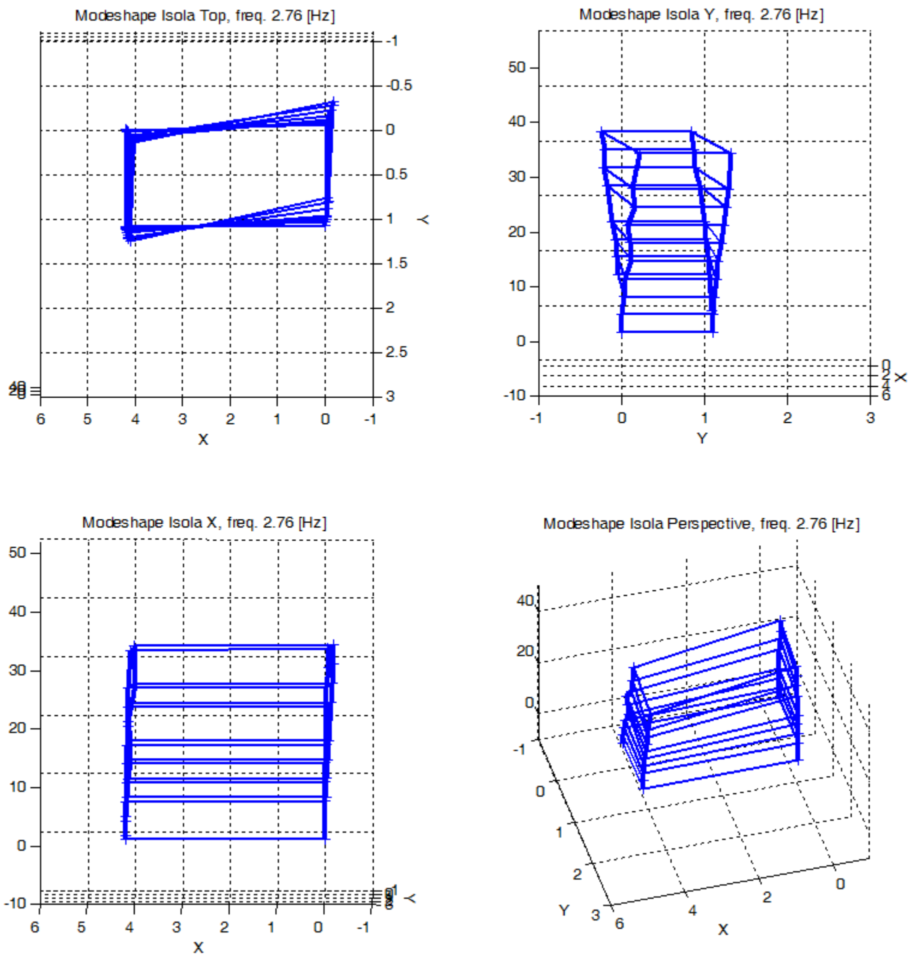

Operational Modal analysis
Frequency Domain Decomposition (FDD)

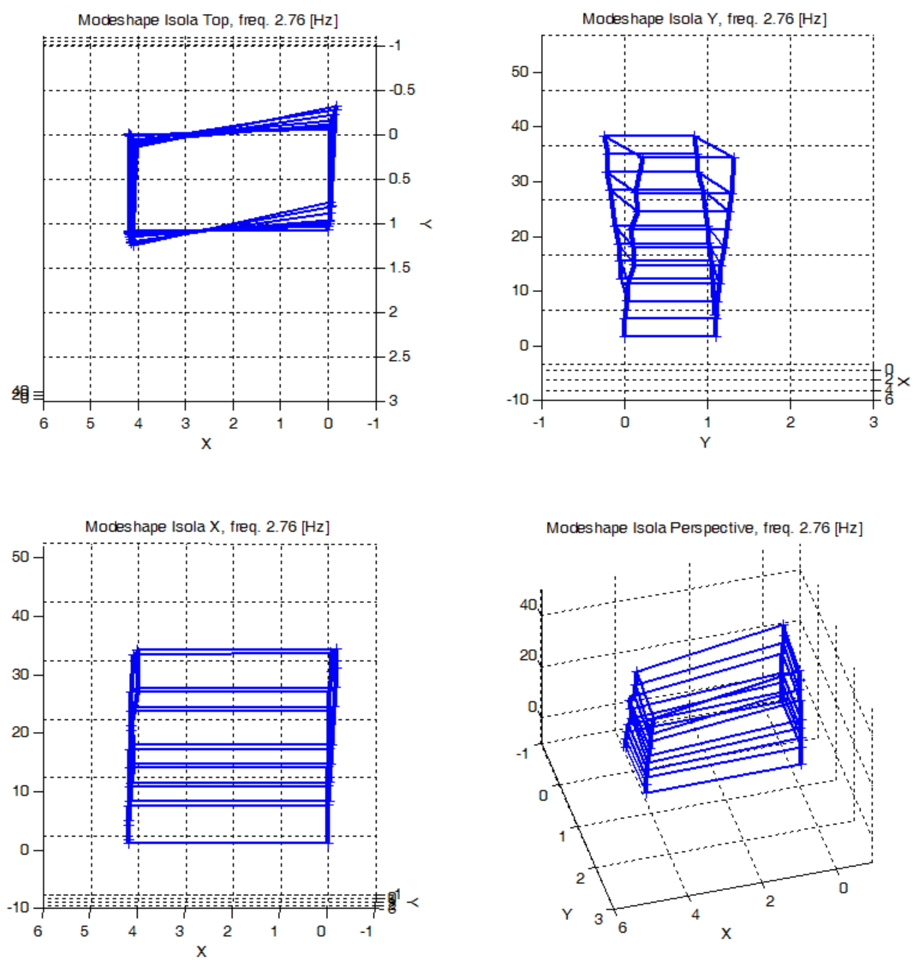

torsional mode
f=2.74 Hz

Operational Modal analysis
Frequency Domain Decomposition (FDD)

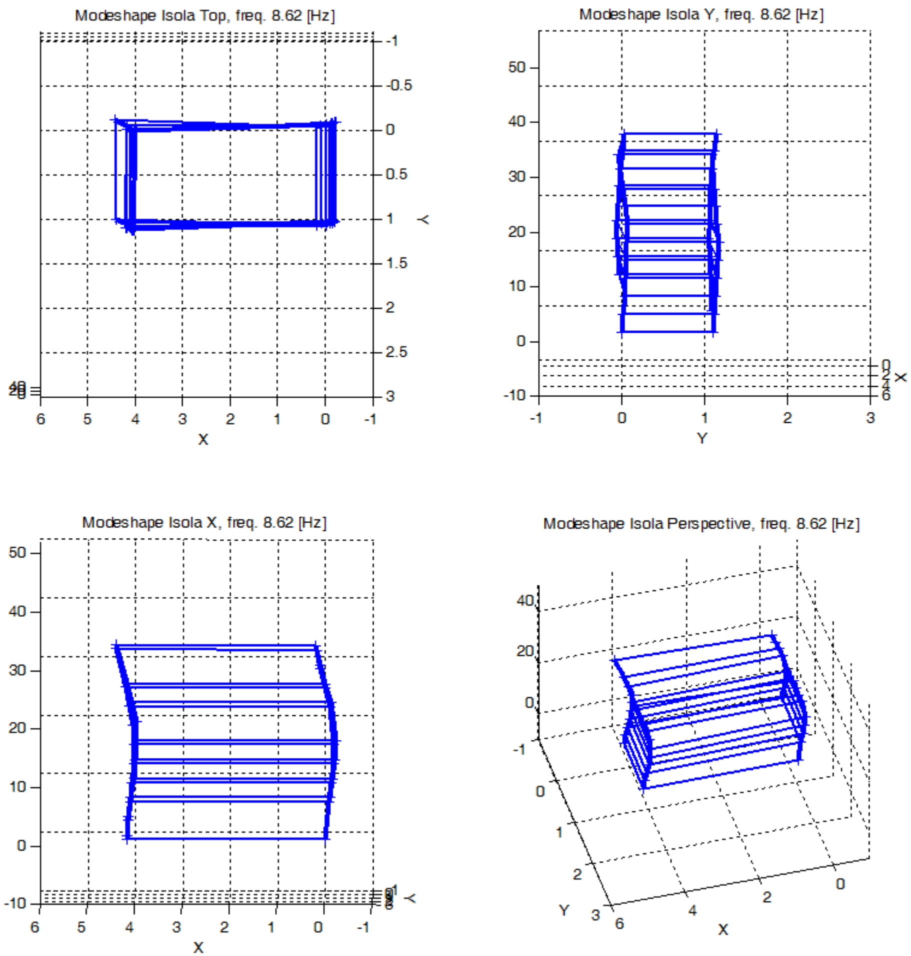

Operational Modal analysis
Frequency Domain Decomposition (FDD)

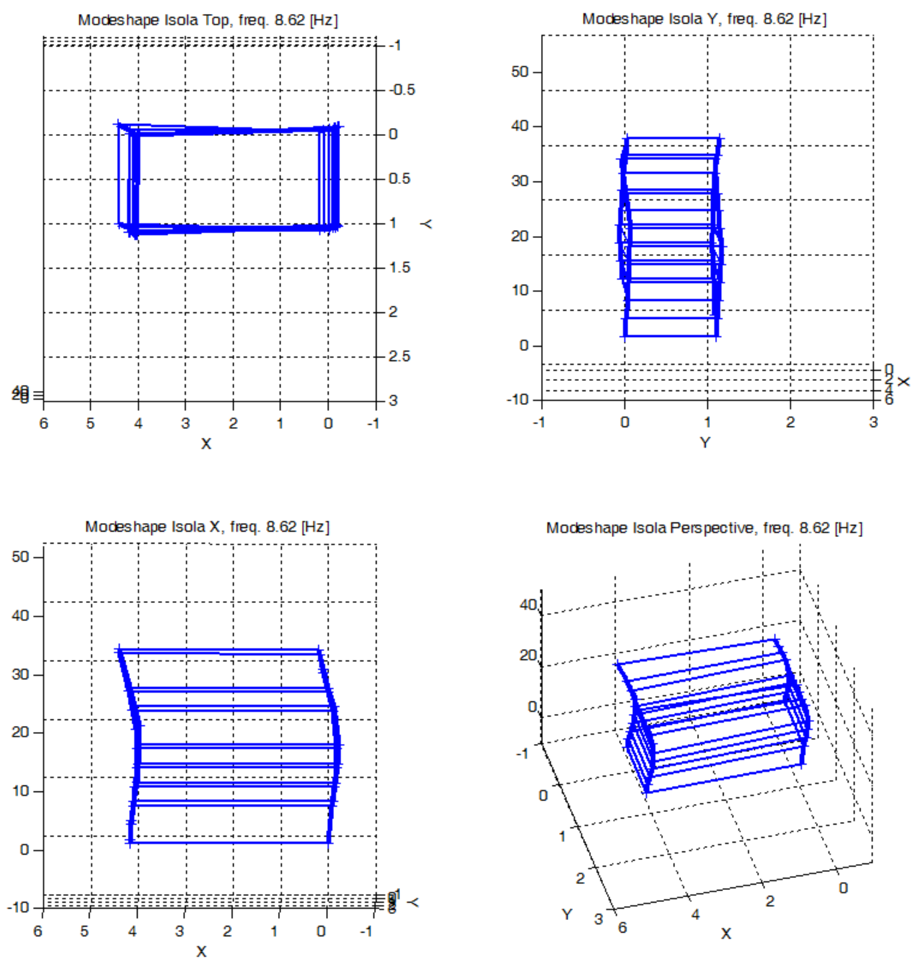

2. bending mode in transverse direction f=8.55 Hz

Operational Modal analysis
Frequency Domain Decomposition (FDD)

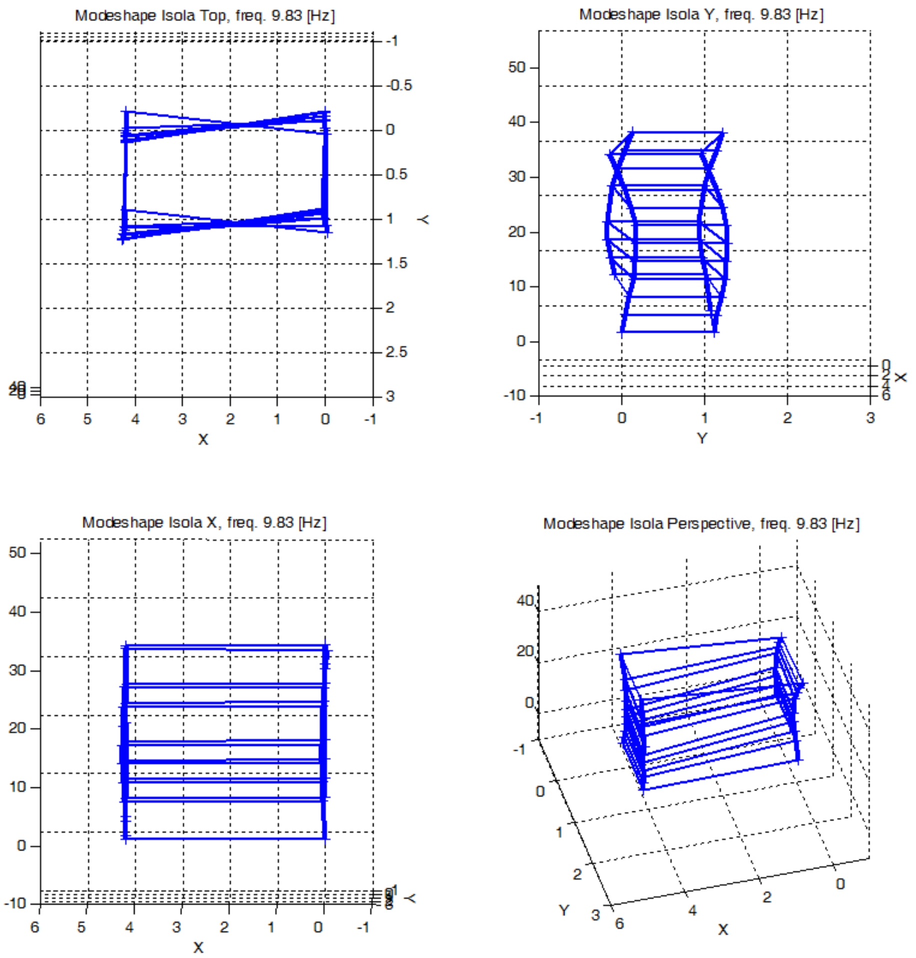

Operational Modal analysis
Frequency Domain Decomposition (FDD)

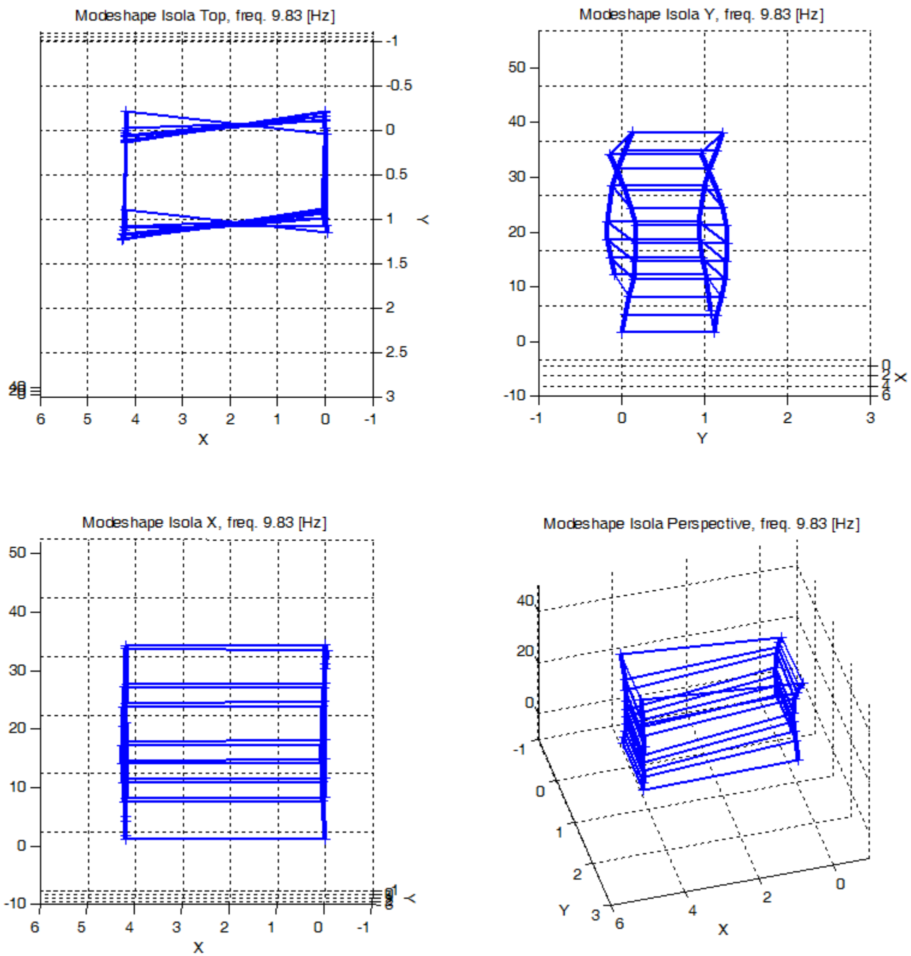

Coupled bending and torsional mode
f=9.65 Hz

The Finite Element Model

- The model includes:
  - Foundation
  - Columns and shear walls
  - All girders and slabs
  - The principal internal and external masonry walls
  - The bays
- The model does not include:
  - The reinforcement
  - Secondary separating walls
  - Additional roof elements

The Finite Element Model (FEM)

Finite element model of the building

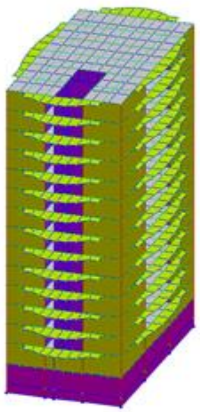

view

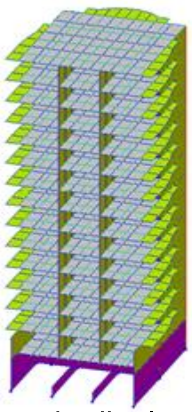

longitudinal cut

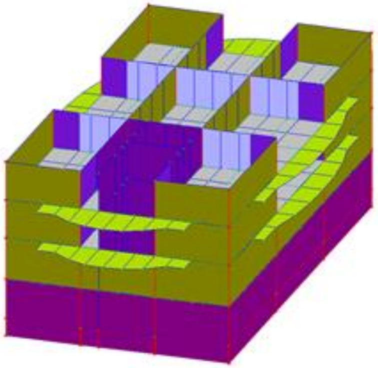

cross-section

- The model includes:
  - Foundation
  - Columns and shear walls
  - All girders and slabs
  - The principal internal and external masonry walls
  - The bays
- The model does not include:
  - The reinforcement
  - Secondary separating walls
  - Additional roof elements

Comparison of the results of the FEM model and the empirical data

Vibration mode shapes of the building (calculated by LIRA)

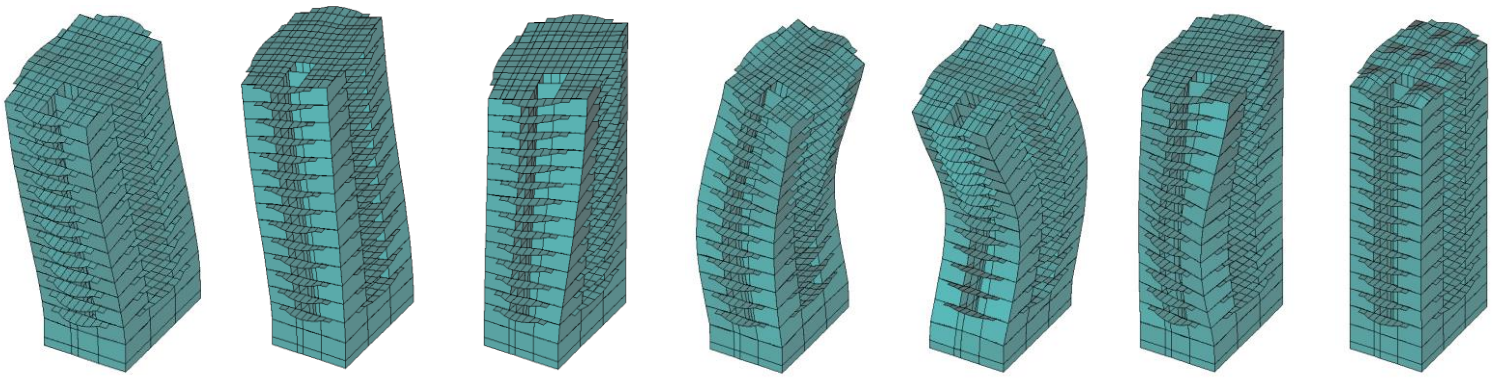

1st bending **1st bending** **1st torsion** **2nd bending** **2nd bending** **2nd torsion** **tension**

Comparison of calculated and measured natural frequencies

Comment	1st bending	1st bending	1st torsion	2nd bending	2nd bending	2nd torsion	tension	bending+ torsion	bending+ torsion
Frequency [Hz] LIRA	1.21	1.27	1.40	3.79	4.02	4.29	7.07	7.23	7.59
Frequency [Hz] OMA	1.29	1.39	1.56	3.81	4.38	4.92	7.07	7.54	8.30

Comparison of the results of the FEM model and the empirical data

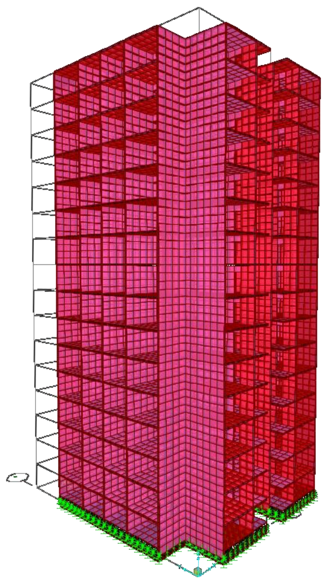

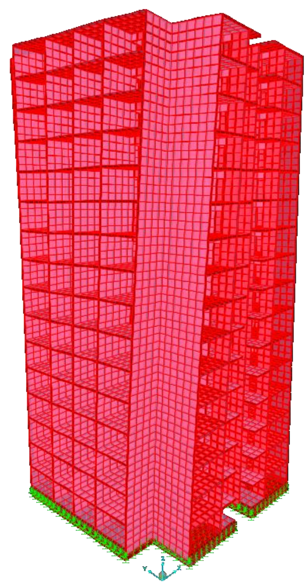

1. Torsional mode

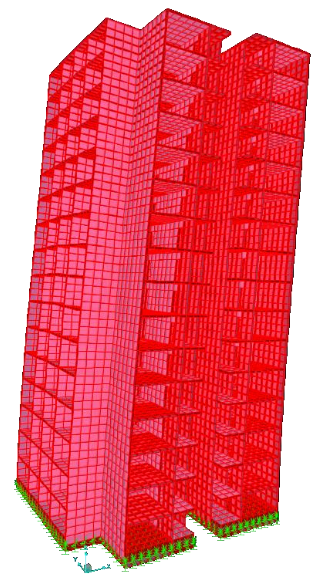

1. bending mode in x direction

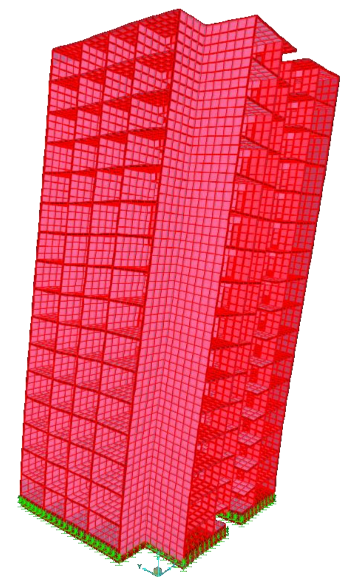

1. bending mode in y direction

Comparison of the results of the FEM model and the empirical data

Mode No.	Frequency f (Hz)				Mode type
	In-situ recordings		Analytical study		
	FAS	Transfer function	Fixed base case	Winkler springs case	
1	1.01	1.00	1.00	0.90	1st bending in x-dir.
2	1.26		0.84	0.76	1st torsional
3	1.35	1.37	1.60	1.43	1st bending in y-dir.
4	3.84	3.85	3.92	3.76	2nd bending in x-dir.
5	4.15	-	3.21	3.06	2nd torsional
6	5.04	5.13	5.36	5.23	2nd bending in y-dir.
7		8.13	8.12	7.93	3rd bending in x-dir.
8	-		6.67	6.48	3rd torsional
9	-		8.01	8.79	3rd bending in y-dir.

Stiffness of exterior infill walls which contribute to the torsional rigidity of the structure, are neglected in the model.

Seismic interferometry

Gives us an insight into the wave propagation through buildings and/or soil

Can be applied to

- Earthquake recordings
- Ambient vibration measurements
- Generated vibration measurements

Seismic interferometry

Claerbout’s conjecture

“By cross correlating noise traces recorded at two locations on the surface, we can construct the wavefield that would be recorded at one of the locations if there was a source at the other.”

Seismic interferometry

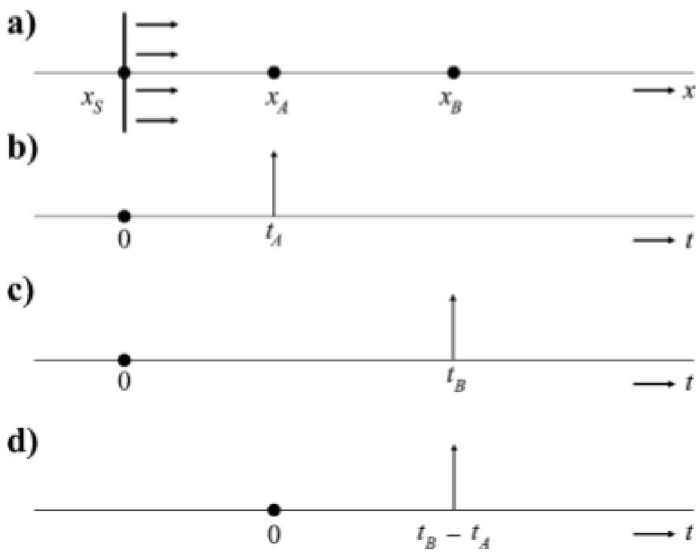

Figure 1. A 1D example of direct-wave interferometry. (a) A plane wave traveling rightward along the x-axis, emitted by an impulsive source at $x = x_S$ and $t = 0$. (b) The response observed by a receiver at x_A. This is the Green's function $G(x_A,x_S,t)$. (c) As in (b) but for a receiver at x_B. (d) Crosscorrelation of the responses at x_A and x_B. This is interpreted as the response of a source at x_A, observed at x_B, i.e., $G(x_B,x_A,t)$.

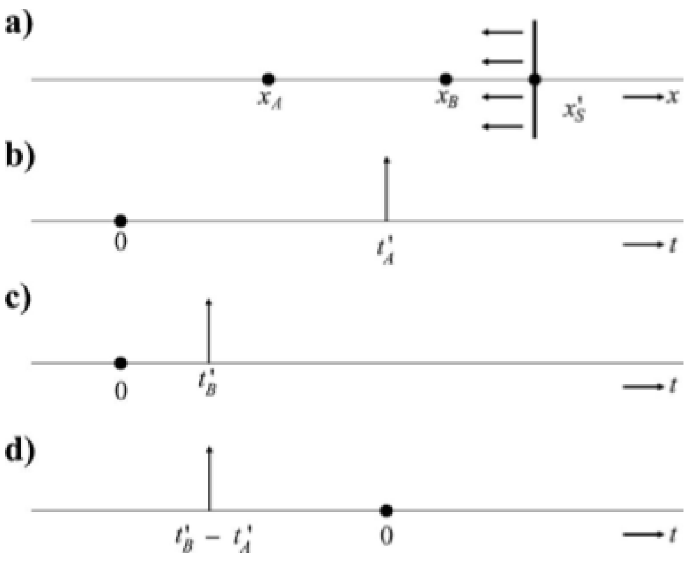

Figure 3. As in Figure 1 but this time for a leftward-traveling impulsive plane wave. The crosscorrelation in (d) is interpreted as the time-reversed Green's function $G(x_B,x_A,-t)$.

Seismic interferometry

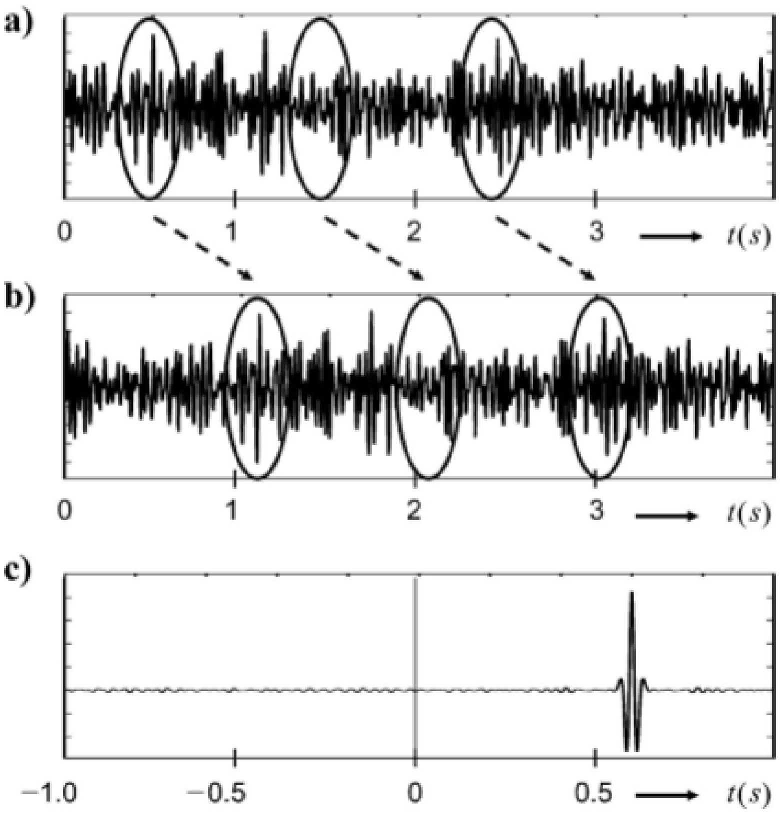

Figure 2. As in Figure 1 but this time for a noise source $N(t)$ at x_S. (a) The response observed at x_A, i.e., $u(x_A,x_S,t) = G(x_A,x_S,t) * N(t)$. (b) As in (a) but for a receiver at x_B. (c) The crosscorrelation, which is equal to $G(x_B,x_A,t) * S_N(t)$, with $S_N(t)$ the autocorrelation of the noise.

Convolution, Cross-correlation, Autocorrelation

Convolution between two real functions in the time domain

$$h(t) = f(t) * g(t) = \int_{-\infty}^{+\infty} f(\tau) g(t-\tau) d\tau$$

Fourier Transform of h(t) is given by

$$H(\omega) = 2\pi F(\omega) G(\omega)$$

Correlation between two real functions in the time domain

$$h(t) = f(t) \otimes g(t) = f(-t) * g(t) = \int_{-\infty}^{+\infty} f(\tau) g(t+\tau) d\tau$$

Fourier Transform of h(t) is given by

$$H(\omega) = 2\pi F(\omega)^{*} G(\omega)$$

Convolution, Cross-correlation, Autocorrelation

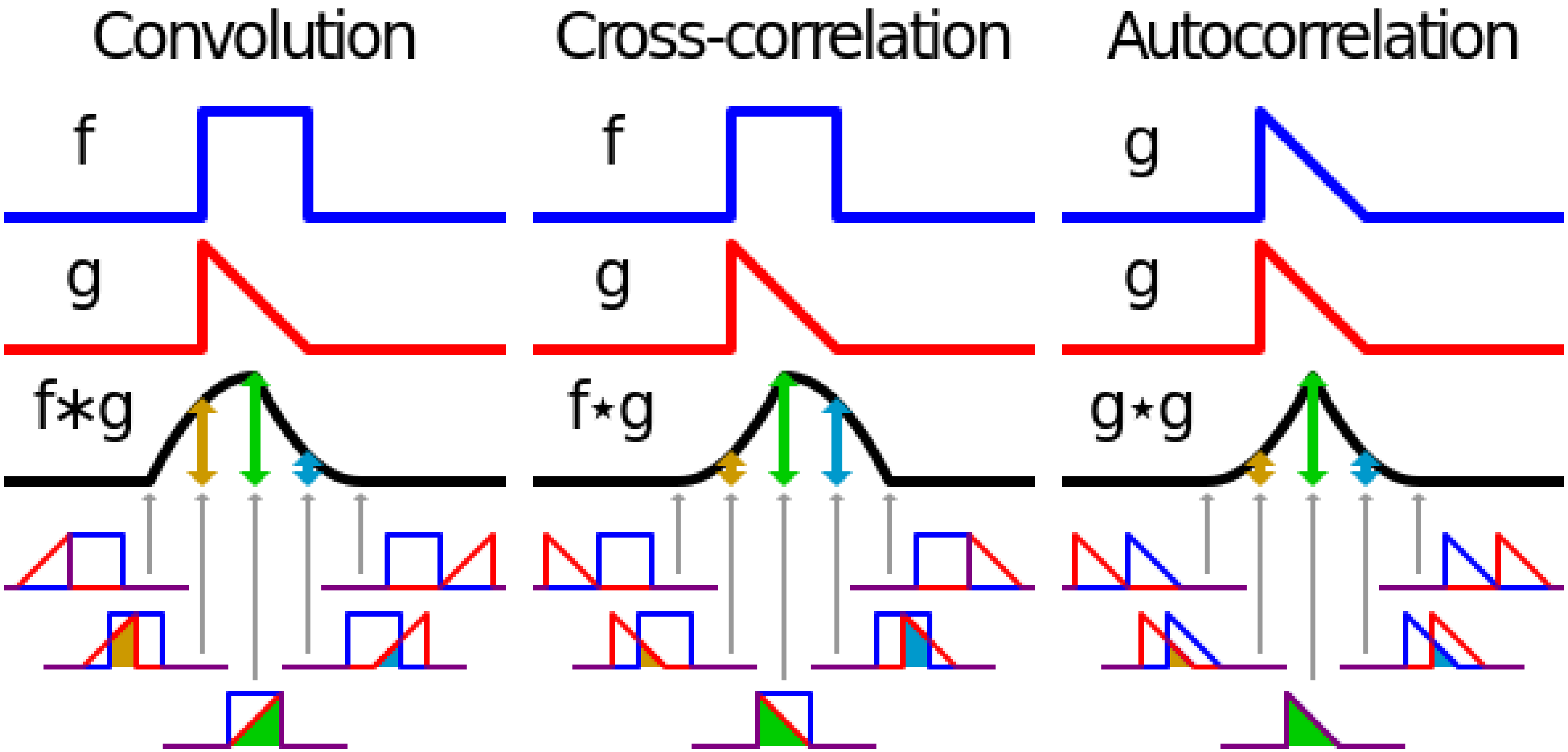

Deconvolution

algorithm-based process used to reverse the effects of **convolution** on recorded data.

objective: find solution of a convolution equation:

$$f(t) * g(t) = h(t)$$

Deconvolution in the frequency domain:

$$F(\omega) = H(\omega)/G(\omega)$$

followed by inverse Fourier Transform.

Deconvolution

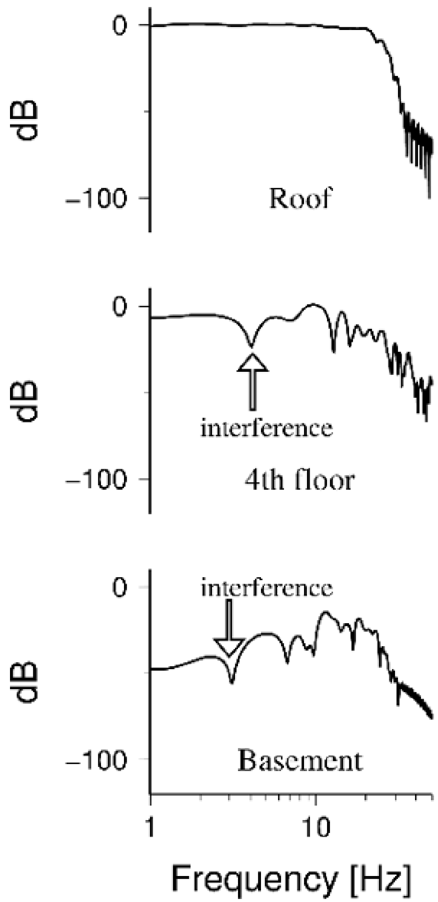

Deconvolution

$$D(\omega) = \frac{\hat{u}(\omega)}{\hat{u}_{ref}(\omega)}$$

Regularized deconvolution

$$D(\omega) = F(\omega)\hat{u}(\omega)$$

$$F(\omega) = \frac{\hat{u}^*_{ref}(\omega)}{|\widehat{u_{ref}}(\omega)|^2 + \varepsilon}$$

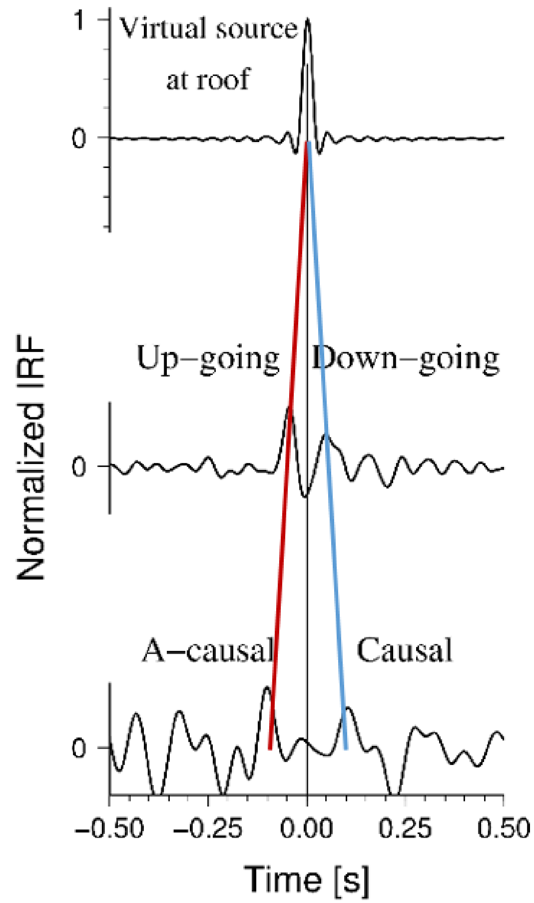

[Bindi et al., 2015]

Wave propagation through a homogeneous layer

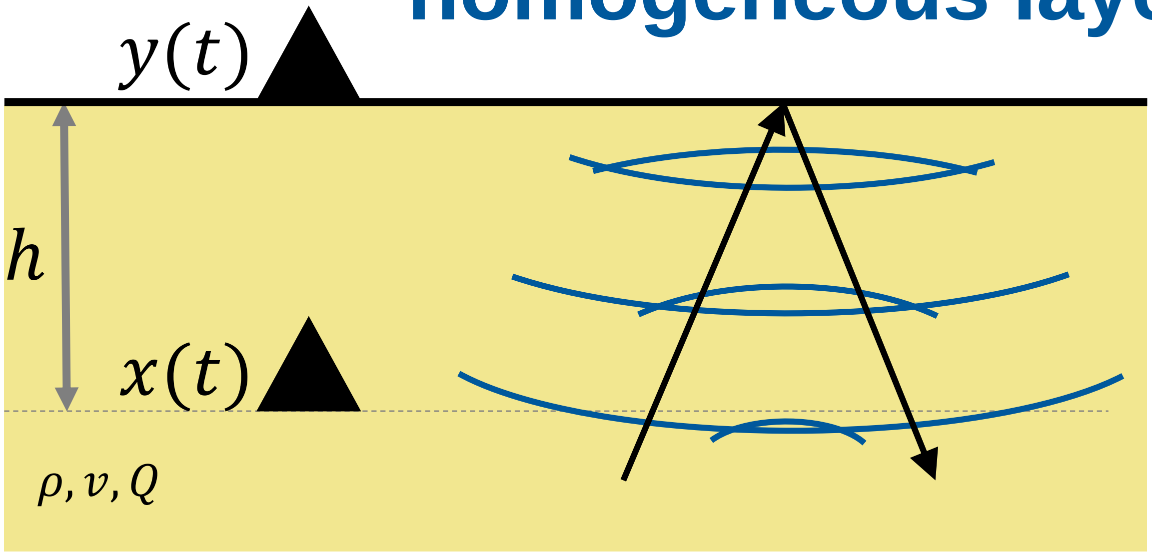

ρ - density
v - velocity
Q - quality factor
τ - travel time
$\tau = h/v$
ω - angular frequency
$\omega = 2\pi f$
f - frequency

$$x(\omega) = \underbrace{x_0(\omega)}_{\text{Incoming wave}} + \underbrace{0.5\, y(\omega)\, e^{-i\omega\tau}}_{\text{Wave reflected at the free surface}}$$

Wave propagation through a homogeneous layer

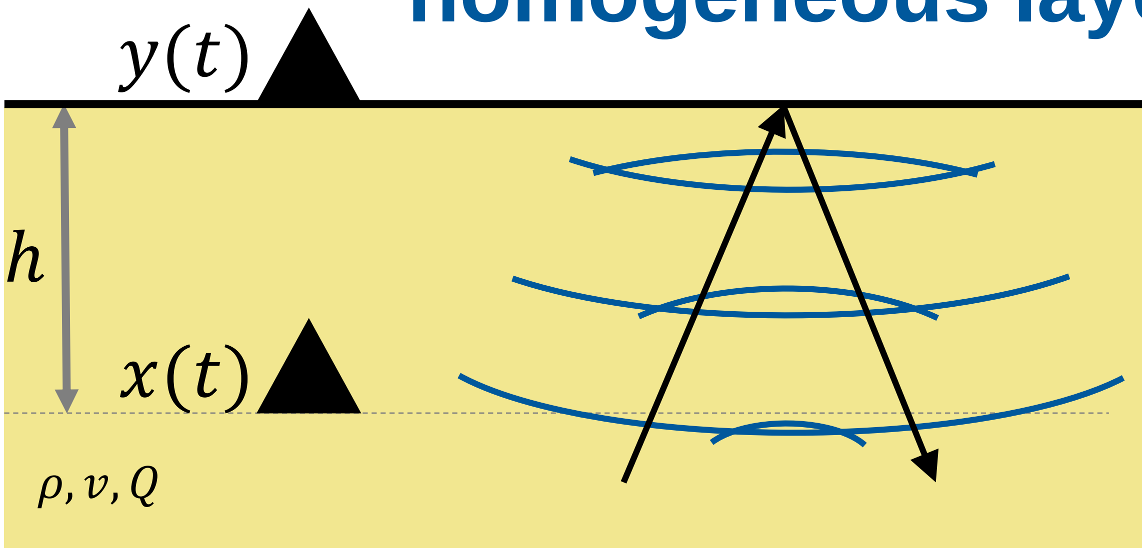

ρ - density

v - velocity

Q - quality factor

τ - travel time

$$\tau = h/v$$

ω - angular frequency

$$\omega = 2\pi f$$

f - frequency

$$x(\omega) = \underbrace{x_0(\omega)}_{\text{Incoming wave}} + \underbrace{0.5\, y(\omega)\, e^{-i\omega\frac{\tau}{}}}_{\text{Wave reflected at the free surface}}$$

Incoming wave — Wave reflected at the free surface

$$y(\omega) = \underbrace{2x_0(\omega)e^{-i\omega\frac{\tau}{}}}_{\text{Incoming wave recorded at free surface}}$$

Incoming wave recorded at free surface

Wave propagation through a homogeneous layer

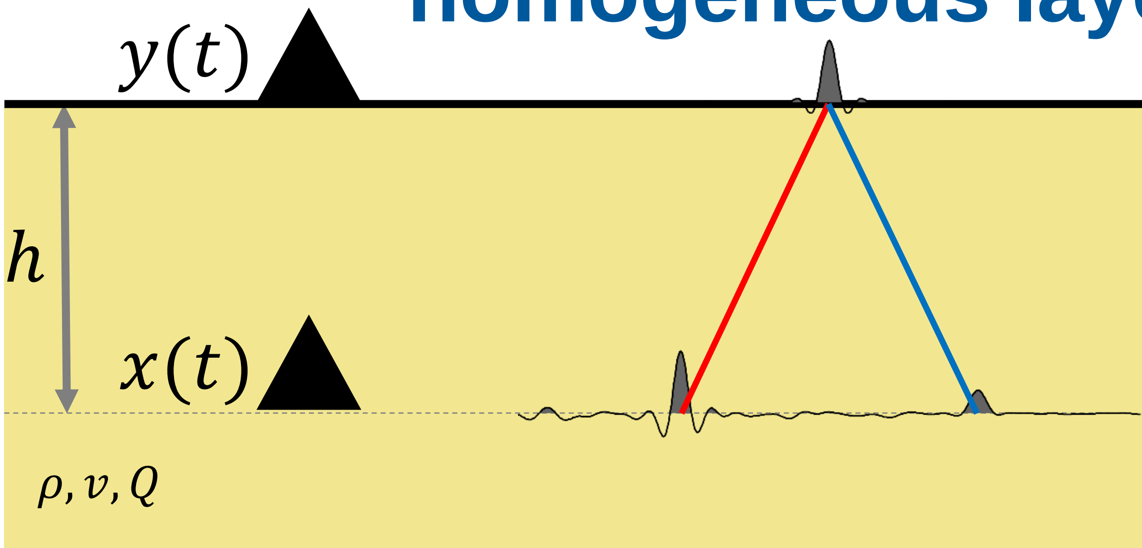

ρ - density

v - velocity

Q - quality factor

τ - travel time

$$\tau = h/v$$

ω - angular frequency

$$\omega = 2\pi f$$

f - frequency

$$x(\omega) = x_0(\omega) + 0.5\, y(\omega)\, e^{-i\omega\frac{\tau}{}}$$

$$y(\omega) = 2x_0(\omega)e^{-i\omega\frac{\tau}{Q}}$$

Deconvolution:

$$D(\omega) = \frac{x(\omega)}{y(\omega)} = 0.5(\underbrace{e^{-i\omega\frac{\tau}{}}}_{\text{up-going}} + \underbrace{e^{i\omega\frac{\tau}{}}}_{\text{down-going}})$$

Seismic interferometry using deconvolution approach

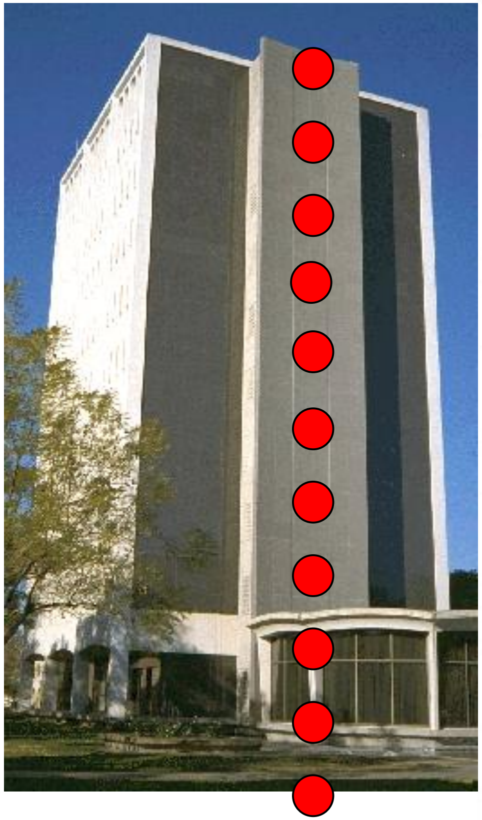

Millikan Library

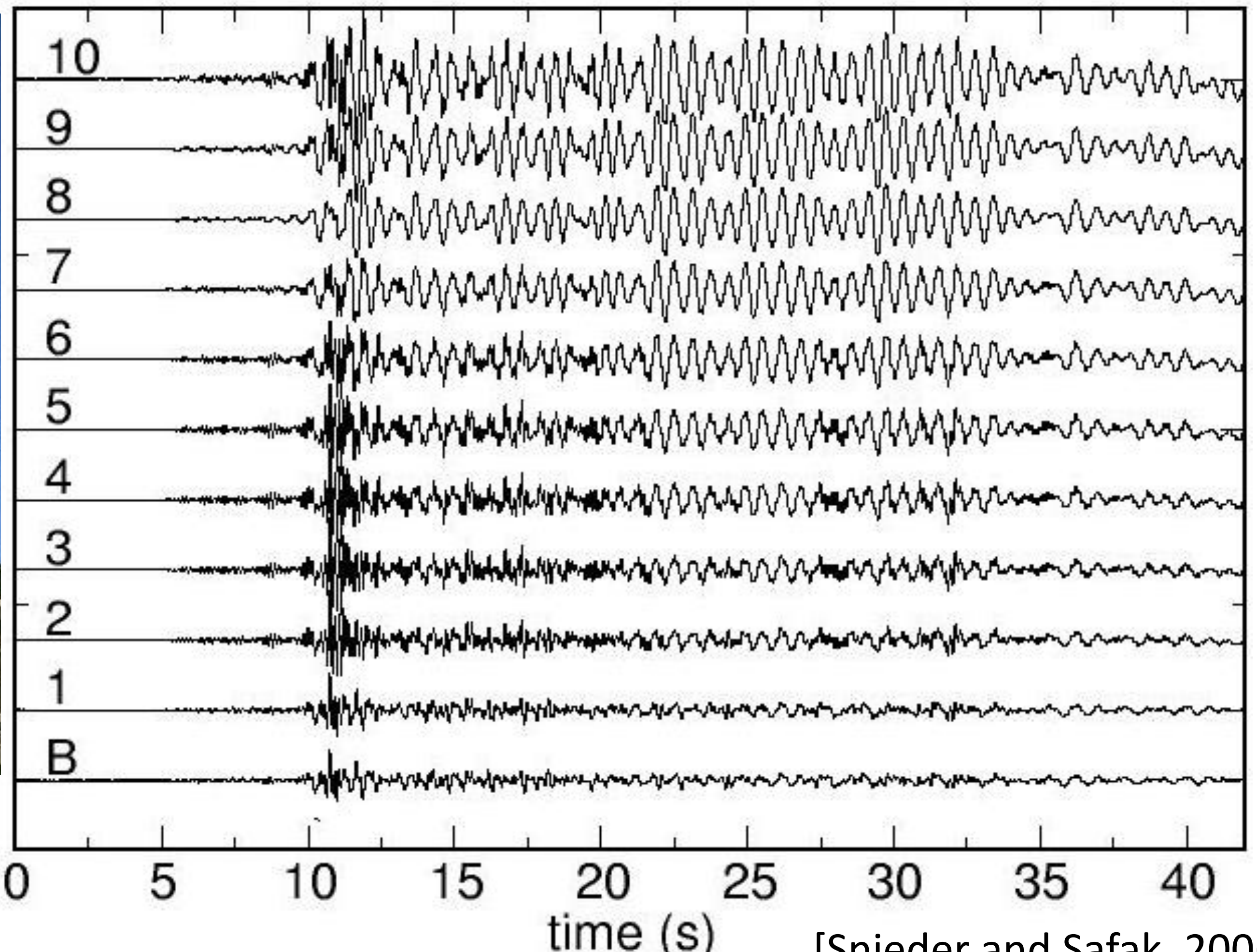

[Snieder and Safak, 2006]

Seismic interferometry - Earthquakes

Snieder and Safak, 2006

Millikan Library

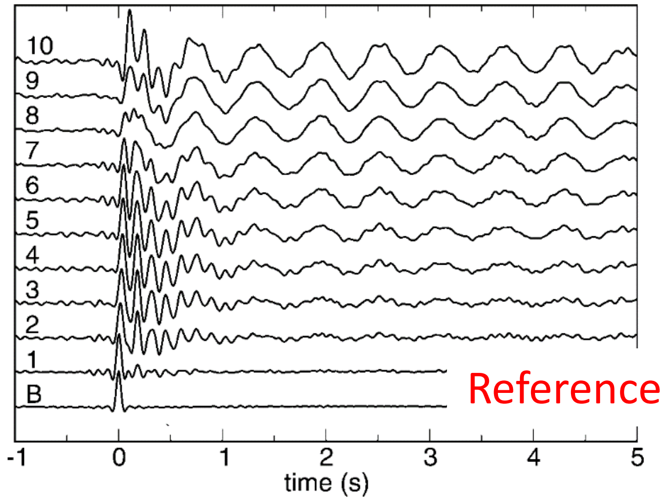

Reference at bottom

$$B(z,\omega) = \sum_{n=0}^{\infty} (-1)^n \left[e^{ik(z+2nH)} e^{-\gamma |k| (z+2nH)} + \right.$$

$$\left. + e^{ik(2(n+1)H - z)} e^{-\gamma |k| (2(n+1)H - z)} \right]$$

the summation index *n* counts the number of bounces off the base

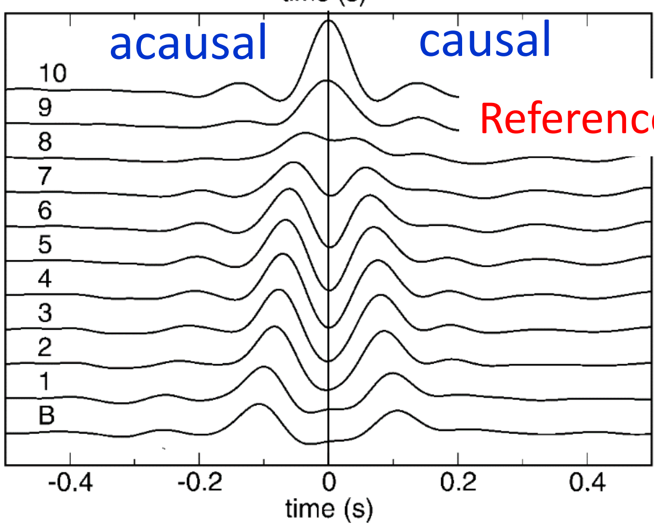

Reference at top

$$T(z,\omega) = \frac{1}{2} \left[e^{ik(z-H)} e^{-\gamma |k| (z-H)} + e^{ik(H-z)} e^{-\gamma |k| (H-z)} \right]$$

Upgoing + downgoing

Deconvolution with the top

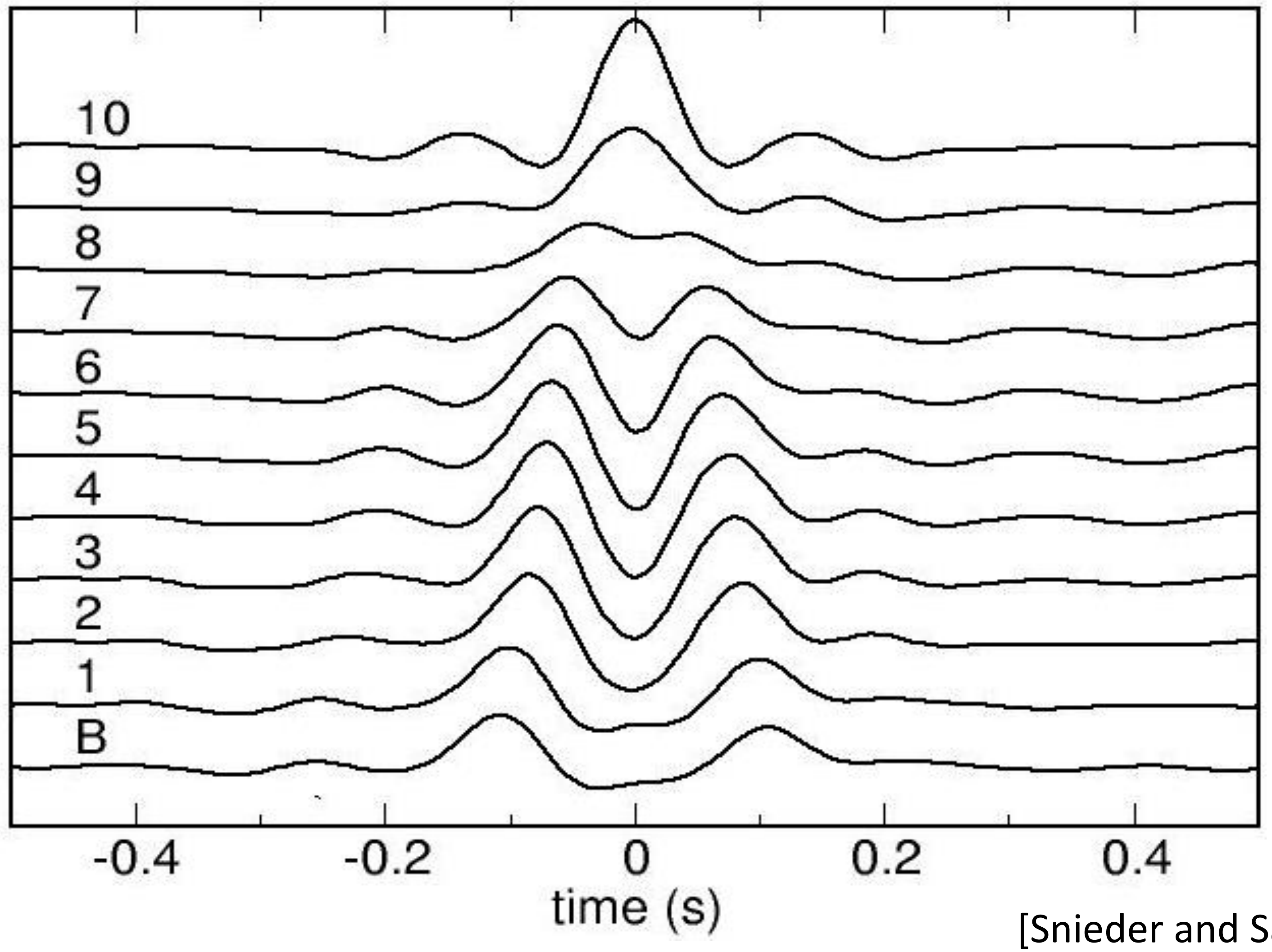

[Snieder and Safak, 2006]

Deconvolution with the top

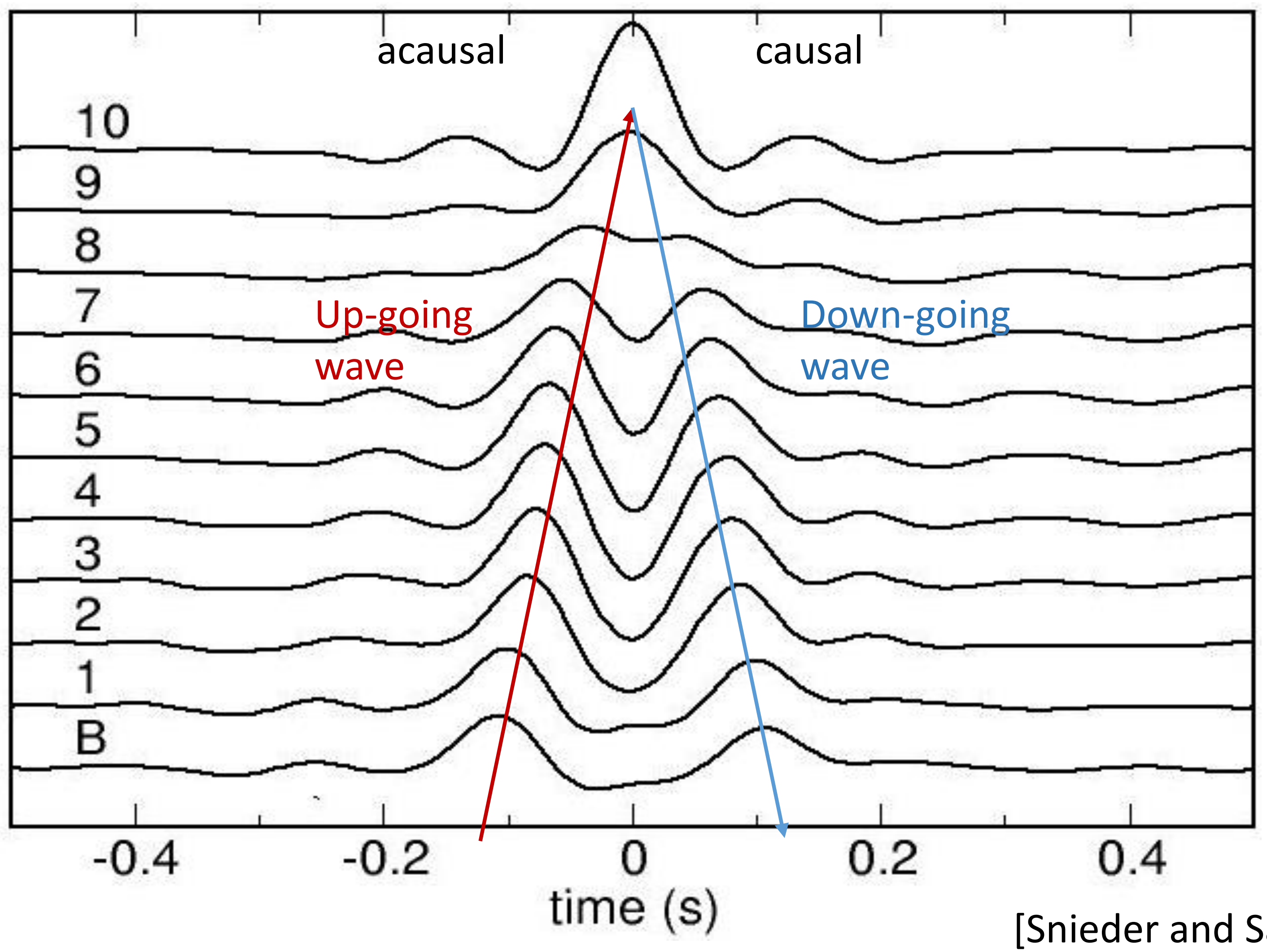

[Snieder and Safak, 2006]

Deconvolution with the bottom

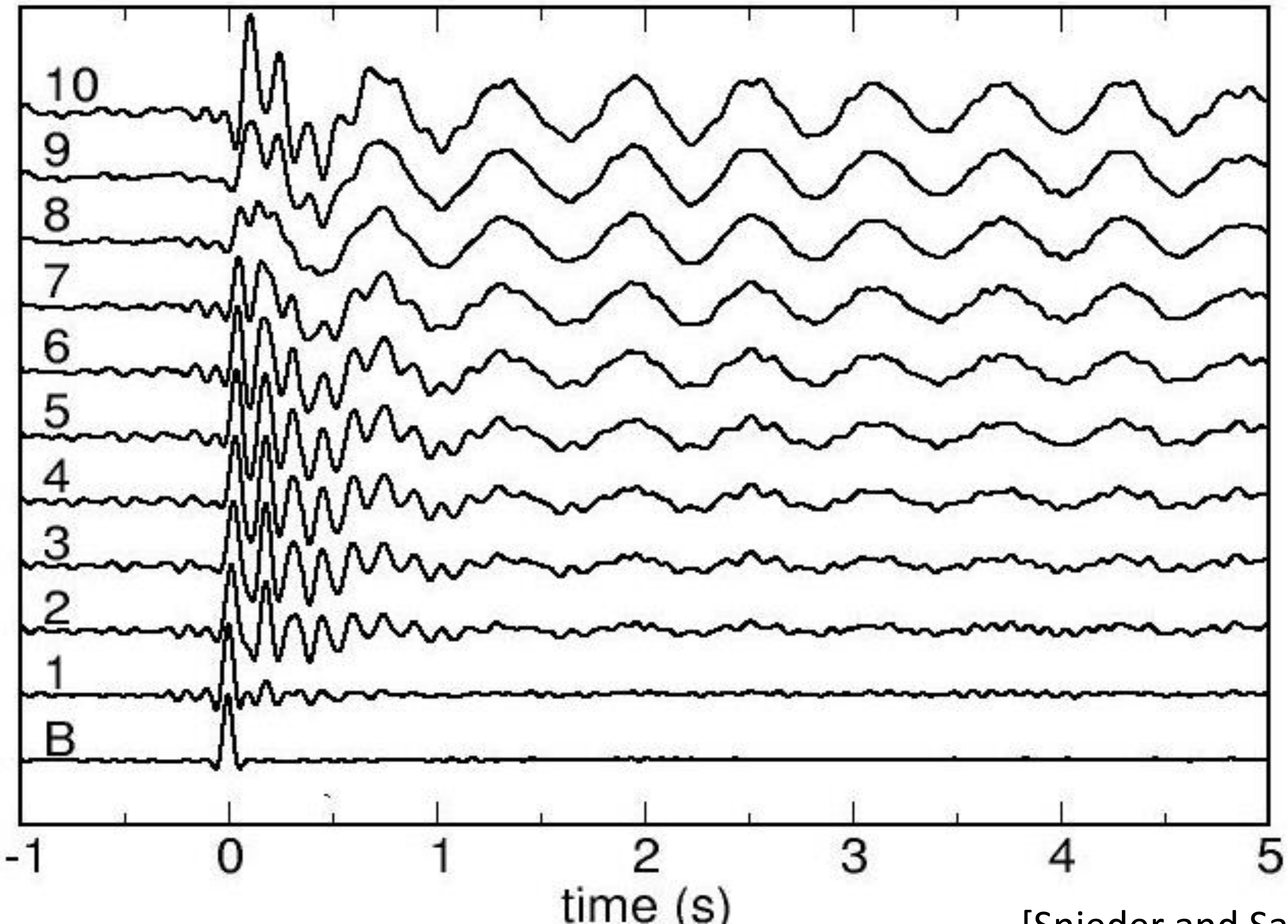

[Snieder and Safak, 2006]

Deconvolution with the bottom

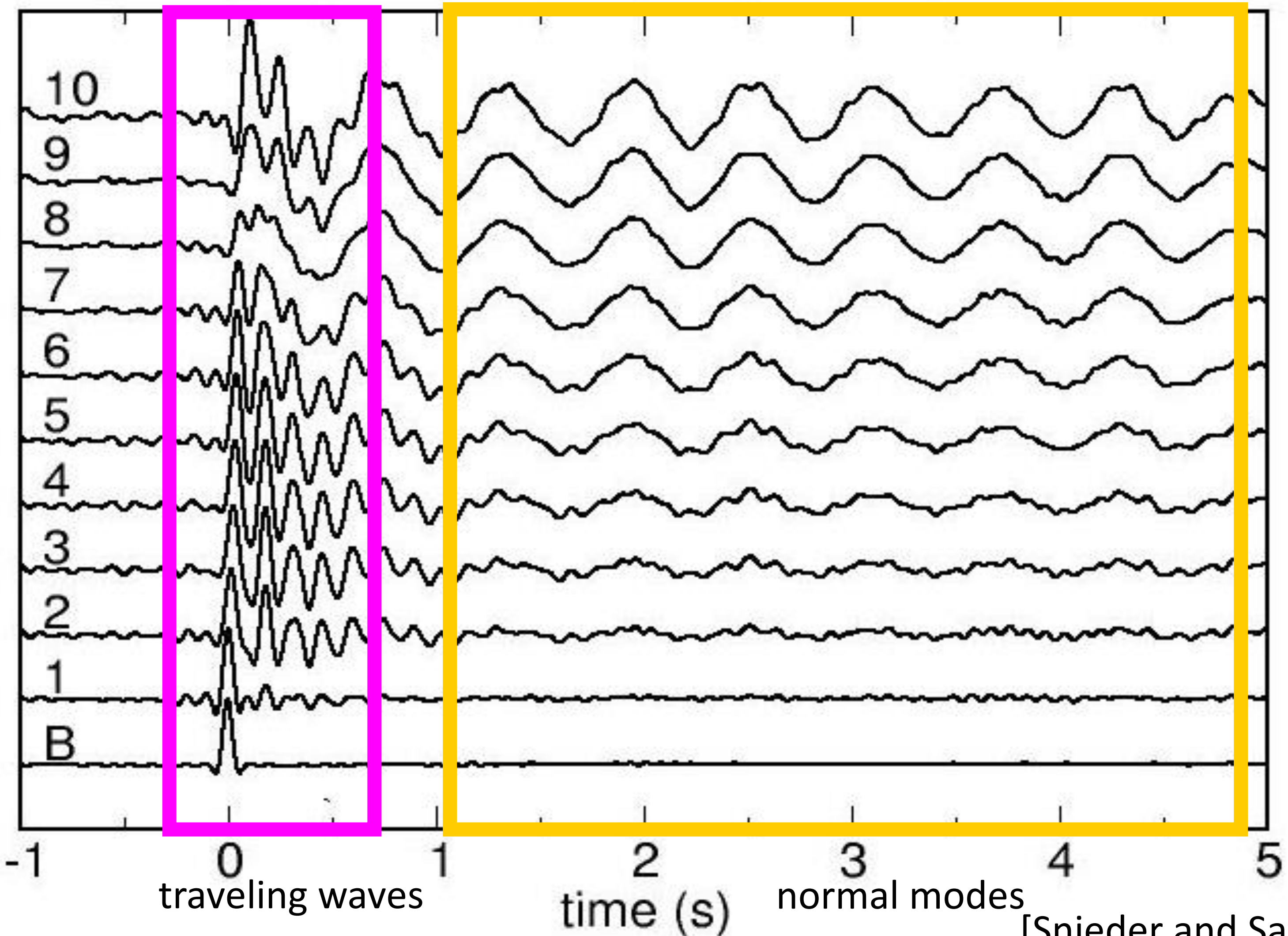

[Snieder and Safak, 2006]

Mode shapes – translational modes

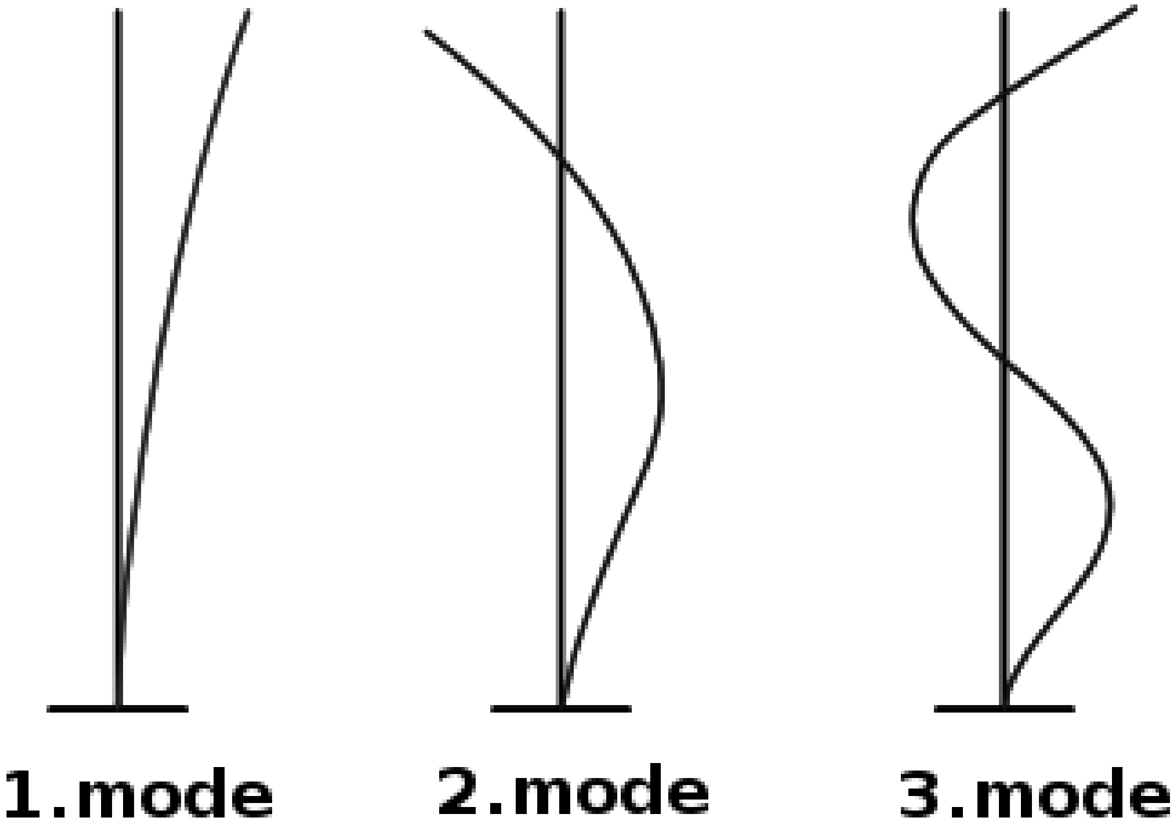

Earthquake recordings

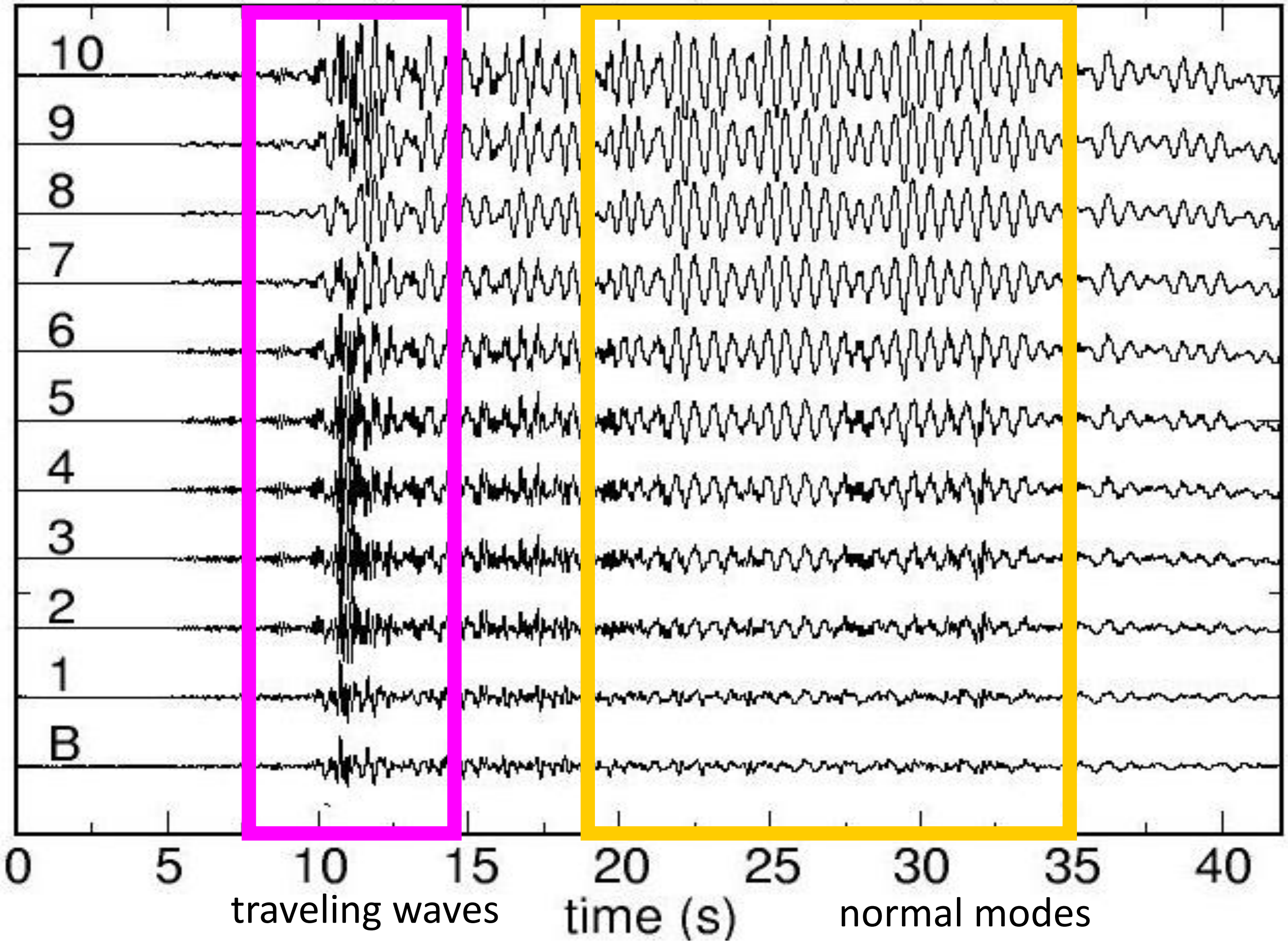

[Snieder and Safak, 2006]

Deconvolution with the bottom

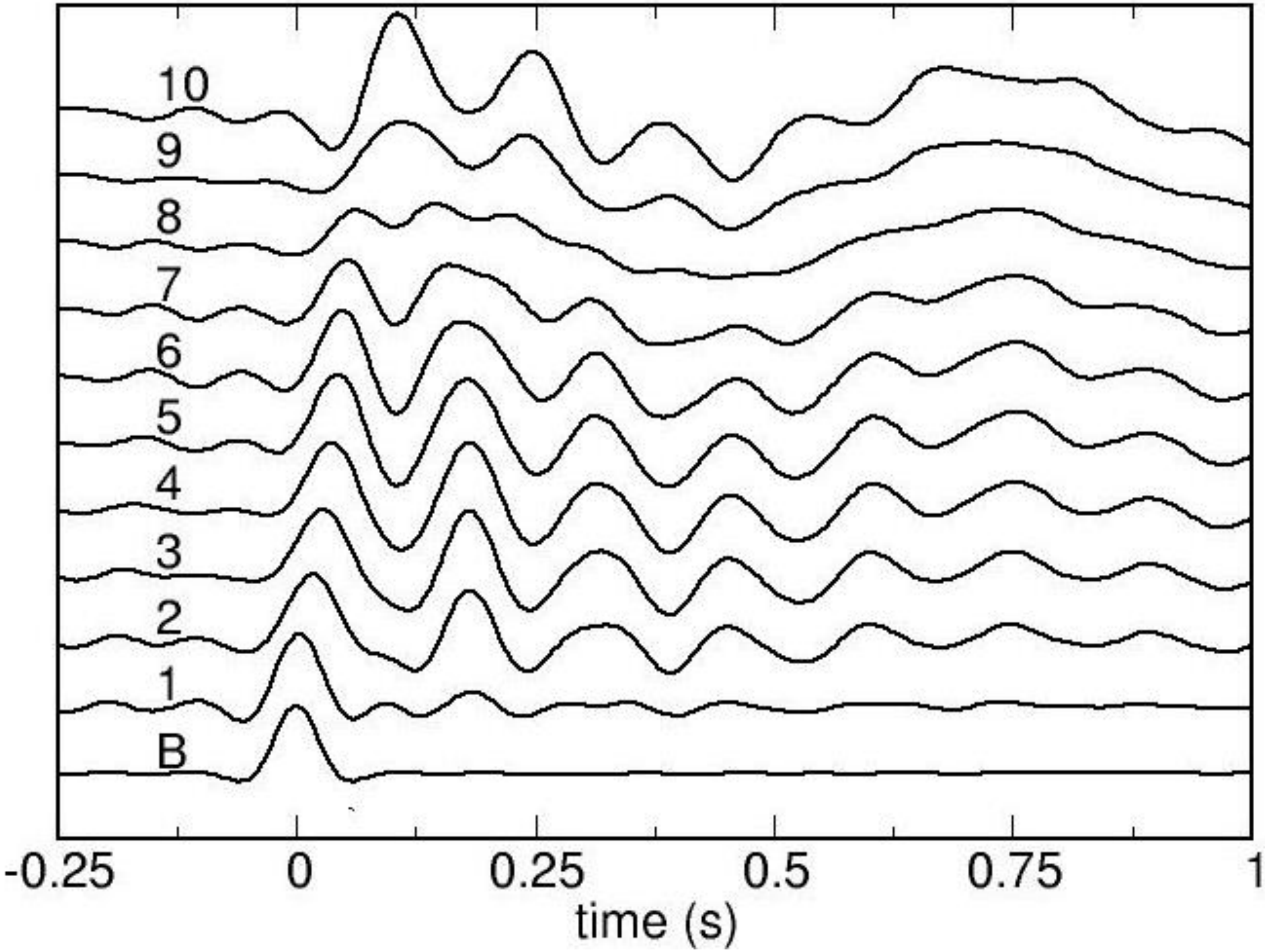

[Snieder and Safak, 2006]

Deconvolution with the bottom

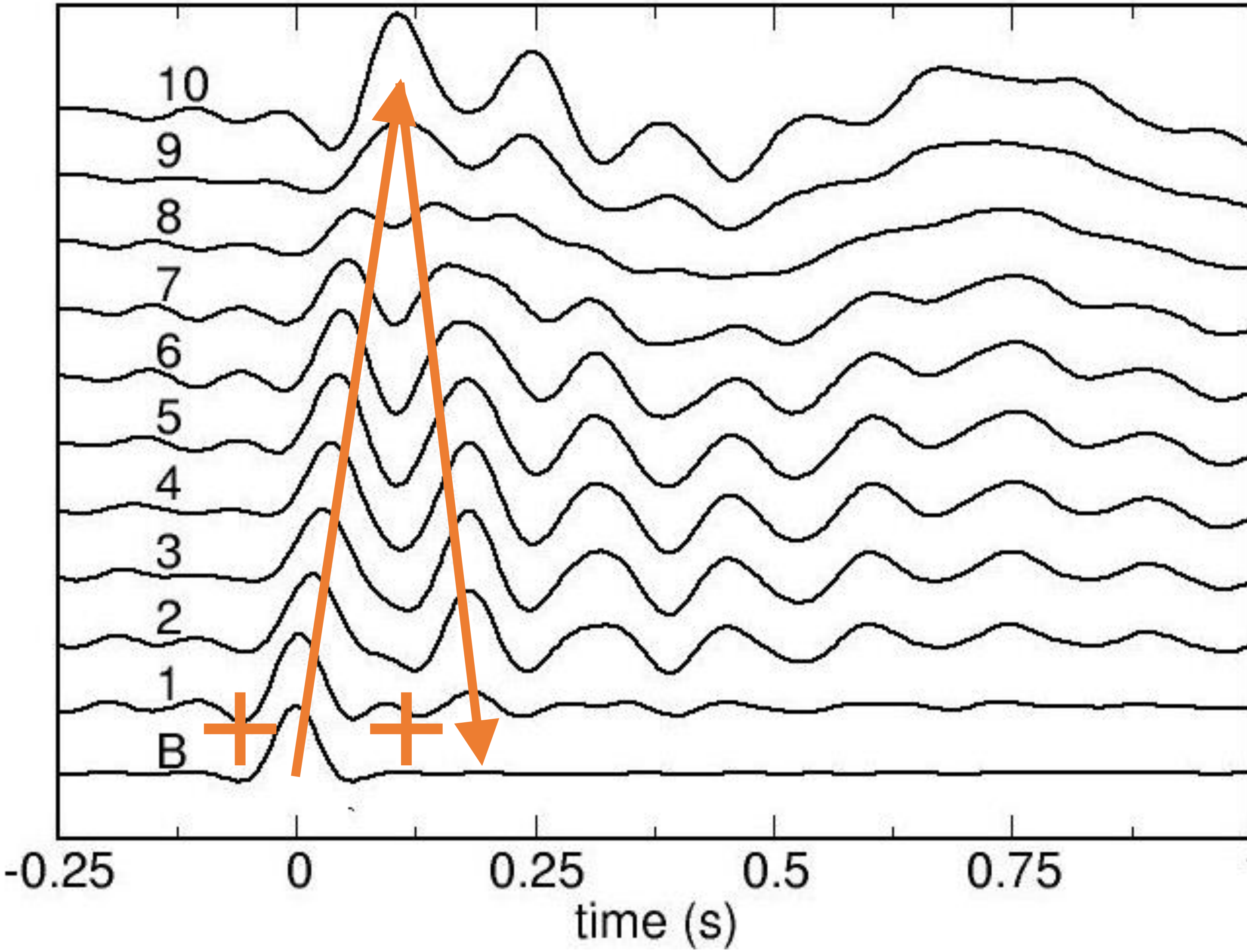

[Snieder and Safak, 2006]

Deconvolution with the bottom

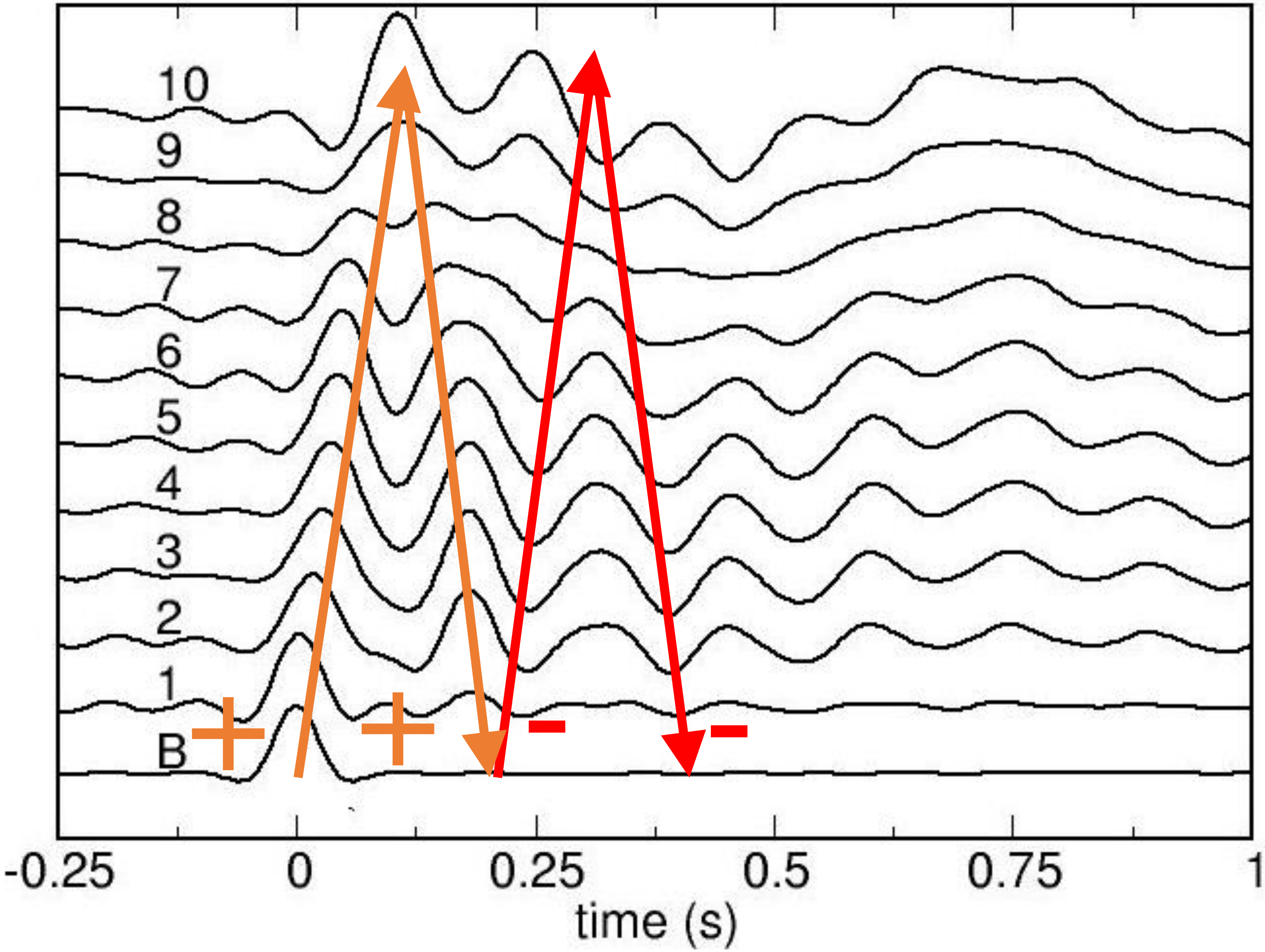

[Snieder and Safak, 2006]

Deconvolution with the bottom

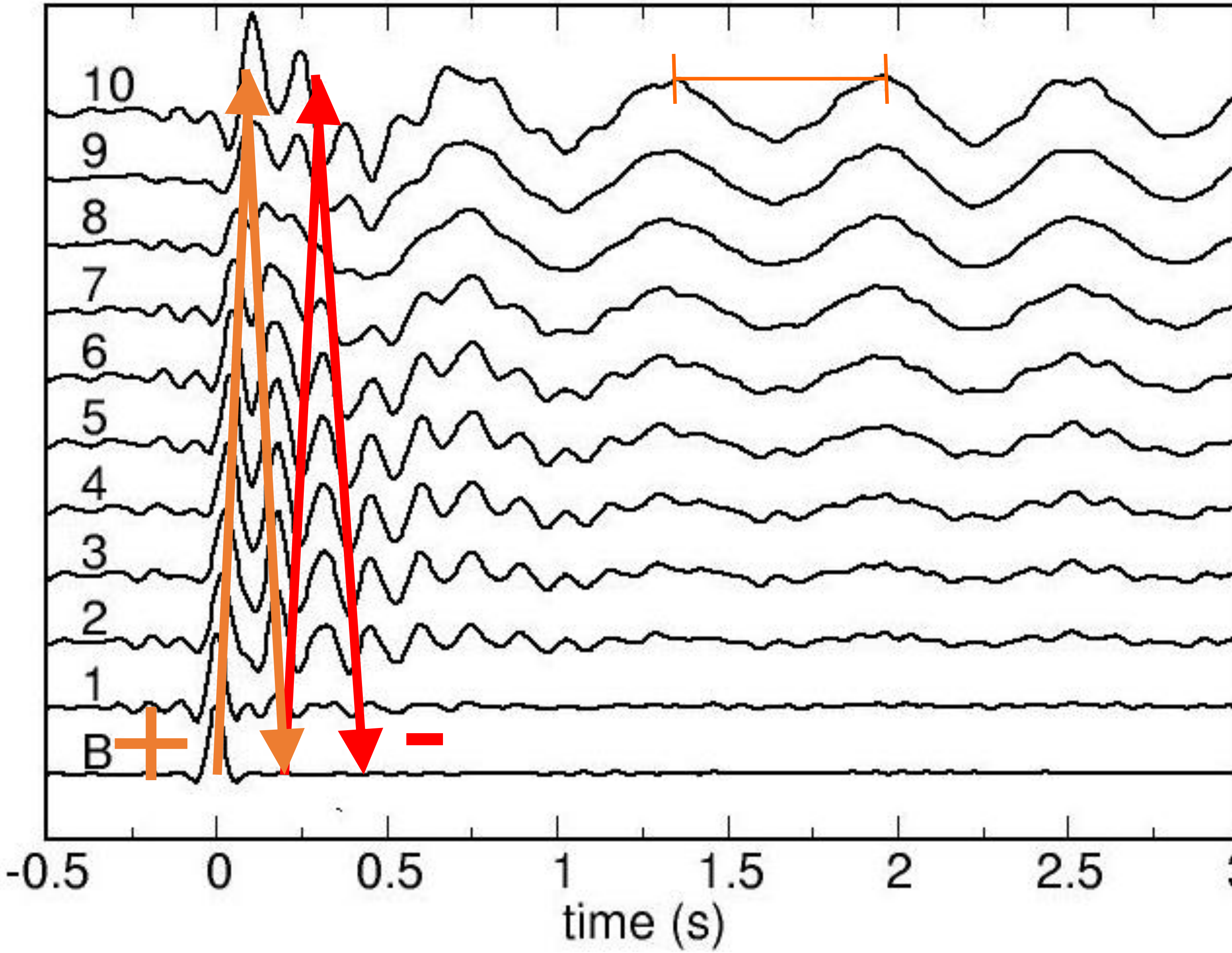

[Snieder and Safak, 2006]

Deconvolution with the bottom

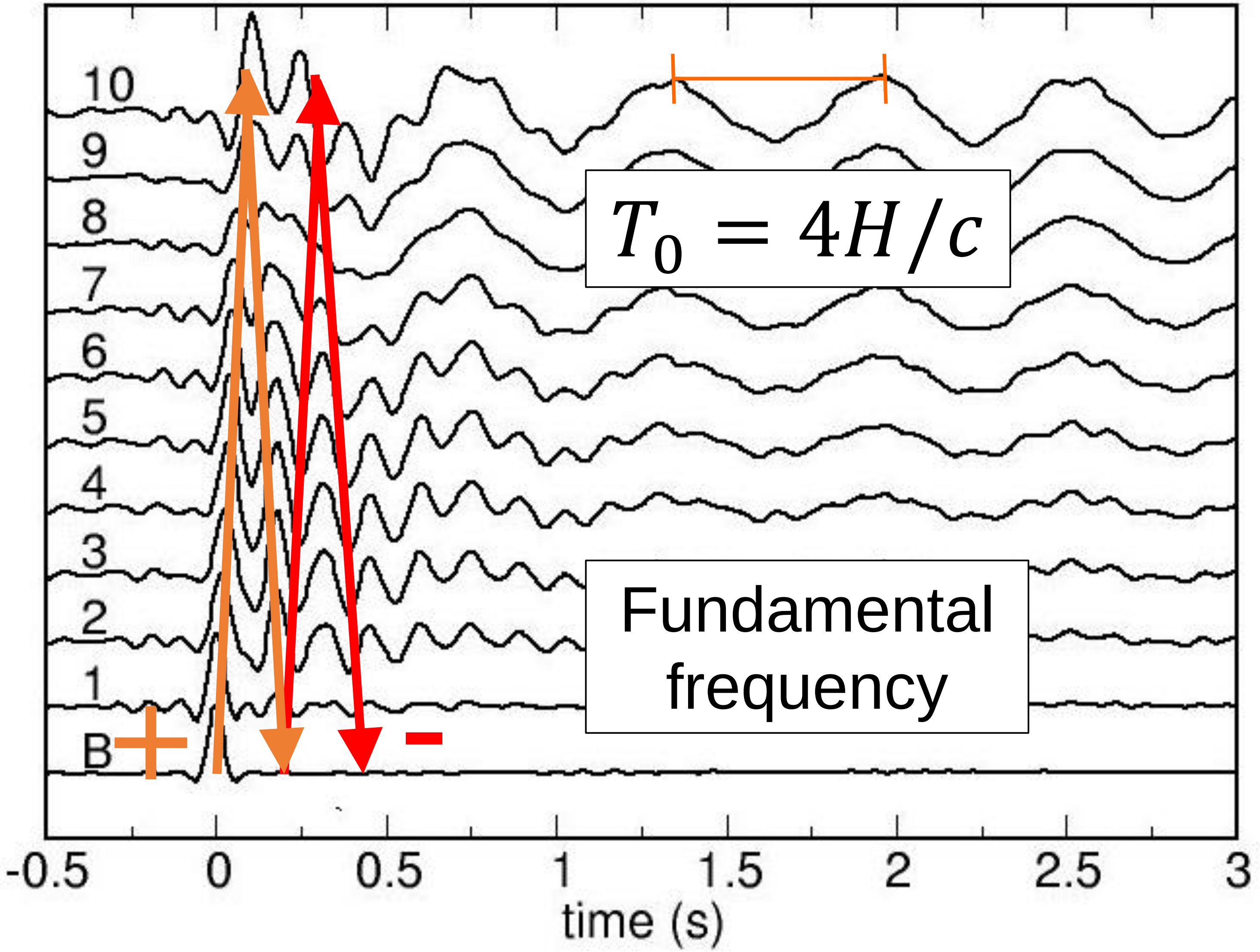

[Snieder and Safak, 2006]

Deconvolution with the bottom
Ambient vibration vs. earthquakes

Bishkek test-site
(GFZ, TU-Berlin, CAIAG)

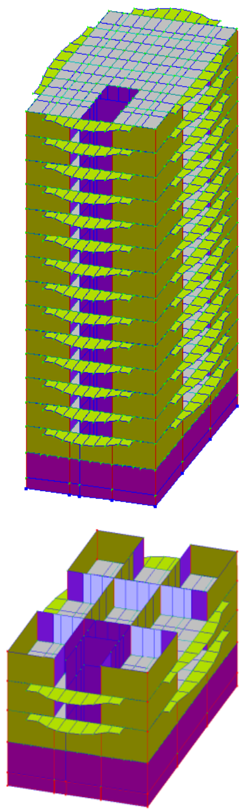

14-floor
RC frame with
masonry infill

Noise (Bishkek)

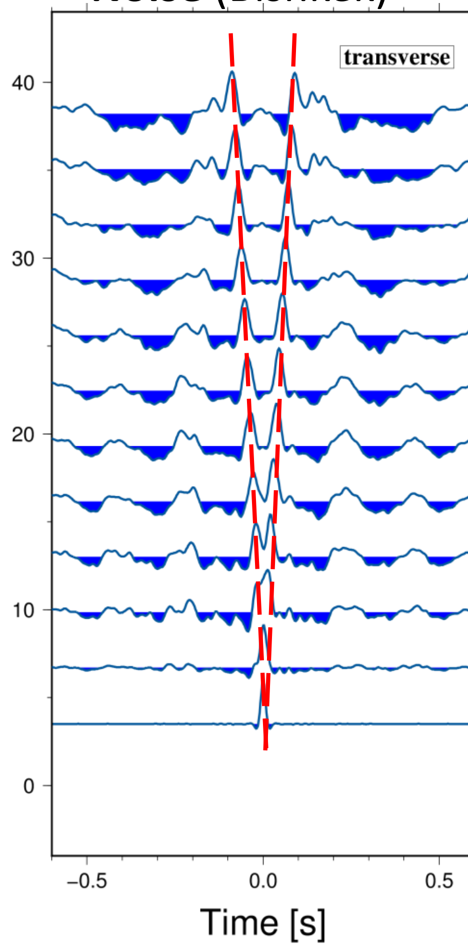

Earthquake (Milikan)

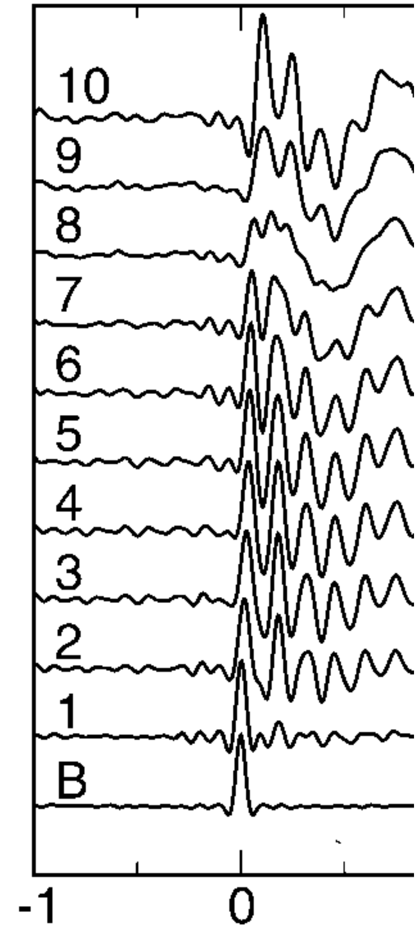

Seismic interferometry - Earthquakes

Velocity estimation

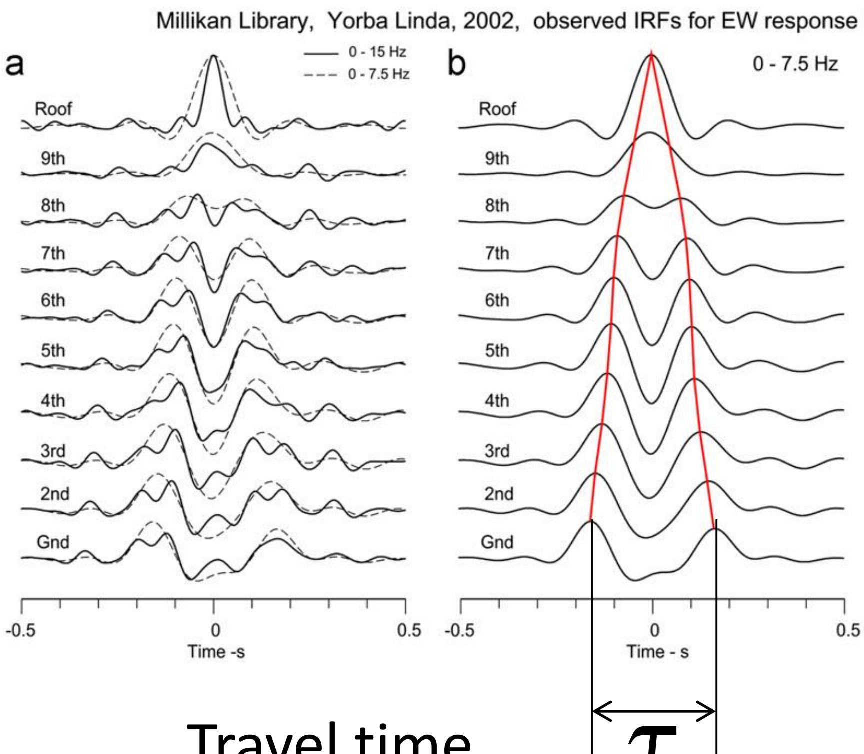

Travel time τ

Attenuation estimation

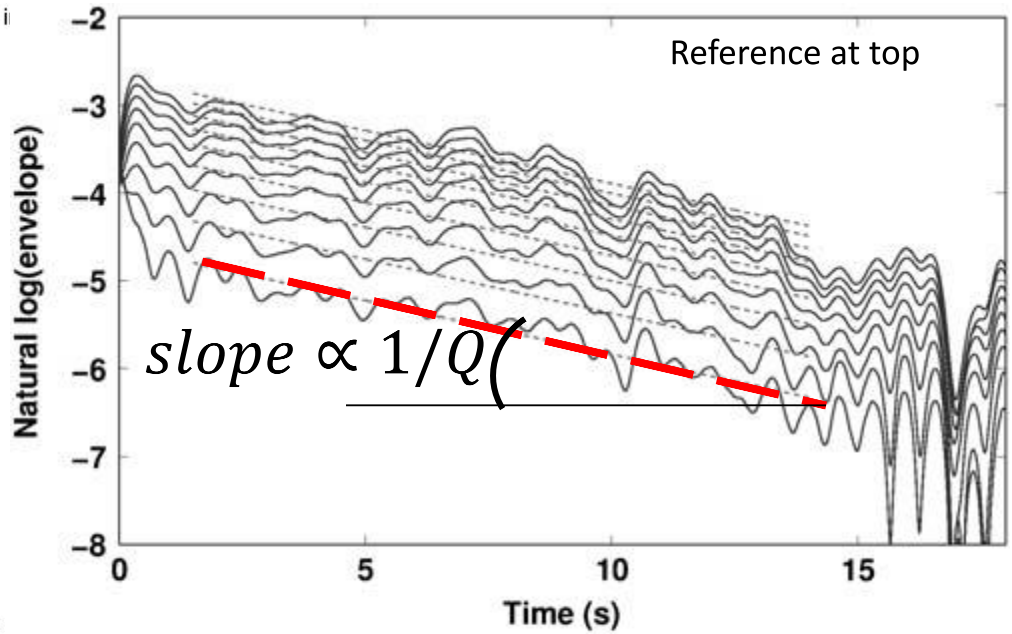

$\zeta = 1/2Q$

[e.g.Rahmani and Todorovska, 2013; Newton and Snieder, 2012]

Studies dealing with velocity in buildings
Deconvolution approach

The AHEPA hospital
in Thessaloniki, Greece

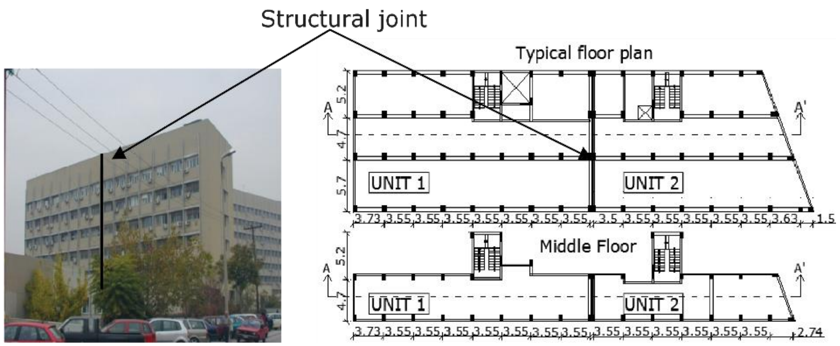

[Bindi et al. 2015]

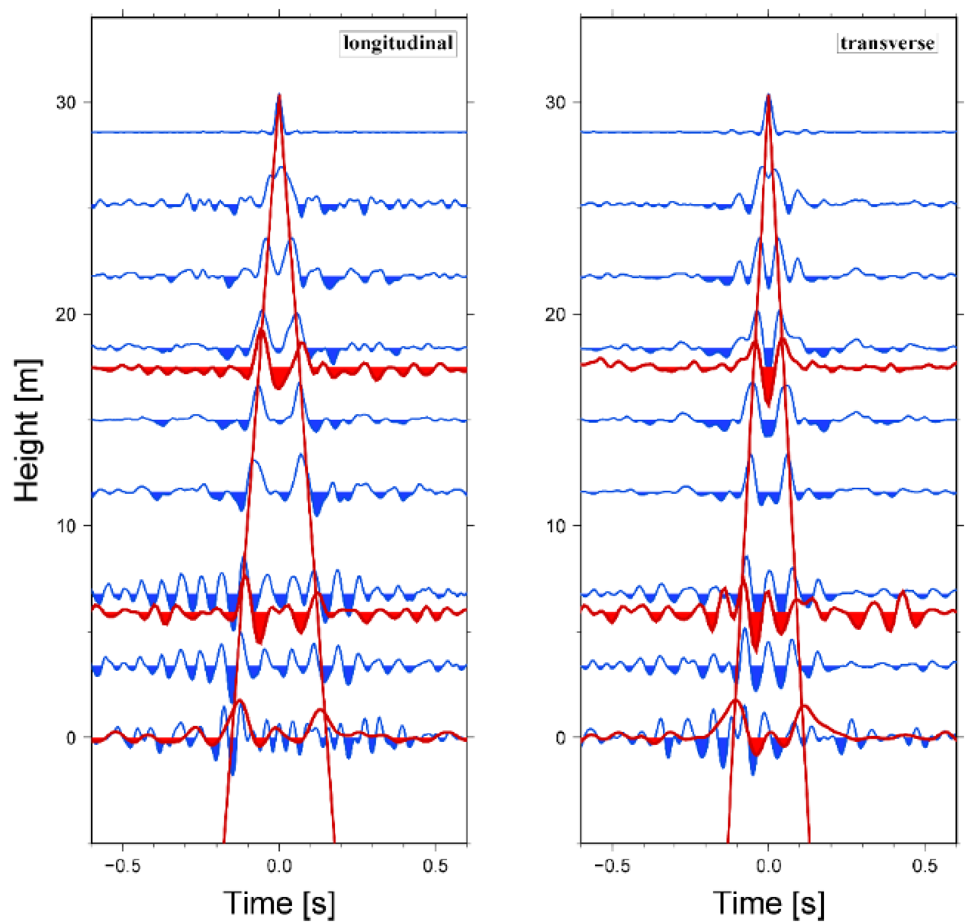

Ambient vibration

Earthquake recordings

[Bindi et al. 2015]

Studies dealing with velocity in buildings
Deconvolution approach

The B22 building

[Petrovic et al. 2017a]

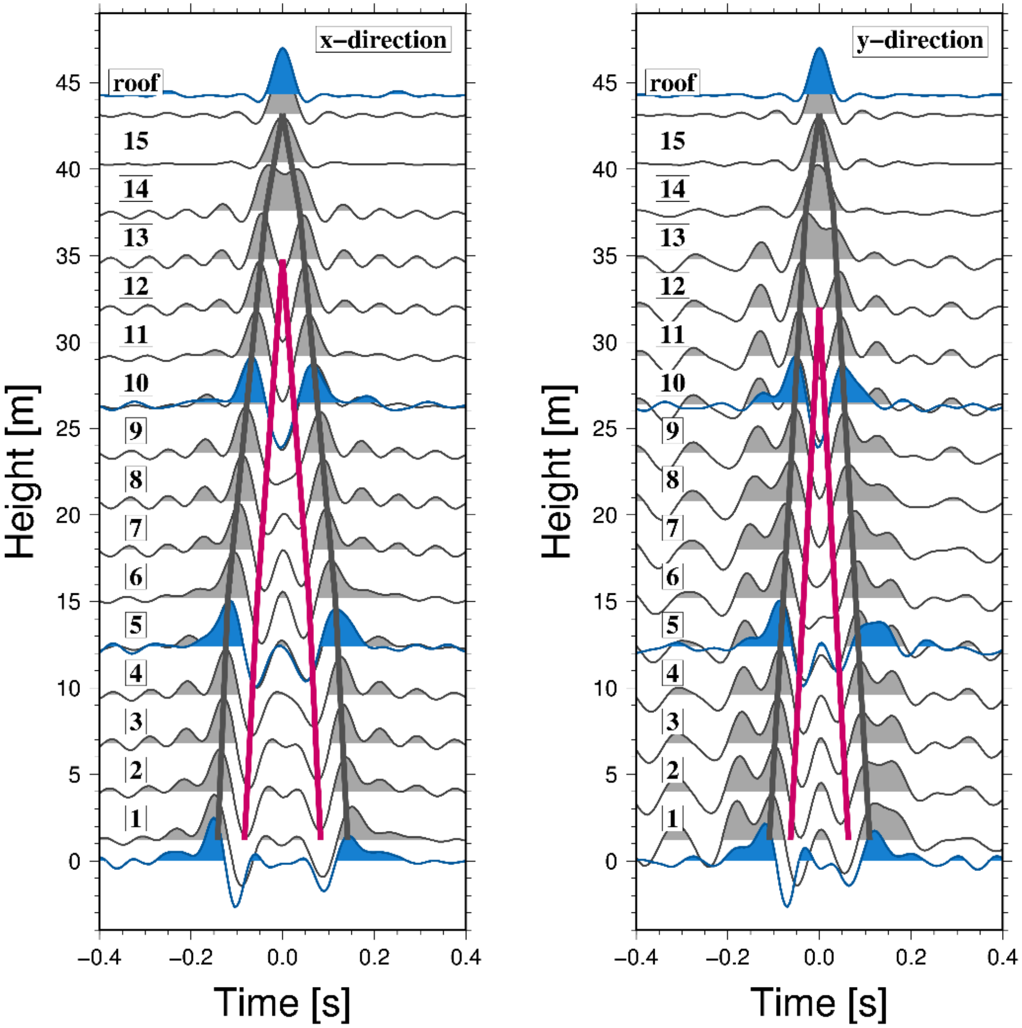

Studies dealing with velocity in buildings Deconvolution approach

The B22 building in Istanbul, Turkey

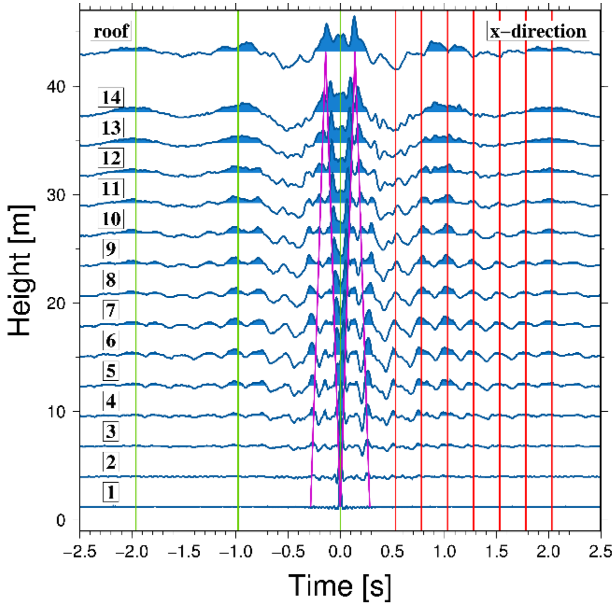

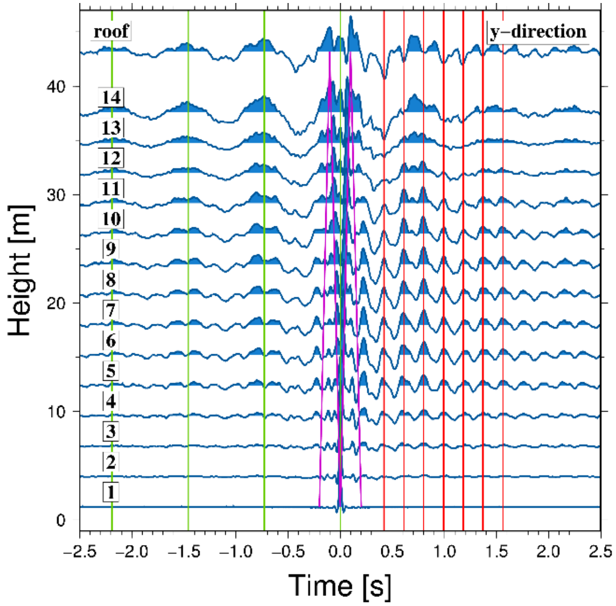

[Petrovic et al. 2017a]

Studies dealing with velocity in buildings Deconvolution approach

The B22 building in Istanbul, Turkey

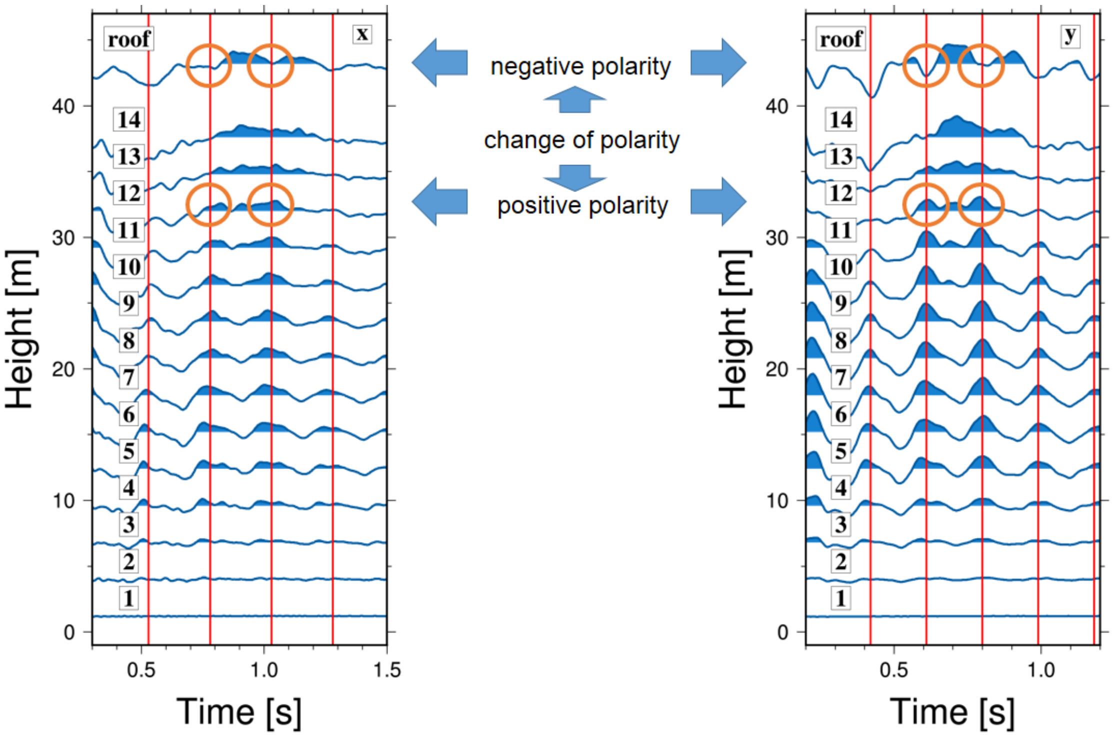

[Petrovic et al. 2017a]

Studies dealing with velocity in buildings
Deconvolution approach

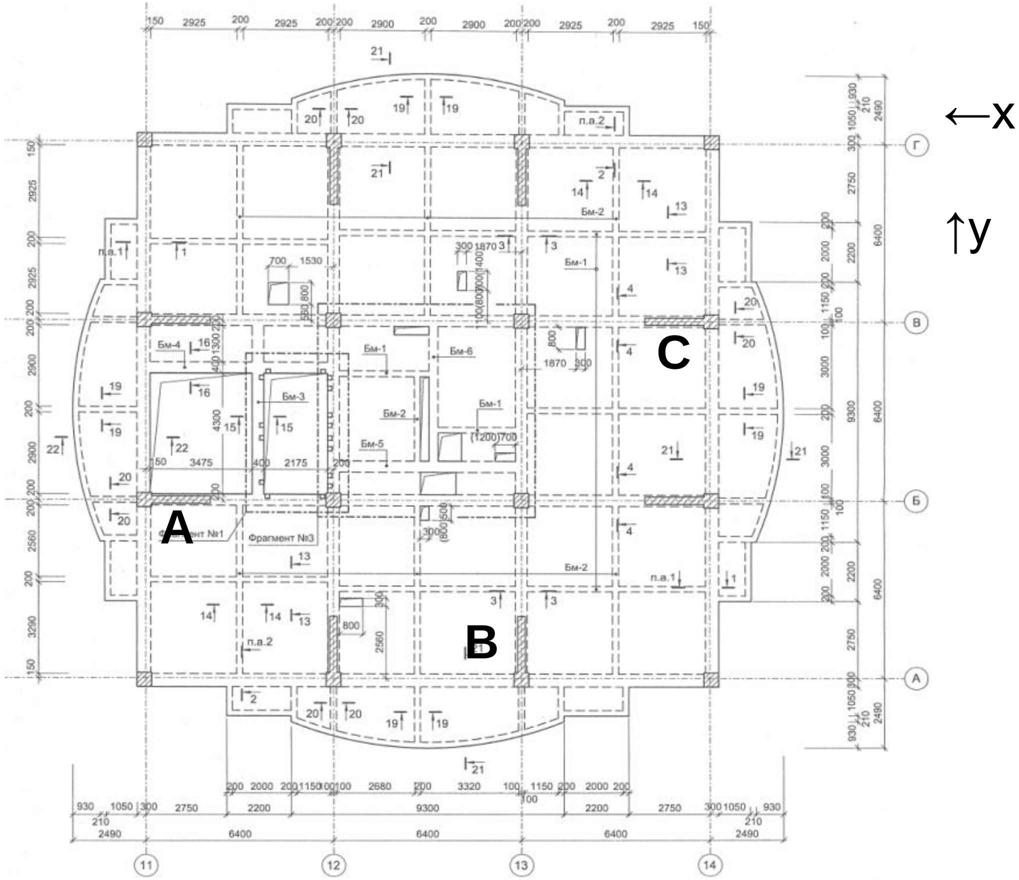

Deconvolution approach

Variation of shear wave velocity through the building at different points

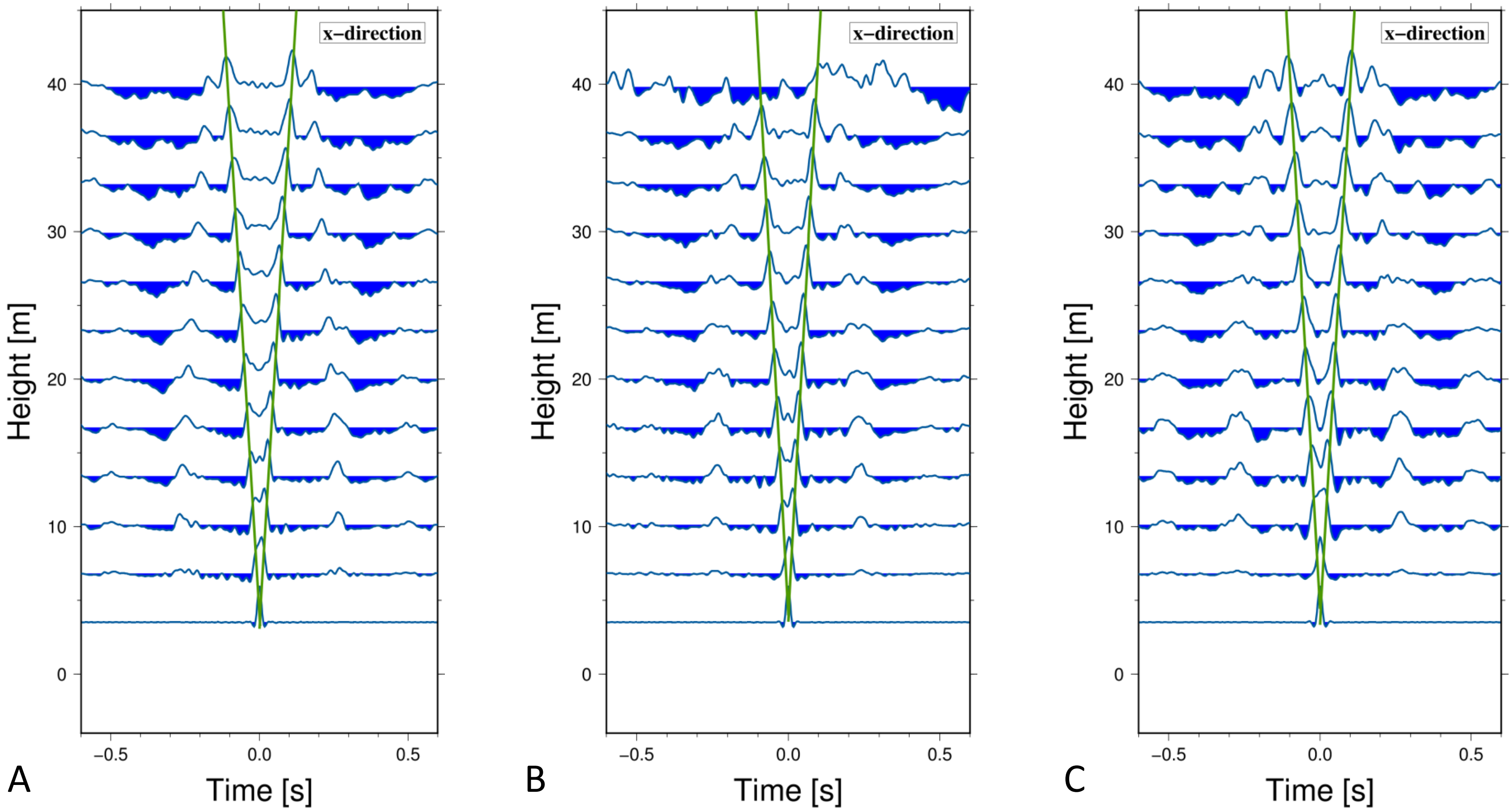

Deconvolution approach
Variation of shear wave velocity through the building at different points

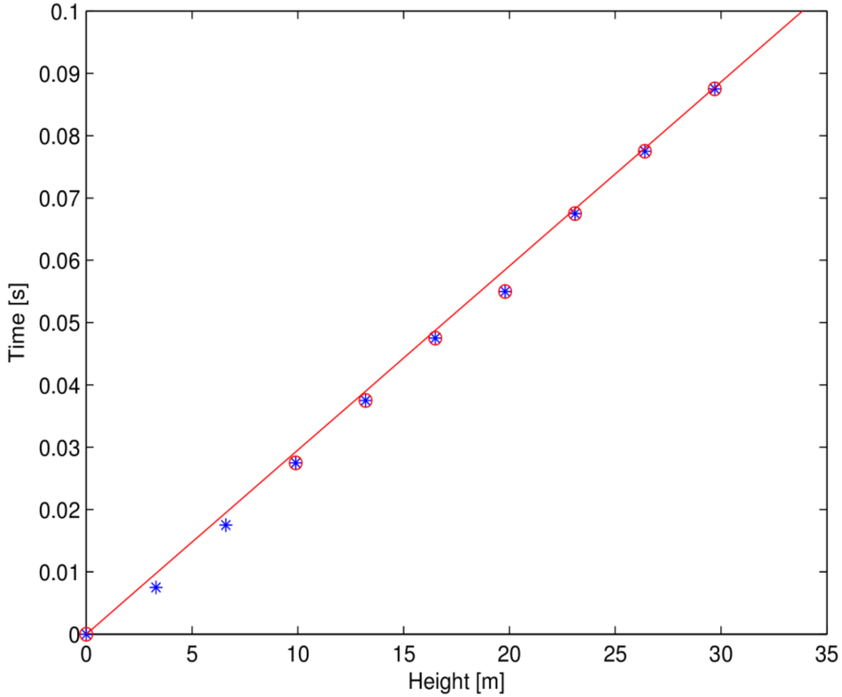

X direction

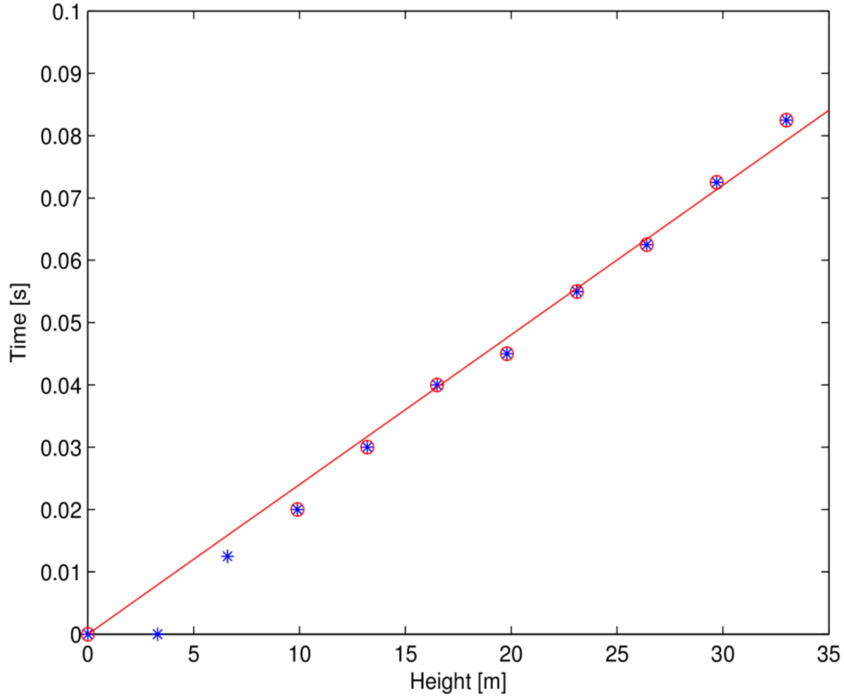

Y direction

Deconvolution approach
Variation of shear wave velocity through the building at different points

	V_x in m/s	v_y in m/s
A	338±5	416±6
B	386±4	426±6
C	364±3	413±3

How can we exploit seismic interferometry for damage detection?

Global: Changes in total travel time is related to changes in the fundamental frequency (level1)

Local: look for changes in travel time between different floors or block of floors (level 2)

Local: quantify changes in velocities as changes in stiffness (level 3)

Seismic Interferometry -Damage

Global: Changes in total travel time can be related to changes in the fundamental frequency that can be related to damages (level1)

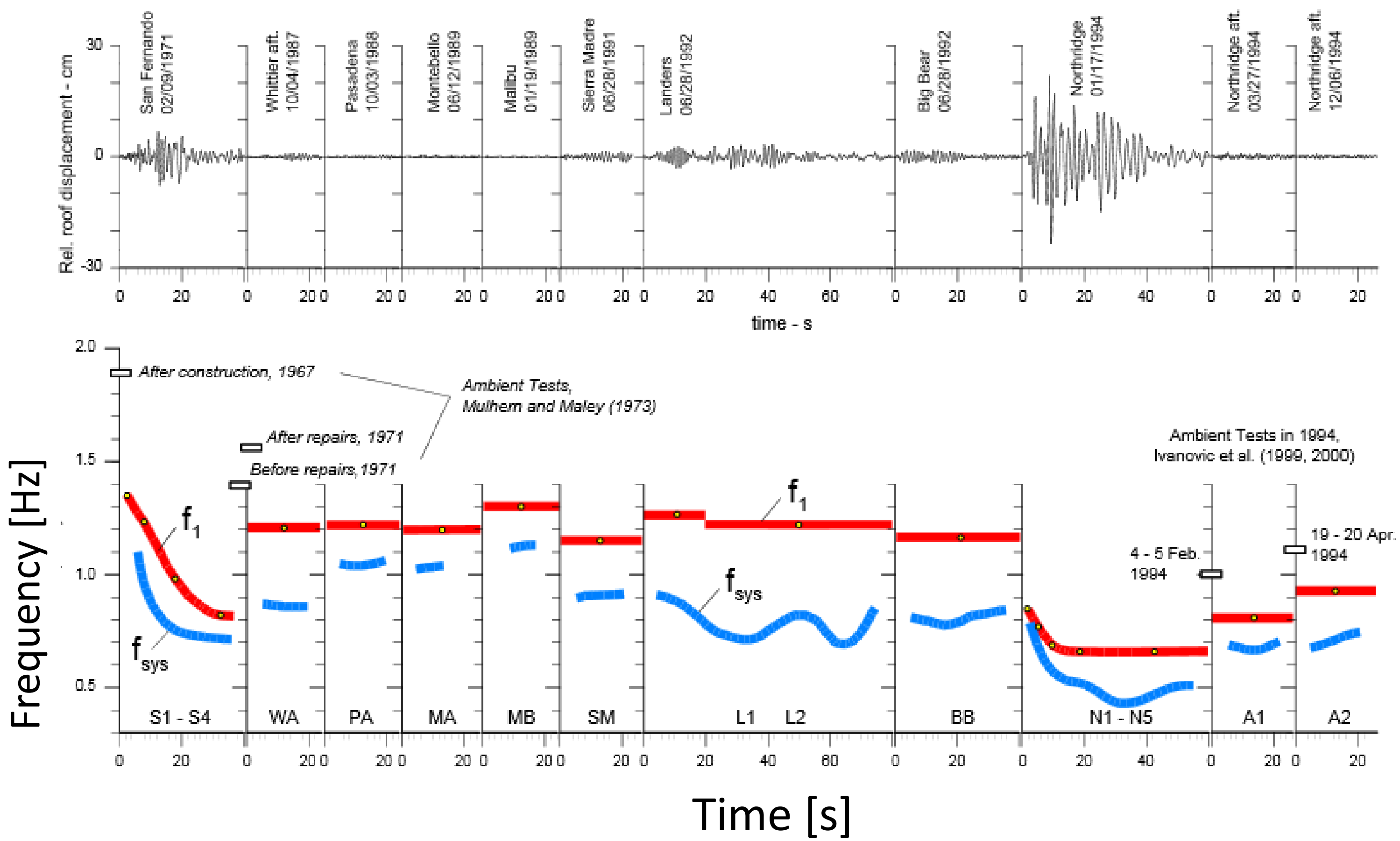

[Todorovska and Trifunac, 2008b]

Seismic Interferometry -Damage

Local: Changes in total travel time between floors (level 2)

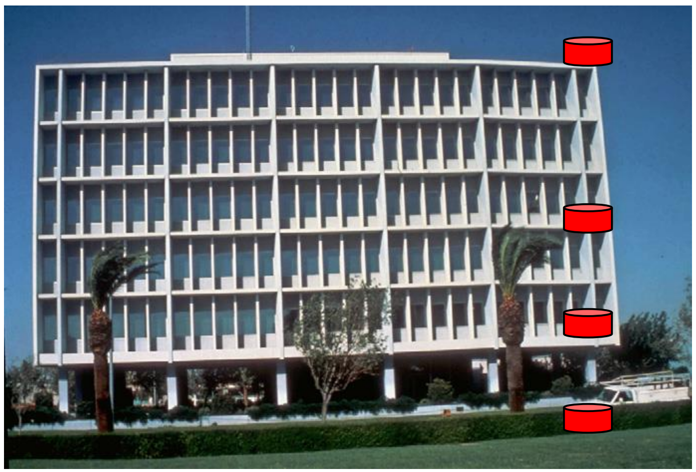

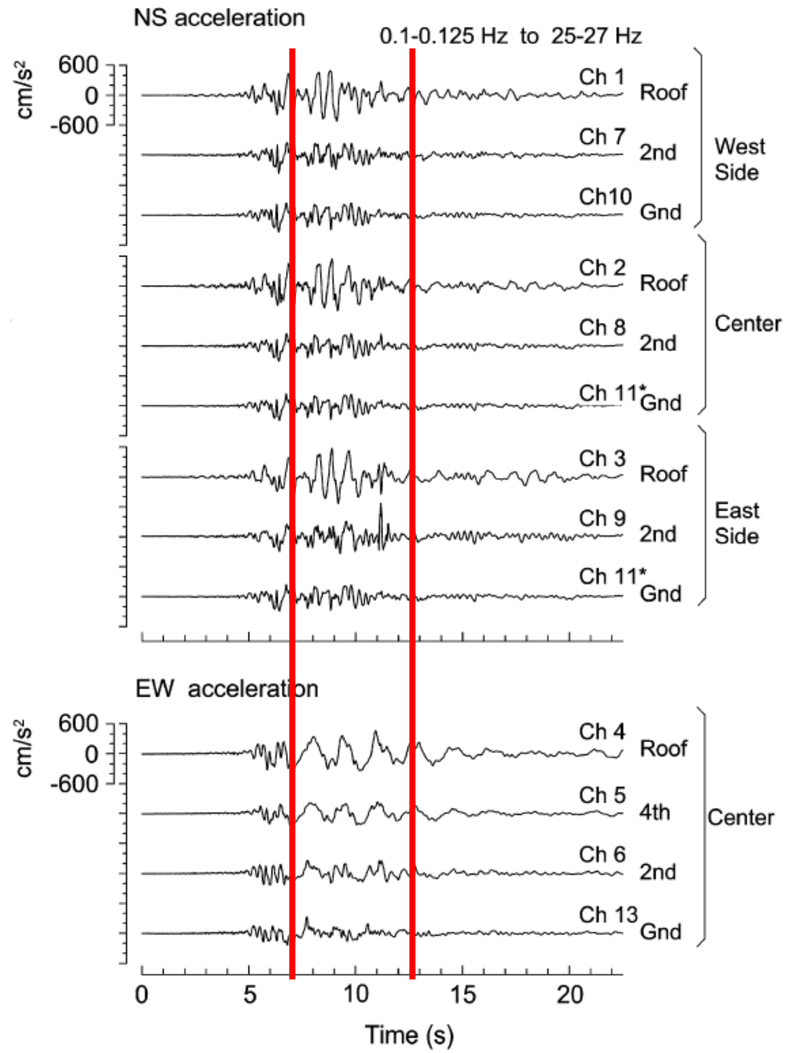

ICS building damaged by the 1979 Imperial valley Mw 6.6 earthquake

[Todorovska and Trifunac, 2007, 2008a]

Seismic Interferometry -Damage

Local: Changes in total travel time between floors (level 2)

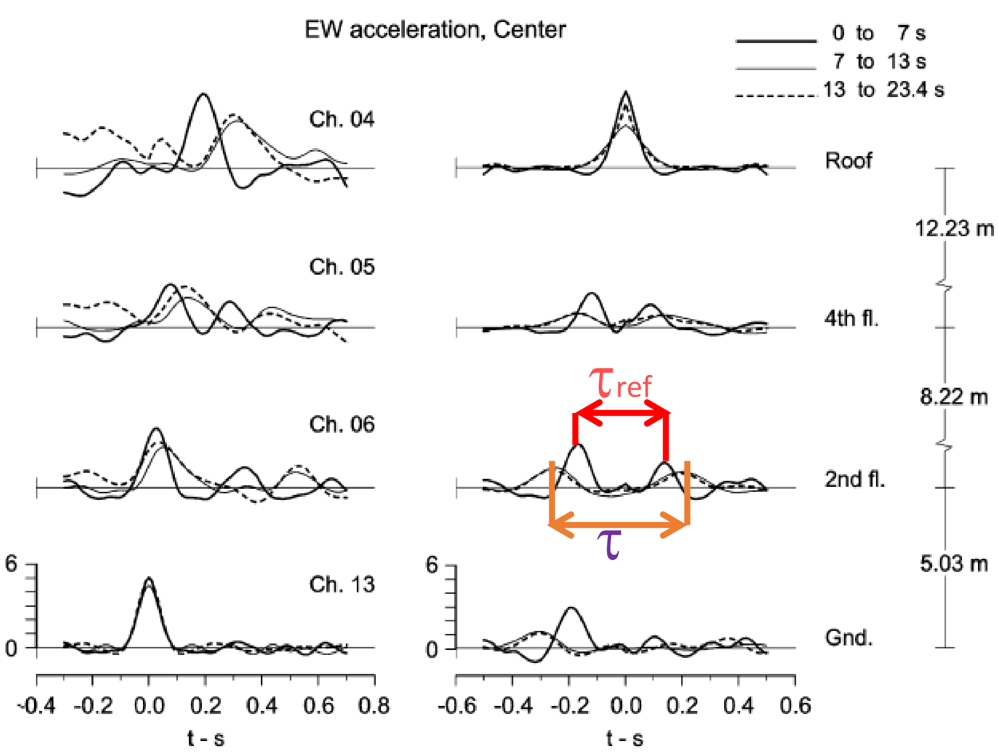

$$\mu \propto v^2$$

$$\Delta v_i / v_{ref} = \left(v_i - v_{ref}\right) / v_{ref} = \tau_{ref} / \tau_i - 1$$

$$\Delta \mu_i / \mu_{ref} = \left(\tau_{ref} / \tau_i\right)^2 - 1$$

[Todorovska and Trifunac, 2008a]

Studies on non-linearity during strong motion earthquakes

Combined Stockwell Transform and deconvolution approach

Local Spectra S(*t*,*f*) + Green's Function

Local Green's Functions

The time lag at each time of shaking motion

Instantaneous shear wave velocity

$$v_s(t) = \frac{H}{\sum_{i=1}^{N} \frac{D_i}{v_i}} = \frac{H}{\frac{D_1}{v_{s_1}} + \frac{D_2}{v_{s_2}}}$$

Time trend of fixed-base frequency

$$f_1(t) = \frac{v_s(t)}{4H}$$

[Pianese et al. 2018]

Studies on non-linearity during strong motion earthquakes

Event 1995- M_w=7.5-PGA=37cm/s^2 DAMAGE OBSERVED

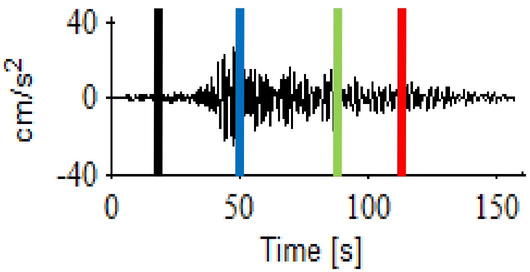

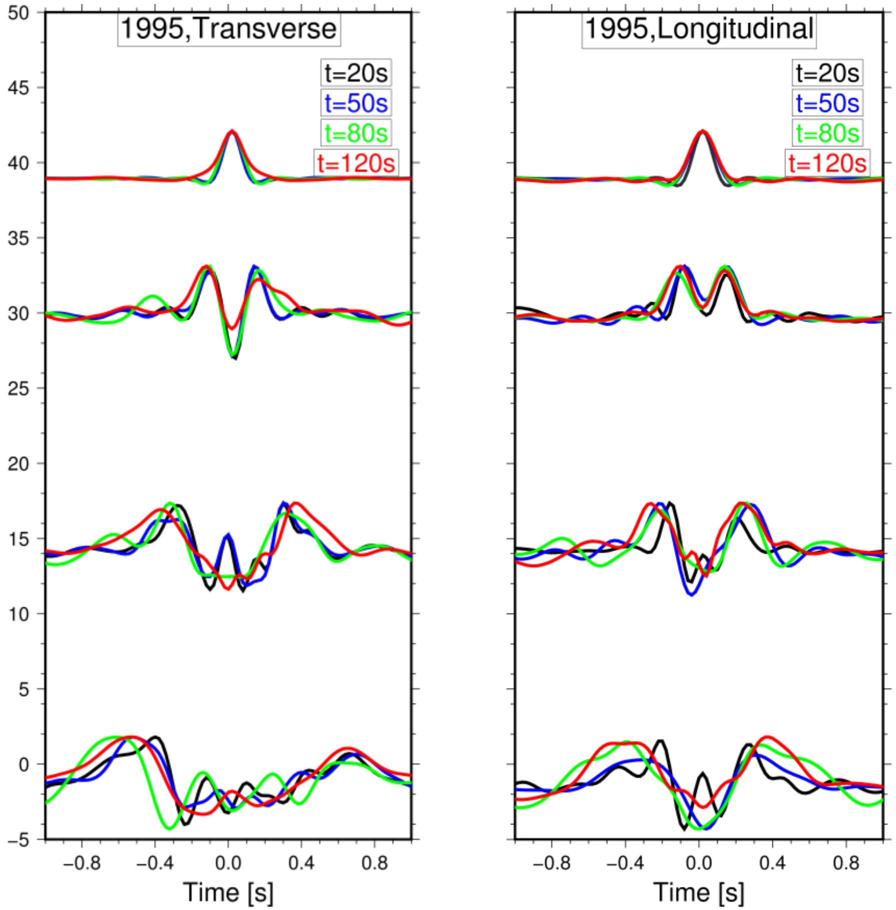

t_{20}=0.19s
t_{160}=0.26s
36%

t_{20}=0.25s
t_{160}=0.35s
39%

[Pianese et al. 2018]

Studies on non-linearity during strong motion earthquakes

Time variation of fixed-base frequency $f_1(t)$, event 1995 – damage observed

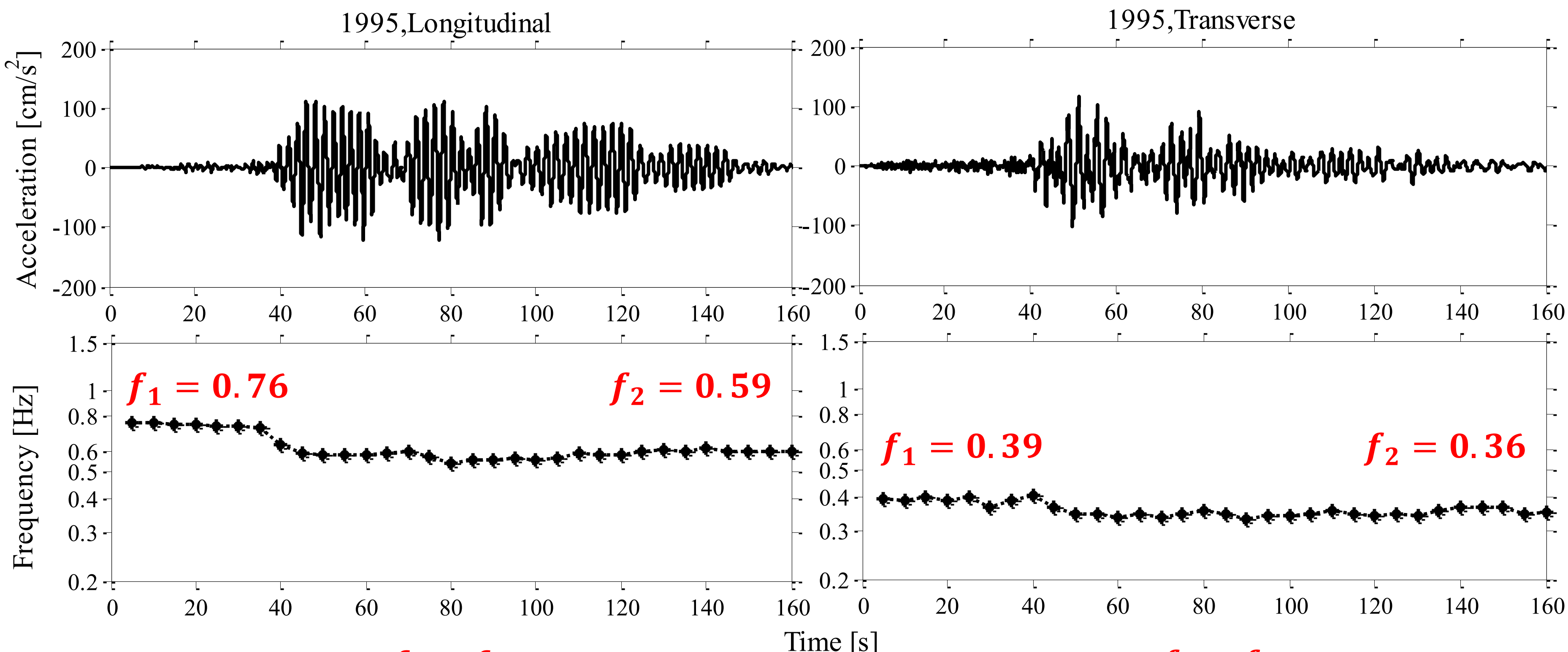

$$\Delta f/f_1 = \frac{f_2 - f_1}{f_1} = -22\%$$

$$\Delta f/f_1 = \frac{f_2 - f_1}{f_1} = -7\%$$

non-linear response of Jalapa building

[Pianese et al. 2018]

Studies on non-linearity during strong motion earthquakes

Event 1993- M_w=6-PGA=8cm/s^2 NO VISIBLE DAMAGE

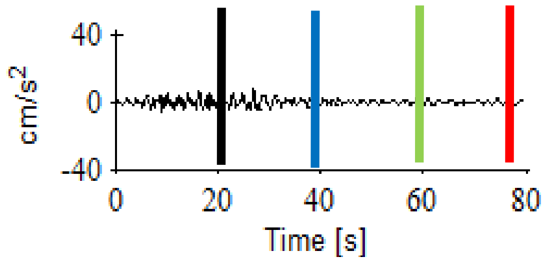

t_{20}=0.28s
t_{80}=0.31s
9%

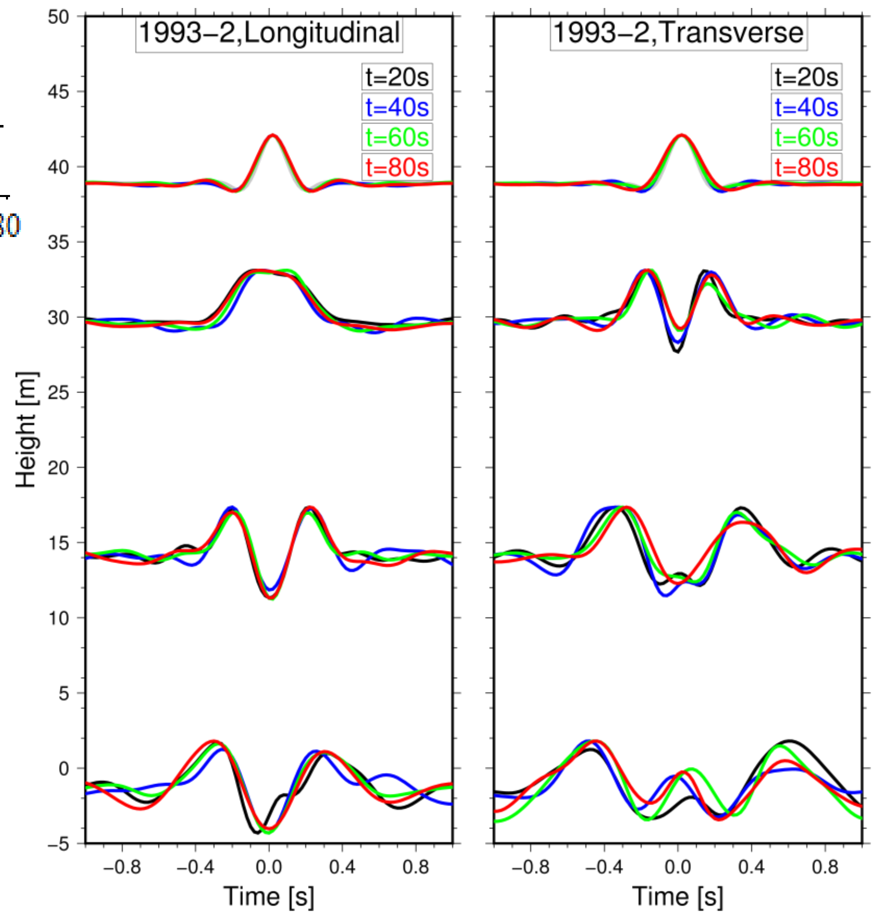

t_{20}=0.56s
t_{80}=0.58s
4%

[Pianese et al. 2018]

Studies on non-linearity during strong motion earthquakes

Time variation of fixed-base frequency $f_1(t)$, event 1993 – no visible damage

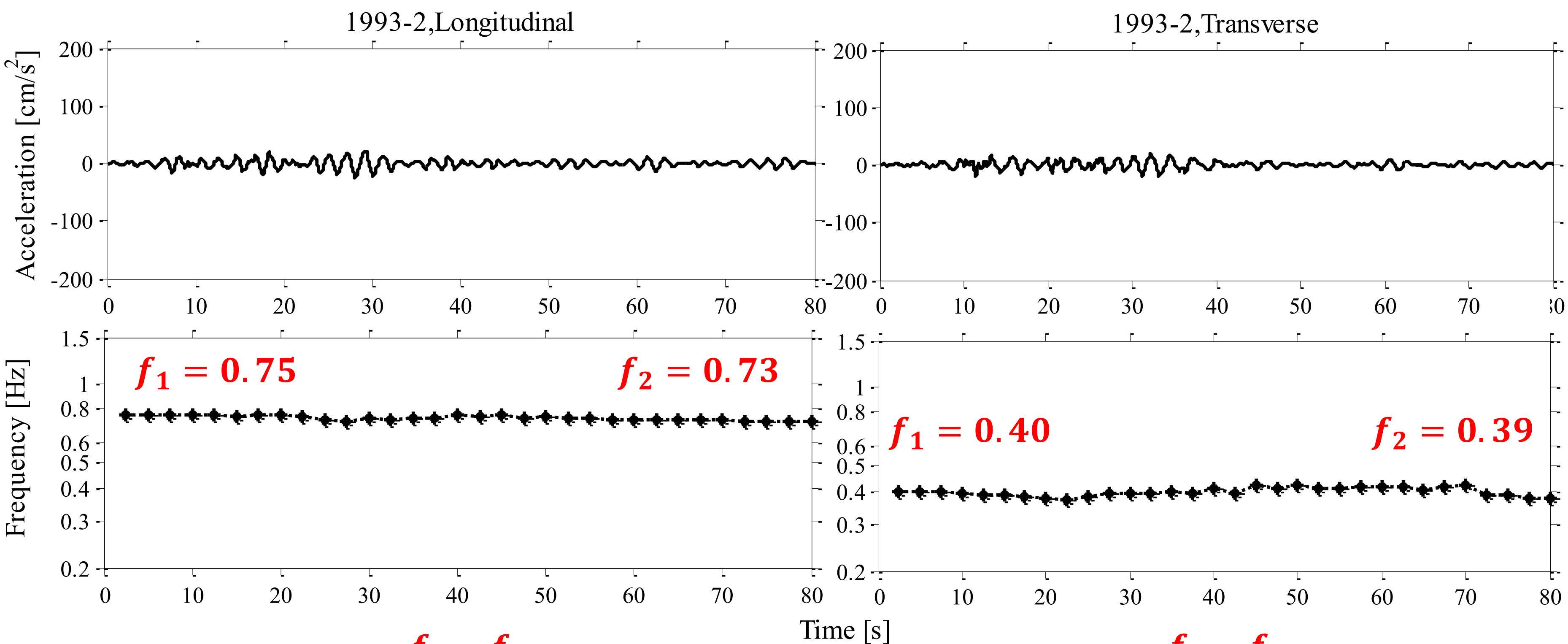

$$\Delta f/f_1 = \frac{f_2 - f_1}{f_1} = -4\%$$

$$\Delta f/f_1 = \frac{f_2 - f_1}{f_1} = -3\%$$

linear response of Jalapa building

[Pianese et al. 2018]

Studying soil-structure interaction effects

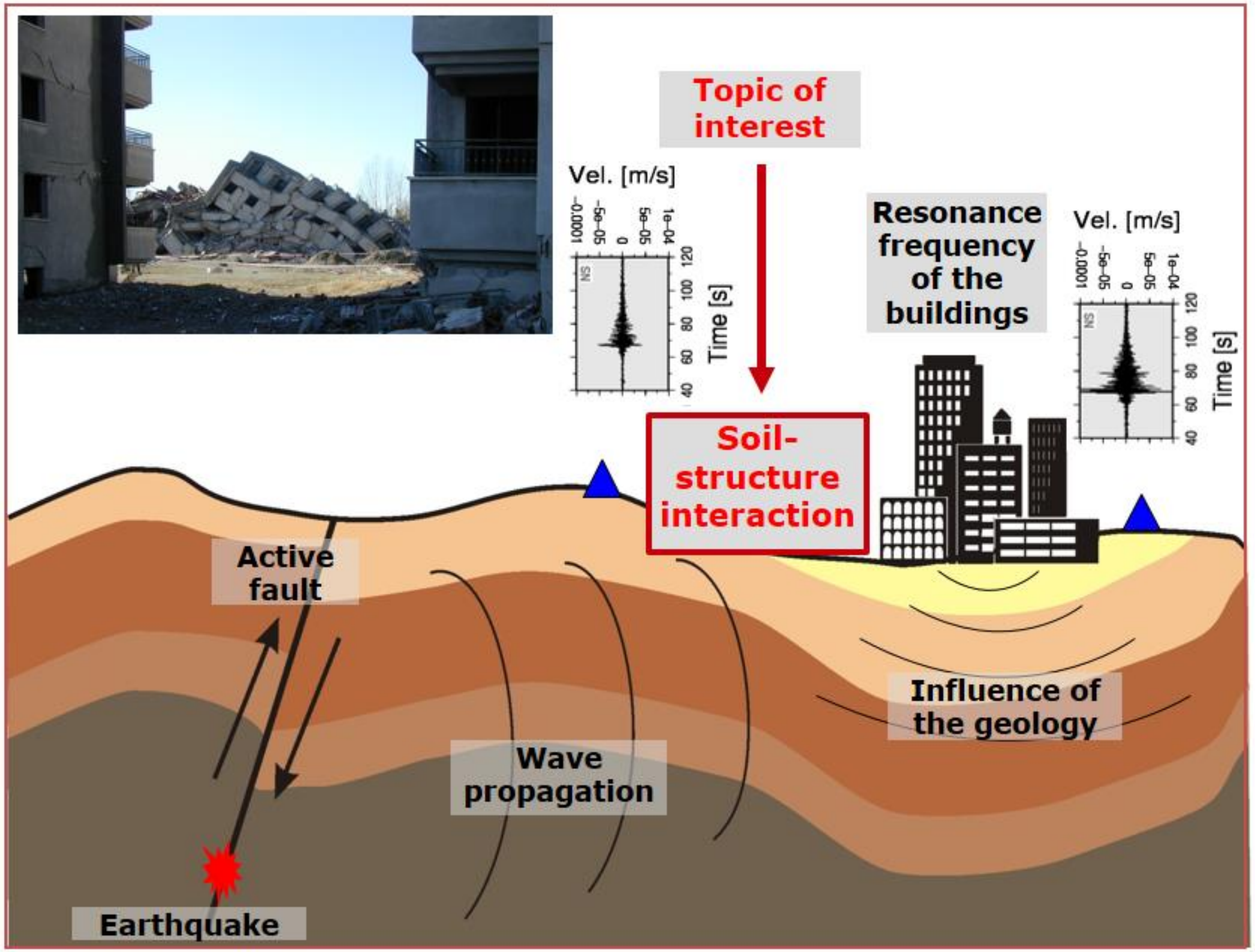

Studying soil-structure and site-city interaction effects using numerical simulations

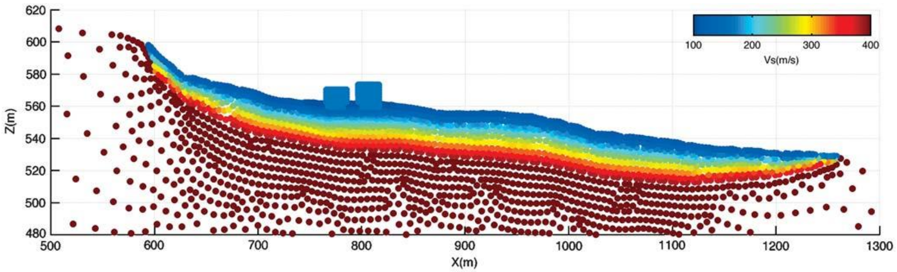

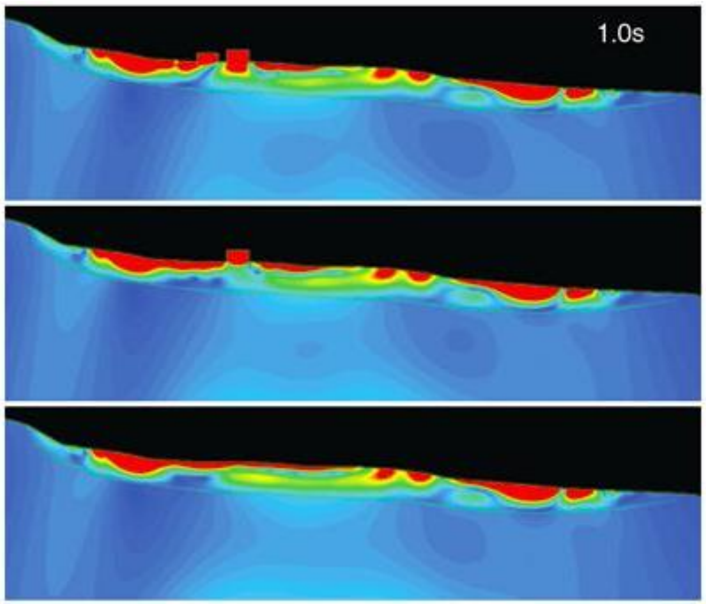

[Laurenzano et al., 2010]

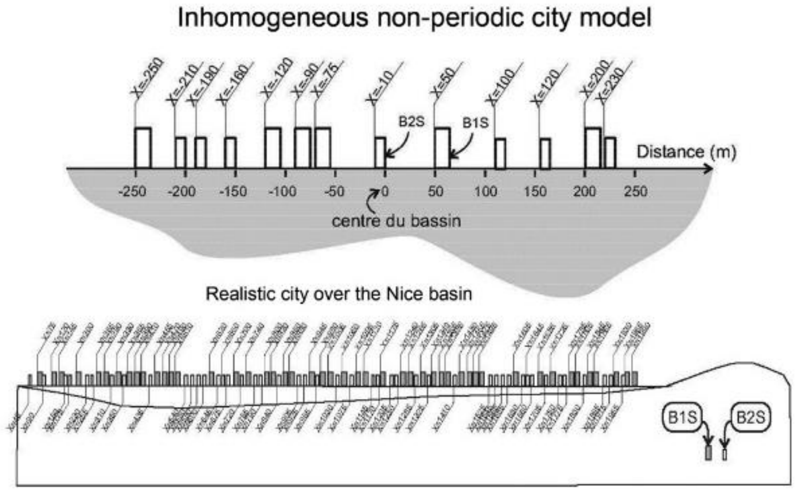

[Bard et al., 2008]

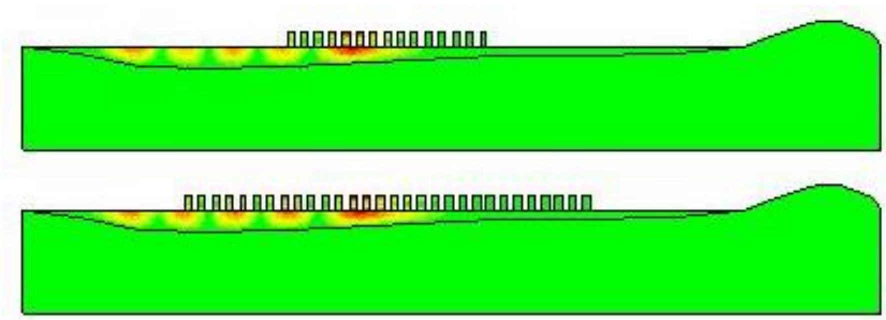

[Semblat et al., 2009]

Aim: Better understanding the wave propagation

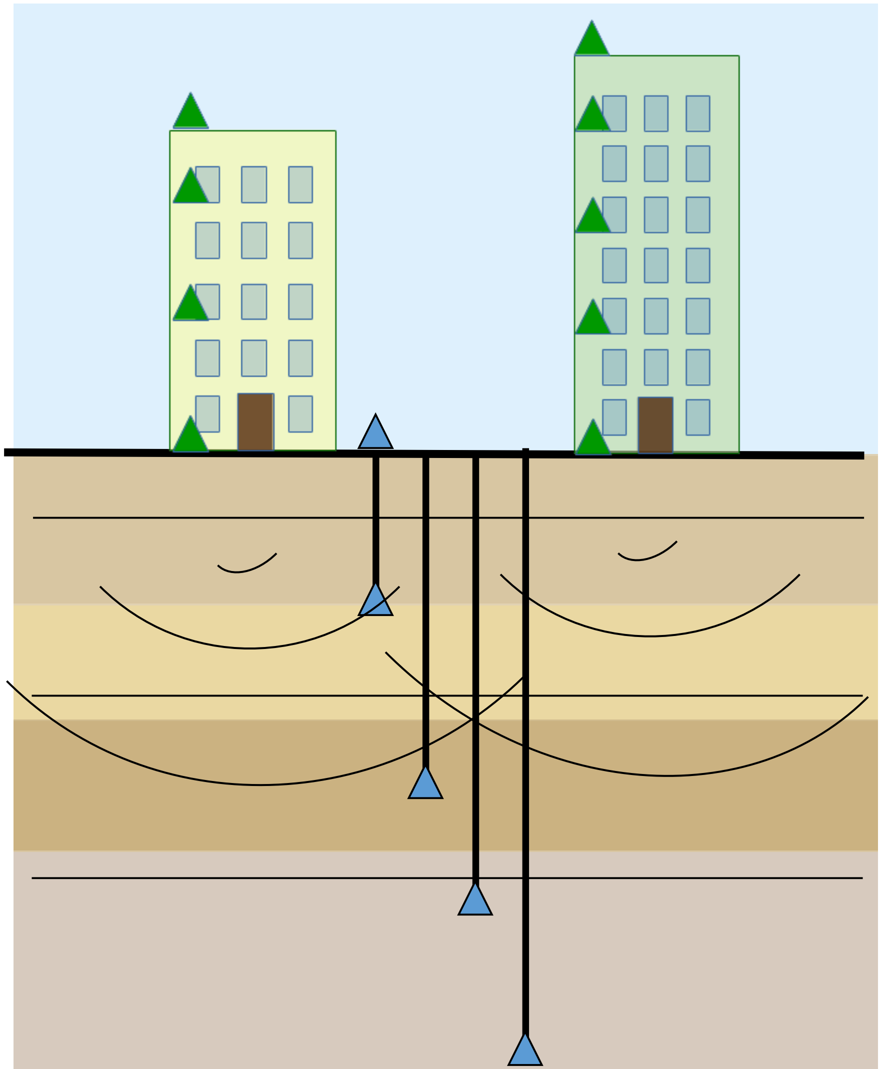

Wave propagation analysis

- through buildings
-> information about buildings‘ dynamic behavior

- through the soil
-> information about shallow geological layers

- thorugh building-soil layers
-> information about interactions taking place

Wave propagation through building-soil-layers

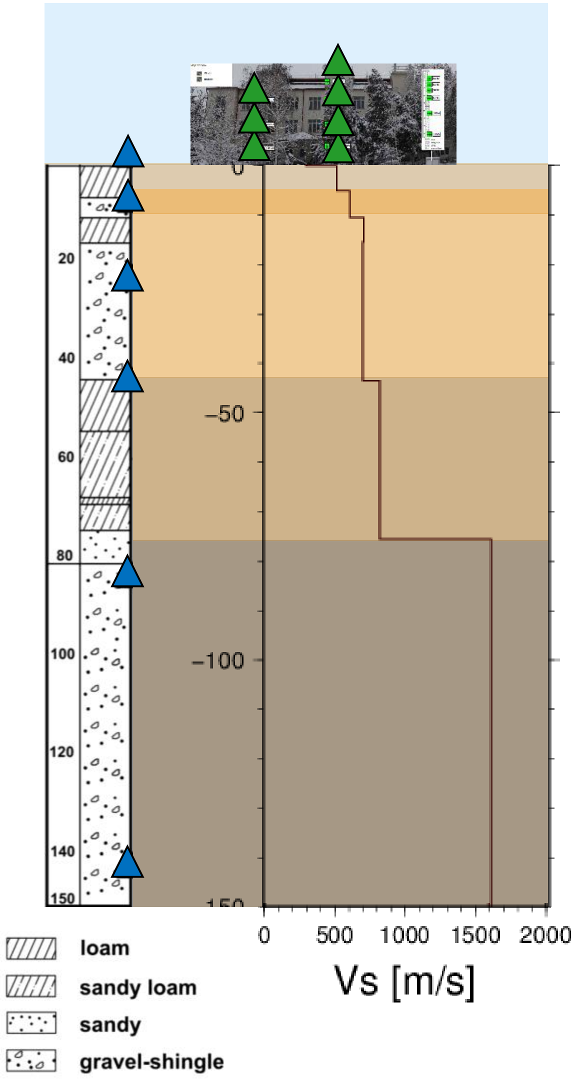

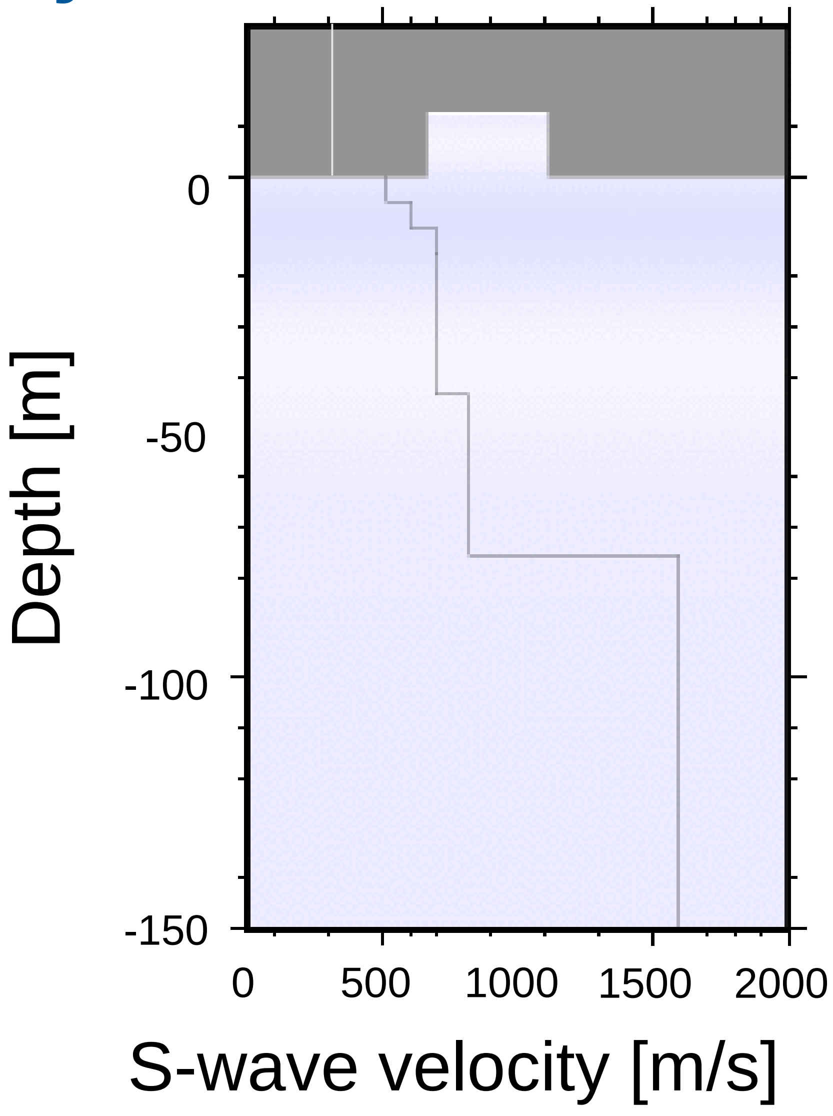

Wave propagation through a 2-layer media

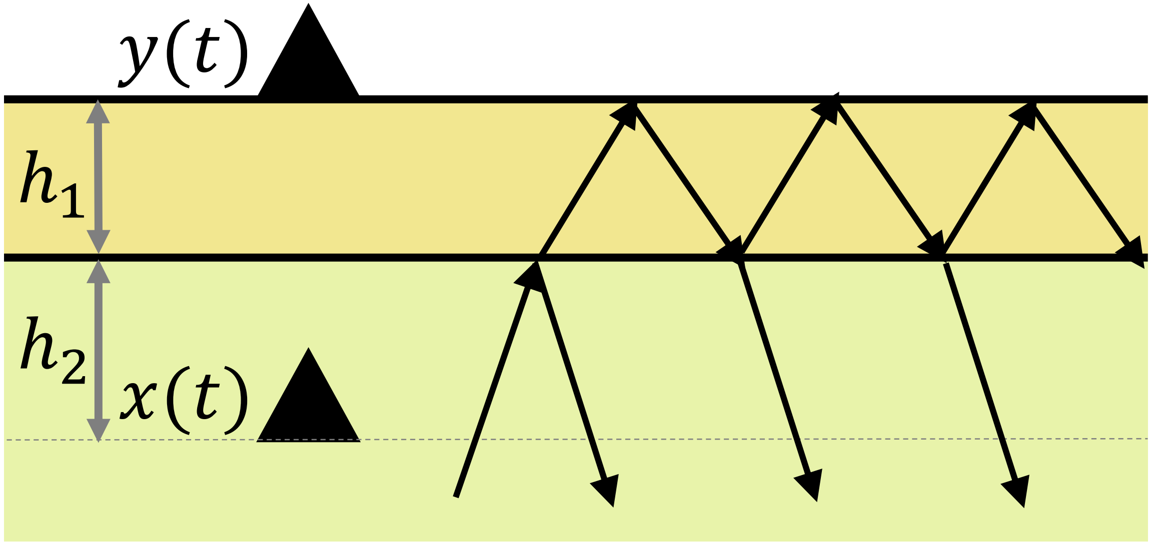

$Q_1, \rho_1, v_1, \tau_1 = h_1/v_1$

$Q_2, \rho_2, v_2, \tau_2 = h_2/v_2$

Reflection coefficient r

$$r = \frac{\rho_2 v_2 - \rho_1 v_1}{\rho_2 v_2 + \rho_1 v_1}$$

Wave propagation through a 2-layer media

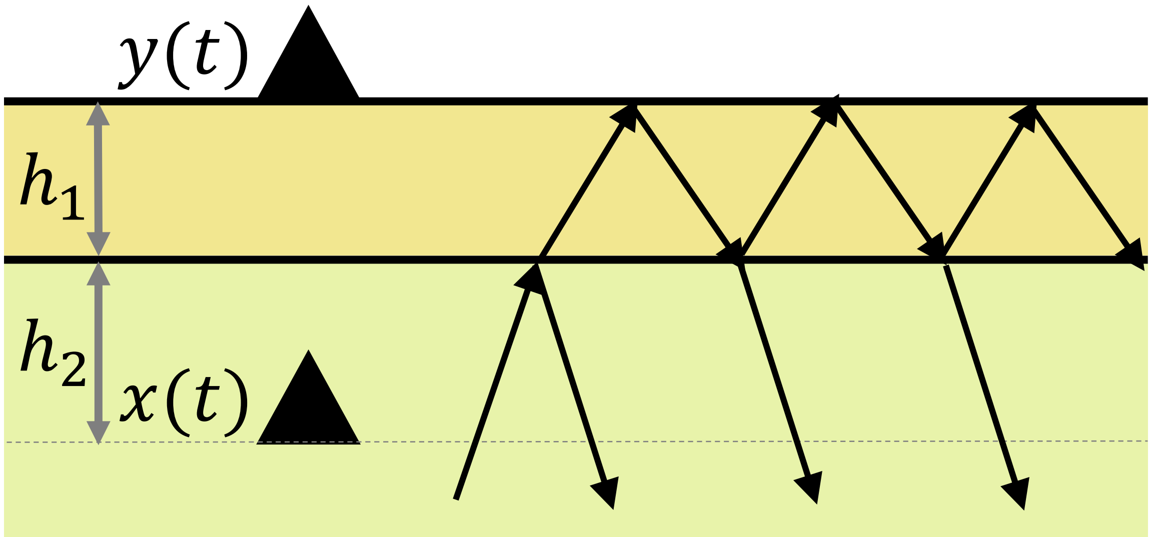

$Q_1, \rho_1, v_1, \tau_1 = h_1/v_1$

$Q_2, \rho_2, v_2, \tau_2 = h_2/v_2$

Reflection coefficient r

$$r = \frac{\rho_2 v_2 - \rho_1 v_1}{\rho_2 v_2 + \rho_1 v_1}$$

$$x(\omega) = \underbrace{x_0(\omega)}_{\text{Incoming waves}} + \underbrace{r x_0(\omega) e^{-i2\omega\frac{\tau_2}{\square}}}_{\text{Waves reflected at the interface}} + \underbrace{0.5 y(\omega)(1 - \mathrm{r}) e^{-i2\omega(\frac{\tau_1}{\square} + \frac{\tau_2}{\square})}}_{\text{Waves reflected at the free surface}}$$

Wave propagation through a 2-layer media

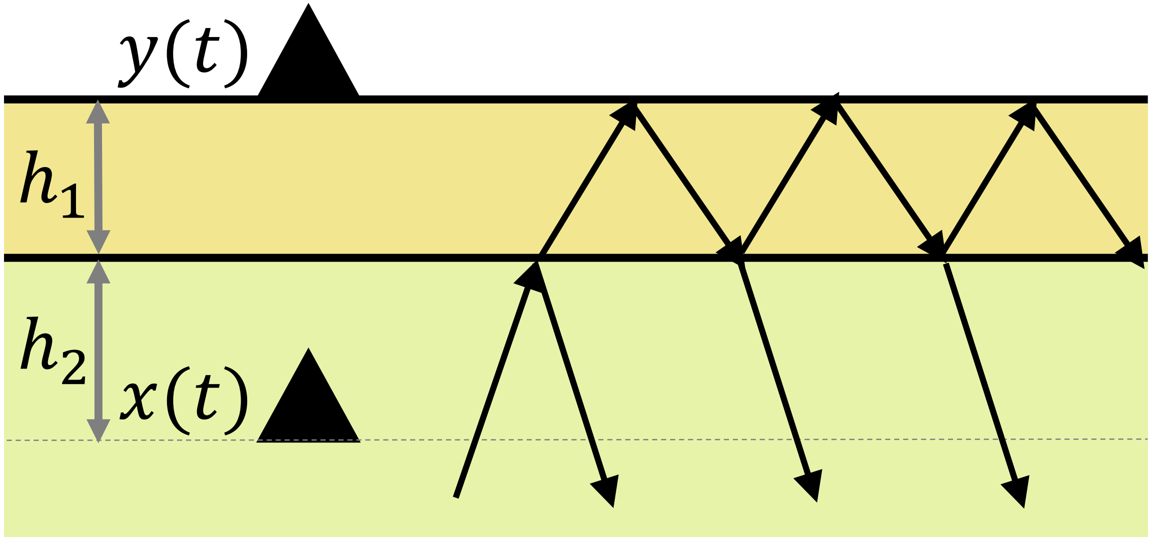

$$Q_1, \rho_1, v_1, \tau_1 = h_1/v_1$$

$$Q_2, \rho_2, v_2, \tau_2 = h_2/v_2$$

Reflection coefficient r

$$r = \frac{\rho_2 v_2 - \rho_1 v_1}{\rho_2 v_2 + \rho_1 v_1}$$

$$x(\omega) = \underbrace{x_0(\omega)}_{\text{Incoming waves}} + \underbrace{r x_0(\omega) e^{-i2\omega\frac{\tau_2}{\square}}}_{\text{Waves reflected at the interface}} + \underbrace{0.5 y(\omega)(1 - \mathrm{r}) e^{-i2\omega(\frac{\tau_1}{\square}+\frac{\tau_2}{\square})}}_{\text{Waves reflected at the free surface}}$$

Incoming waves

Waves reflected at the interface

Waves reflected at the free surface

$$y(\omega) = \underbrace{2((1 + r) x_0(\omega) e^{-i\omega(\frac{\tau_1}{\square}+\frac{\tau_2}{\square})})}_{} - \underbrace{y(\omega) r e^{-i2\omega\frac{\tau_1}{\square}}}_{}$$

Incoming waves transmitted at interface and recorded at free surface

Transmitted incoming waves reflected at the interface and recorded at free surface

Wave propagation through a 2-layer media

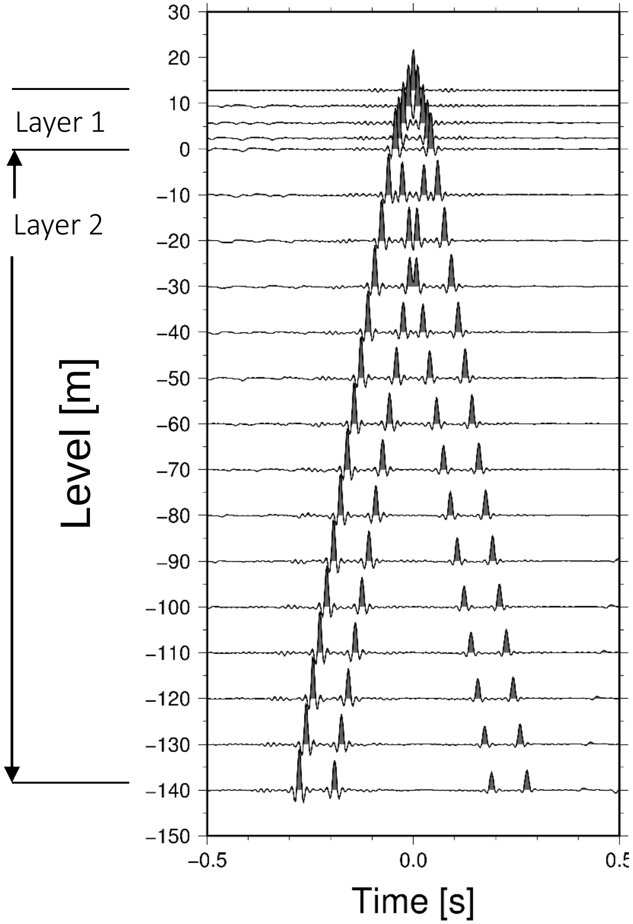

Deconvolved wavefield

Reflection coefficient r

$$r = \frac{\rho_2 v_2 - \rho_1 v_1}{\rho_2 v_2 + \rho_1 v_1}$$

deconvolution

$$D(\omega) = \frac{x(\omega)}{y(\omega)} = \frac{1}{2(1+r)} e^{-i\omega(-\frac{\tau_1}{\square}-\frac{\tau_2}{\square})}$$

$$+ \frac{r}{2(1+r)} e^{-i\omega(\frac{\tau_1}{\square}-\frac{\tau_2}{\square})} + \frac{r}{2(1+r)} e^{-i\omega(-\frac{\tau_1}{\square}+\frac{\tau_2}{\square})}$$

$$+0.5(1-r)e^{-i\omega\left(\frac{\tau_1}{\square}+\frac{\tau_2}{\square}\right)} + \frac{r^2}{2(1+r)} e^{-i\omega(\frac{\tau_1}{\square}+\frac{\tau_2}{\square})}$$

Wave propagation through a 2-layer media

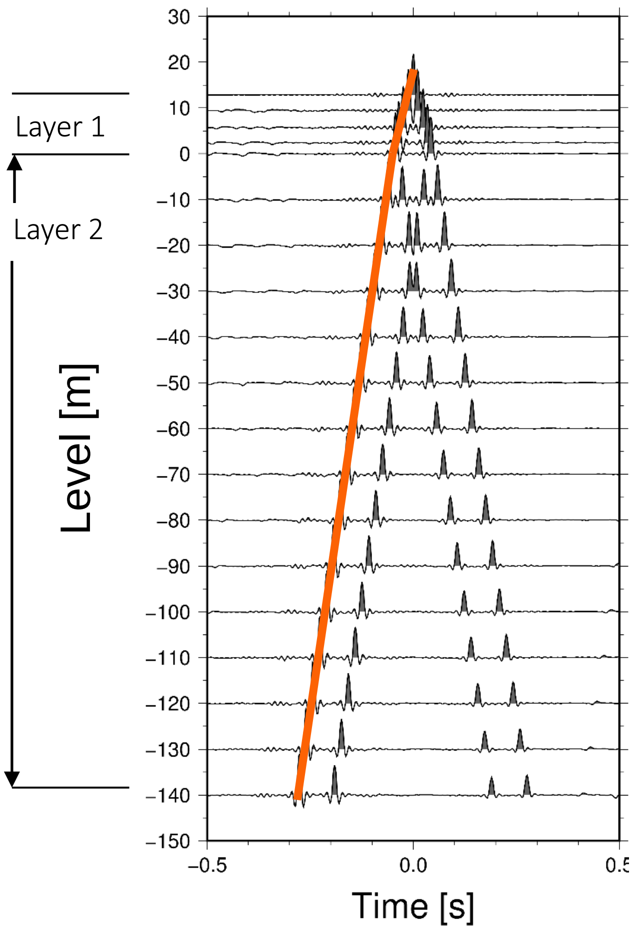

Deconvolved wavefield

Reflection coefficient r

$$r = \frac{\rho_2 v_2 - \rho_1 v_1}{\rho_2 v_2 + \rho_1 v_1}$$

deconvolution

$$D(\omega) = \frac{x(\omega)}{y(\omega)} = \frac{1}{2(1+r)} e^{-i\omega\left(-\frac{\tau_1}{\Box}-\frac{\tau_2}{\Box}\right)}$$

$$+ \frac{r}{2(1+r)} e^{-i\omega\left(\frac{\tau_1}{\Box}-\frac{\tau_2}{\Box}\right)} + \frac{r}{2(1+r)} e^{-i\omega\left(-\frac{\tau_1}{\Box}+\frac{\tau_2}{\Box}\right)}$$

$$+0.5(1-r) e^{-i\omega\left(\frac{\tau_1}{\Box}+\frac{\tau_2}{\Box}\right)} + \frac{r^2}{2(1+r)} e^{-i\omega\left(\frac{\tau_1}{\Box}+\frac{\tau_2}{\Box}\right)}$$

Wave propagation through a 2-layer media

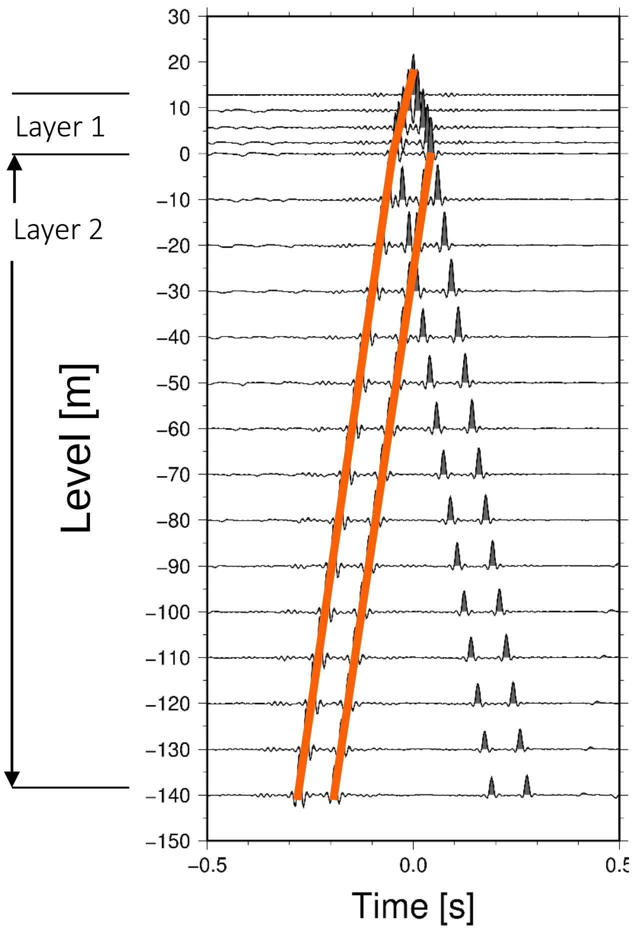

Deconvolved wavefield

Reflection coefficient r

$$r = \frac{\rho_2 v_2 - \rho_1 v_1}{\rho_2 v_2 + \rho_1 v_1}$$

deconvolution

$$D(\omega) = \frac{x(\omega)}{y(\omega)} = \frac{1}{2(1+r)} e^{-i\omega\left(-\frac{\tau_1}{\square}-\frac{\tau_2}{\square}\right)}$$

$$+\frac{r}{2(1+r)} e^{-i\omega\left(\frac{\tau_1}{\square}-\frac{\tau_2}{\square}\right)} + \frac{r}{2(1+r)} e^{-i\omega\left(-\frac{\tau_1}{\square}+\frac{\tau_2}{\square}\right)}$$

$$+0.5(1-r)e^{-i\omega\left(\frac{\tau_1}{\square}+\frac{\tau_2}{\square}\right)} + \frac{r^2}{2(1+r)} e^{-i\omega\left(\frac{\tau_1}{\square}+\frac{\tau_2}{\square}\right)}$$

Wave propagation through a 2-layer media

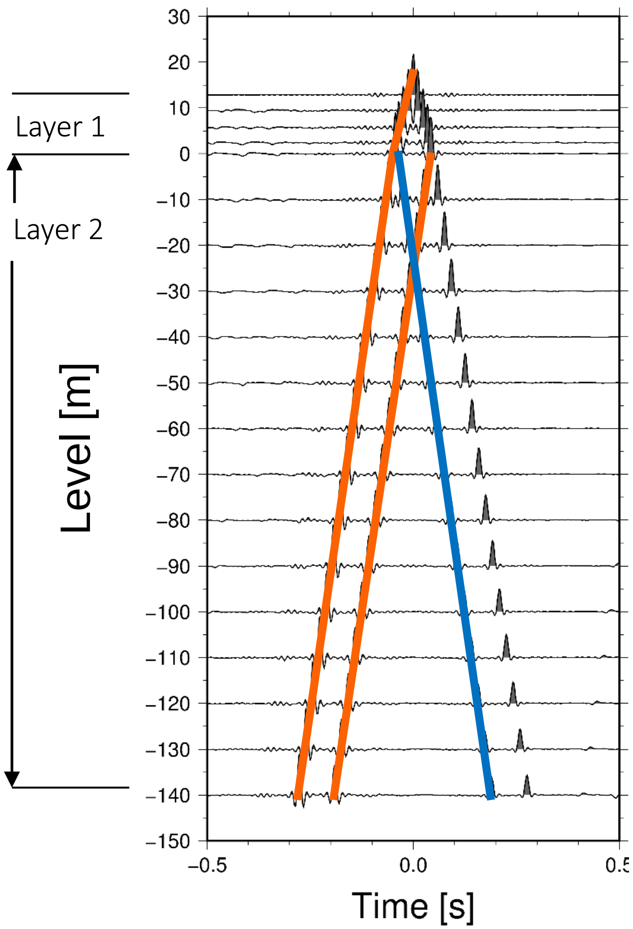

Deconvolved wavefield

Reflection coefficient r

$$r = \frac{\rho_2 v_2 - \rho_1 v_1}{\rho_2 v_2 + \rho_1 v_1}$$

deconvolution

$$D(\omega) = \frac{x(\omega)}{y(\omega)} = \frac{1}{2(1+r)} e^{-i\omega\left(-\frac{\tau_1}{\square}-\frac{\tau_2}{\square}\right)} + \frac{r}{2(1+r)} e^{-i\omega\left(\frac{\tau_1}{\square}-\frac{\tau_2}{\square}\right)} + \frac{r}{2(1+r)} e^{-i\omega\left(-\frac{\tau_1}{\square}+\frac{\tau_2}{\square}\right)}$$

$$+0.5(1-r)e^{-i\omega\left(\frac{\tau_1}{\square}+\frac{\tau_2}{\square}\right)} + \frac{r^2}{2(1+r)} e^{-i\omega\left(\frac{\tau_1}{\square}+\frac{\tau_2}{\square}\right)}$$

Wave propagation through a 2-layer media

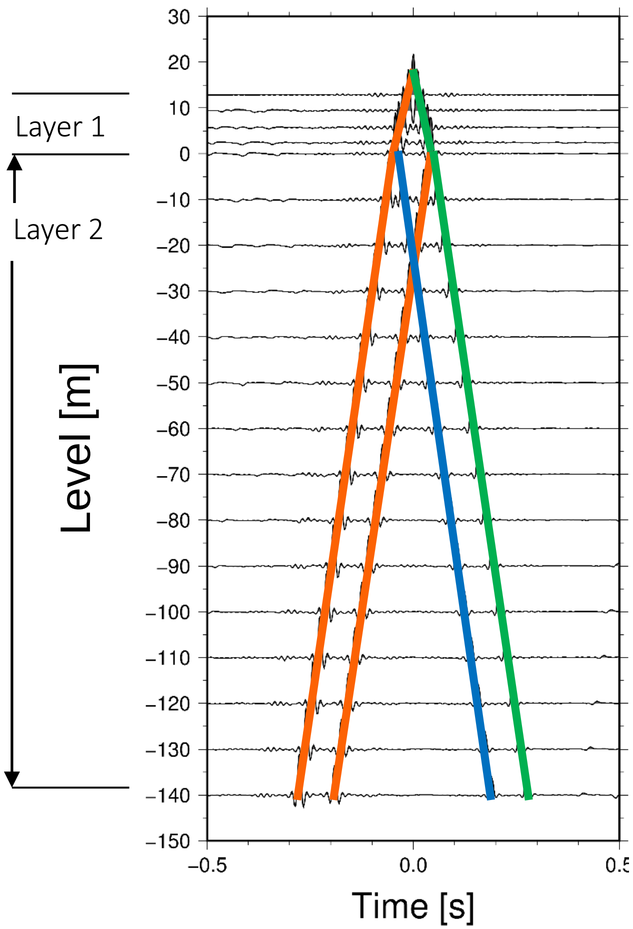

Deconvolved wavefield

Reflection coefficient r

$$r = \frac{\rho_2 v_2 - \rho_1 v_1}{\rho_2 v_2 + \rho_1 v_1}$$

deconvolution

$$D(\omega) = \frac{x(\omega)}{y(\omega)} = \frac{1}{2(1+r)} e^{-i\omega\left(-\frac{\tau_1}{\square}-\frac{\tau_2}{\square}\right)}$$

$$+ \frac{r}{2(1+r)} e^{-i\omega\left(\frac{\tau_1}{\square}-\frac{\tau_2}{\square}\right)} + \frac{r}{2(1+r)} e^{-i\omega\left(-\frac{\tau_1}{\square}+\frac{\tau_2}{\square}\right)}$$

$$+ 0.5(1-r) e^{-i\omega\left(\frac{\tau_1}{\square}+\frac{\tau_2}{\square}\right)} + \frac{r^2}{2(1+r)} e^{-i\omega\left(\frac{\tau_1}{\square}+\frac{\tau_2}{\square}\right)}$$

Wave propagation through a 2-layer media

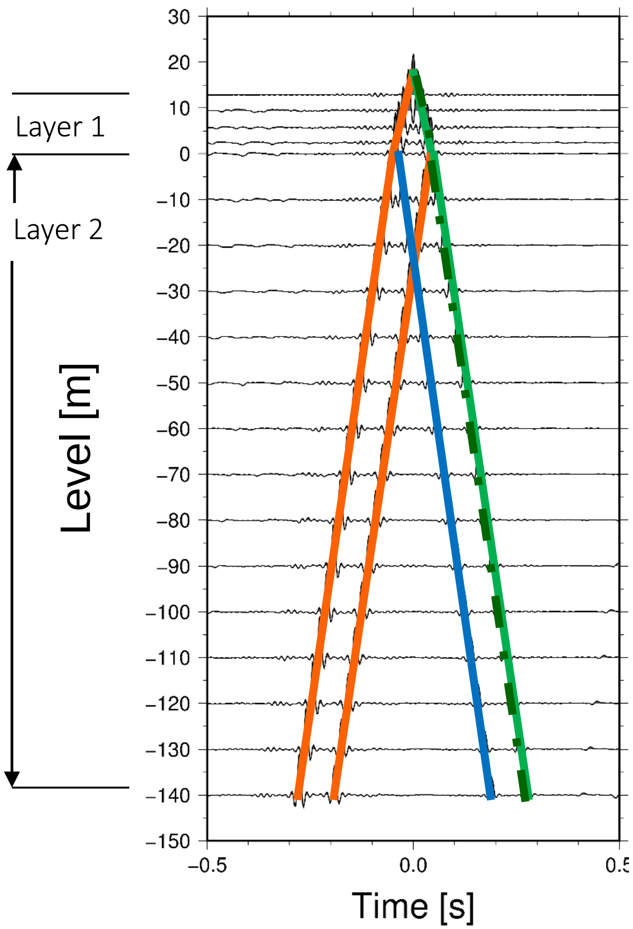

Deconvolved wavefield

Reflection coefficient r

$$r = \frac{\rho_2 v_2 - \rho_1 v_1}{\rho_2 v_2 + \rho_1 v_1}$$

deconvolution

$$D(\omega) = \frac{x(\omega)}{y(\omega)} = \frac{1}{2(1+r)} e^{-i\omega\left(-\frac{\tau_1}{\square} - \frac{\tau_2}{\square}\right)} + \frac{r}{2(1+r)} e^{-i\omega\left(\frac{\tau_1}{\square} - \frac{\tau_2}{\square}\right)} + \frac{r}{2(1+r)} e^{-i\omega\left(-\frac{\tau_1}{\square} + \frac{\tau_2}{\square}\right)} + 0.5(1-r) e^{-i\omega\left(\frac{\tau_1}{\square} + \frac{\tau_2}{\square}\right)} + \frac{r^2}{2(1+r)} e^{-i\omega\left(\frac{\tau_1}{\square} + \frac{\tau_2}{\square}\right)}$$

Methodology: Joint deconvolution of borehole and building recordings

Input data

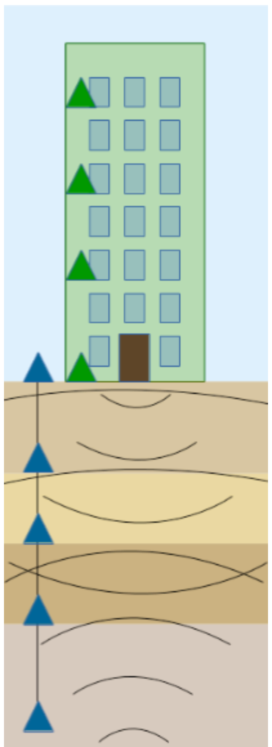

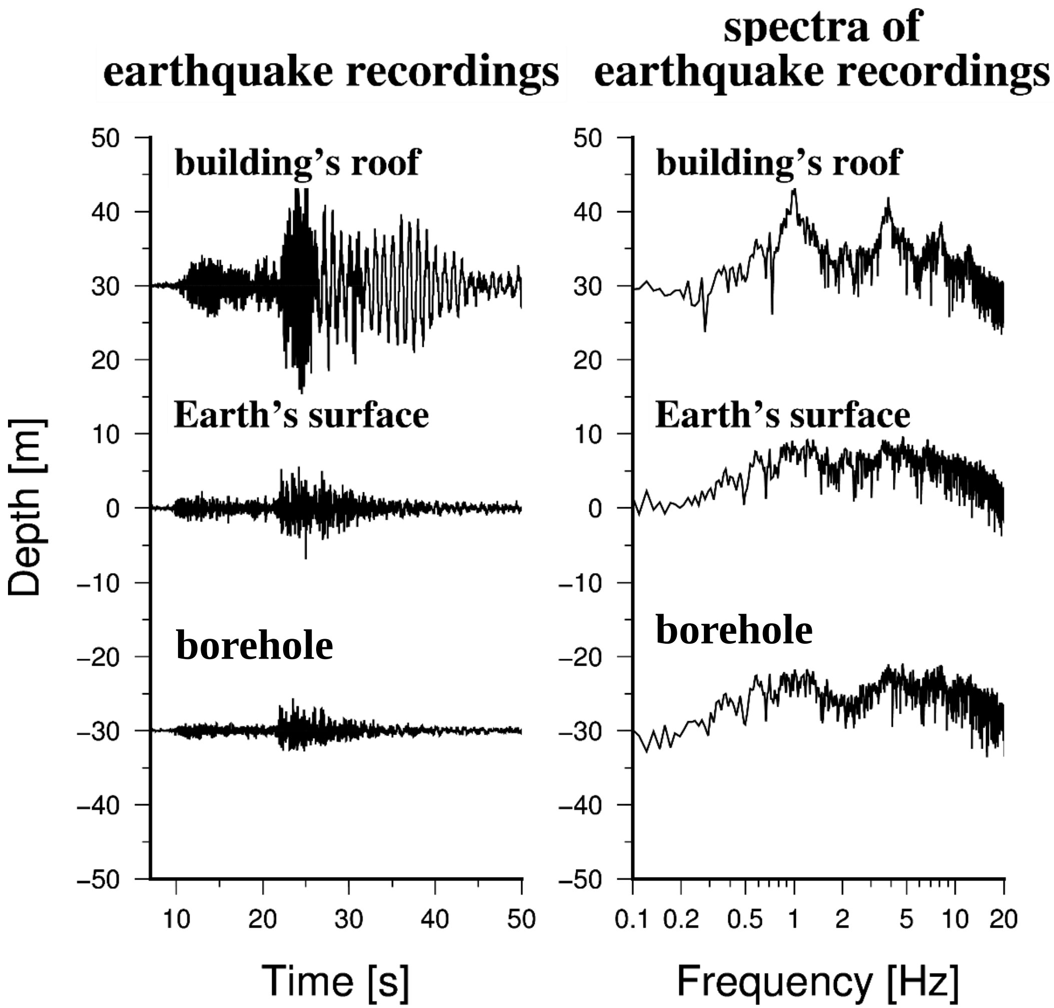

[Petrovic and Parolai, 2016]

Methodology: Joint deconvolution of borehole and building recordings

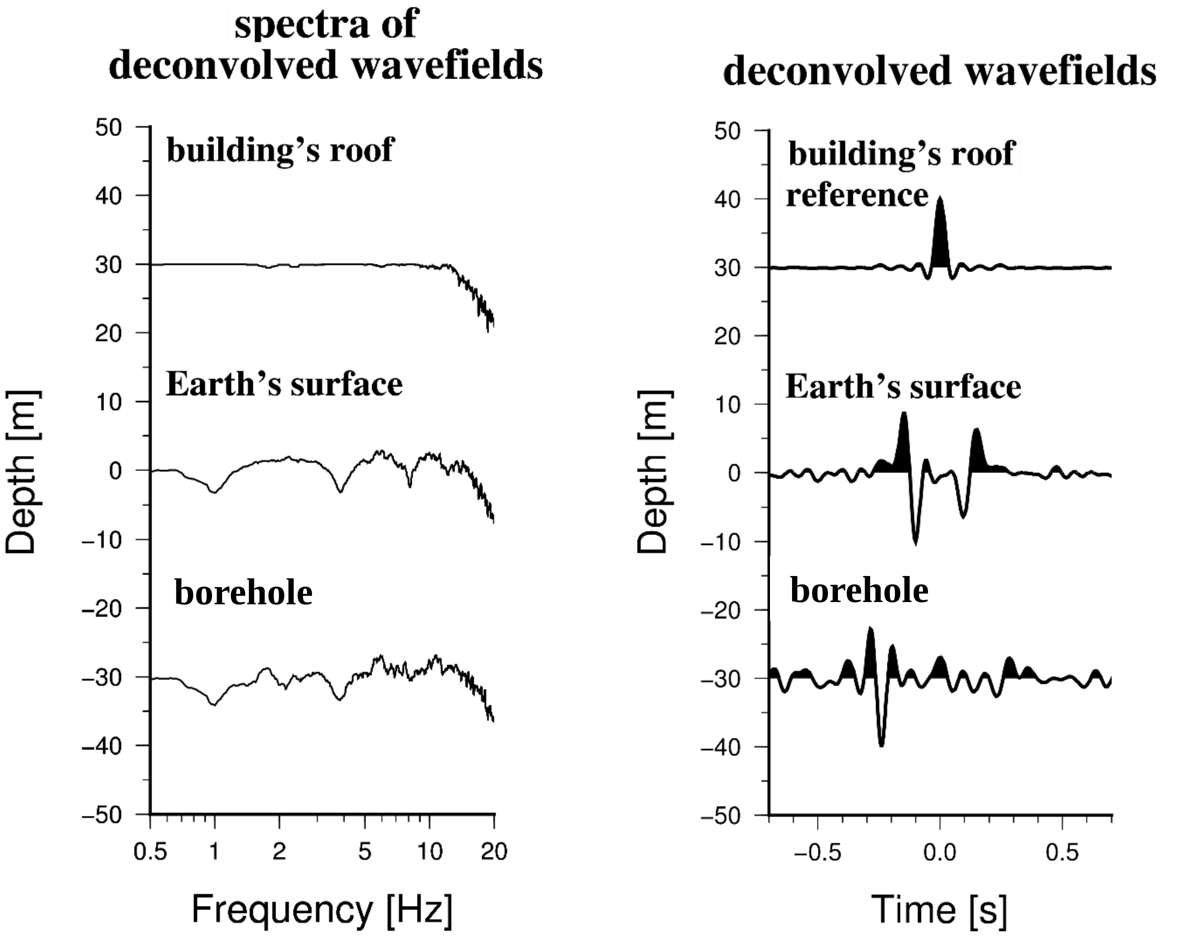

[Petrovic and Parolai, 2016]

Methodology: Joint deconvolution of borehole and building recordings

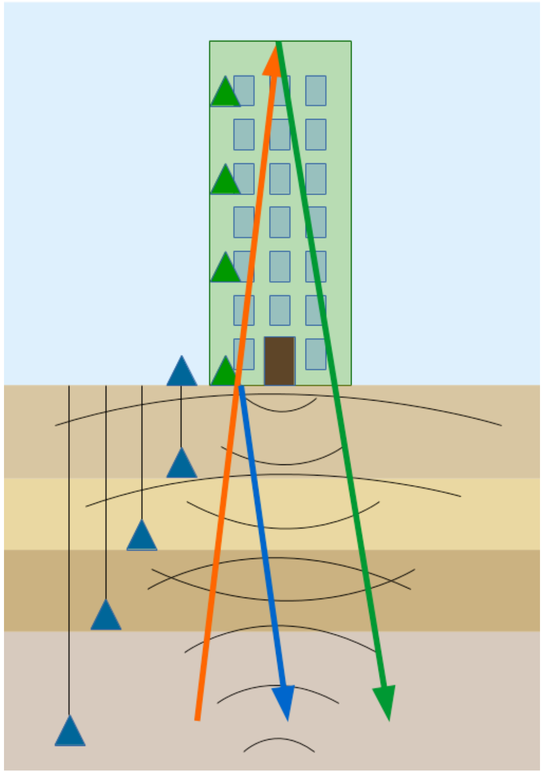

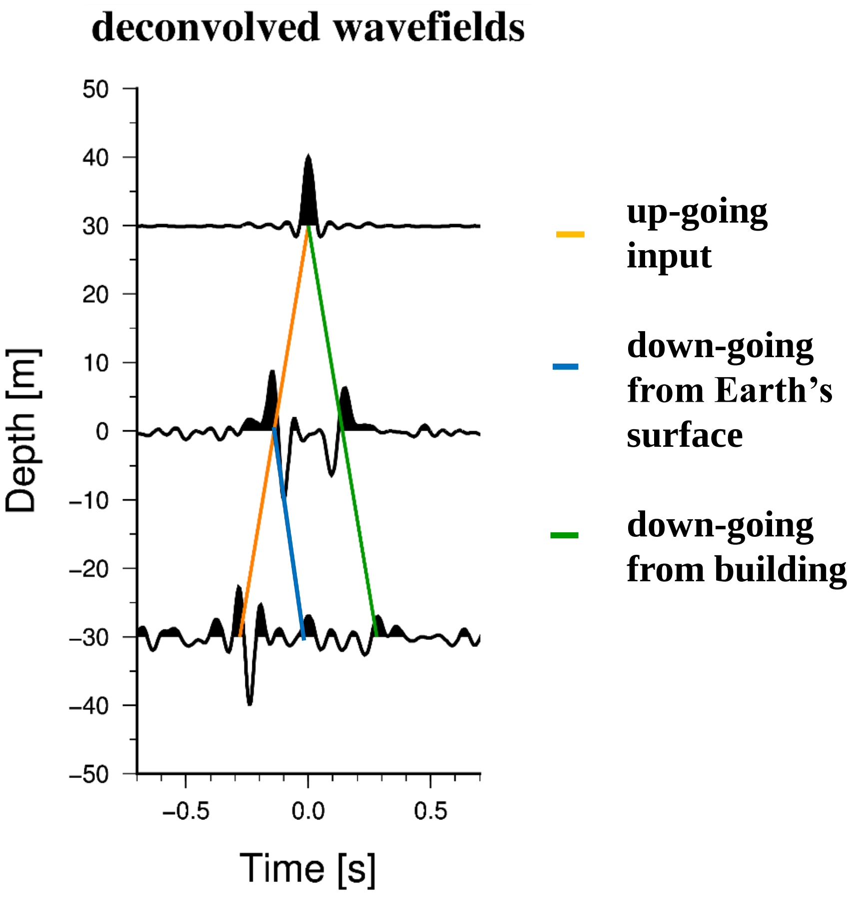

[Petrovic and Parolai, 2016]

Methodology: Estimation of real seismic input

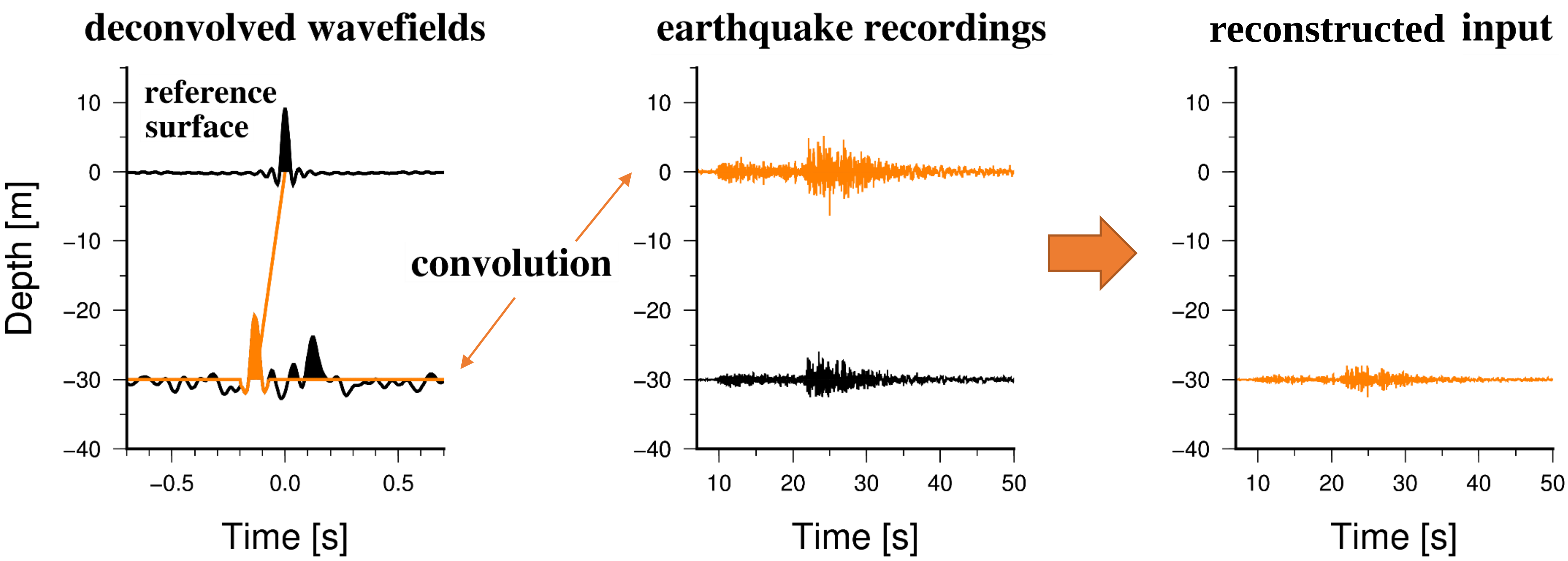

based on constrained deconvolution [Bindi et al., 2010]

[Petrovic and Parolai, 2016]

Constrained deconvolution

The input ground motion at depth is reconstructed from that at the surface without requiring the knowledge of the borehole velocity structure

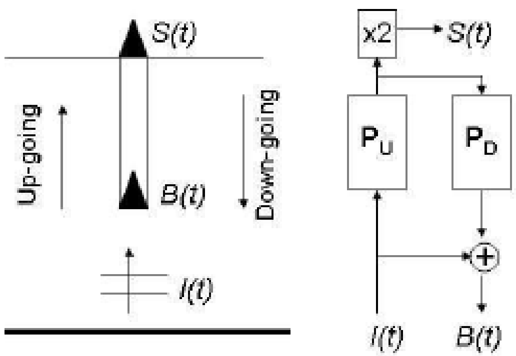

$$\frac{\hat{B}}{\hat{S}} = \frac{\hat{I} + \hat{I}\hat{P}_T}{2\hat{I}\hat{P}_U} = \frac{1+\hat{P}_T}{2\hat{P}_U} = \frac{1}{2\hat{P}_U} + \frac{\hat{P}_D}{2}.$$

$$f_{n+1} = P_C\lfloor f_n + \alpha S^T * (B - S * f_n)\rfloor$$

$$0 < \alpha < \frac{2}{\hat{S}^2_{\max}}, \qquad \hat{S}_{\max} = \max_{\omega} |\hat{S}|.$$

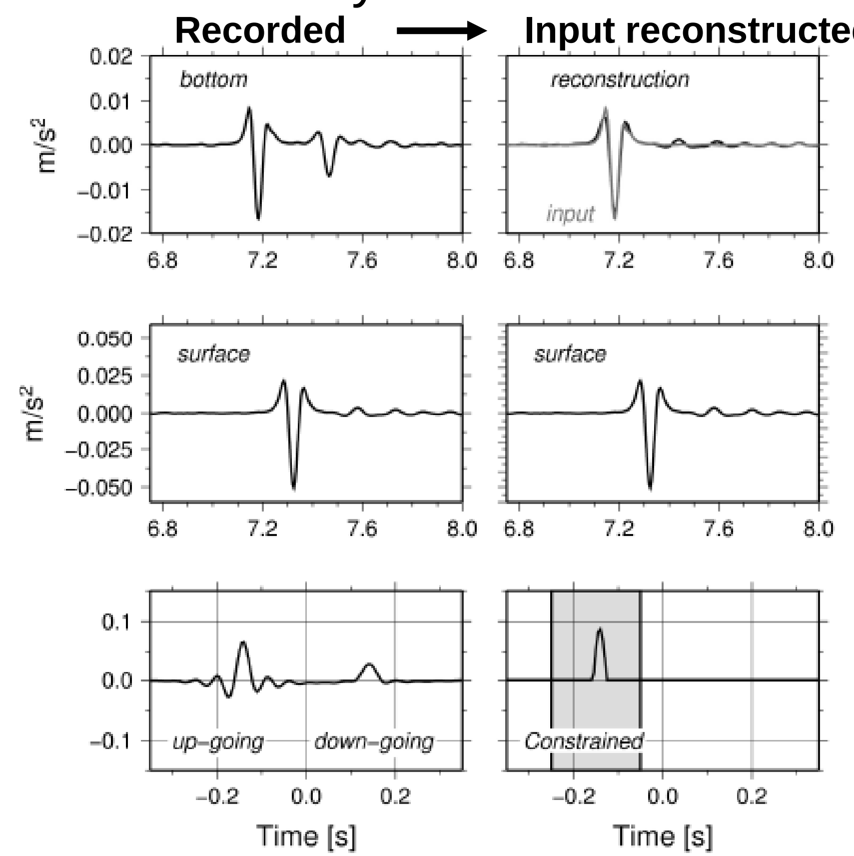

Bindi et al., 2010

Methodology: Estimation of real seismic input

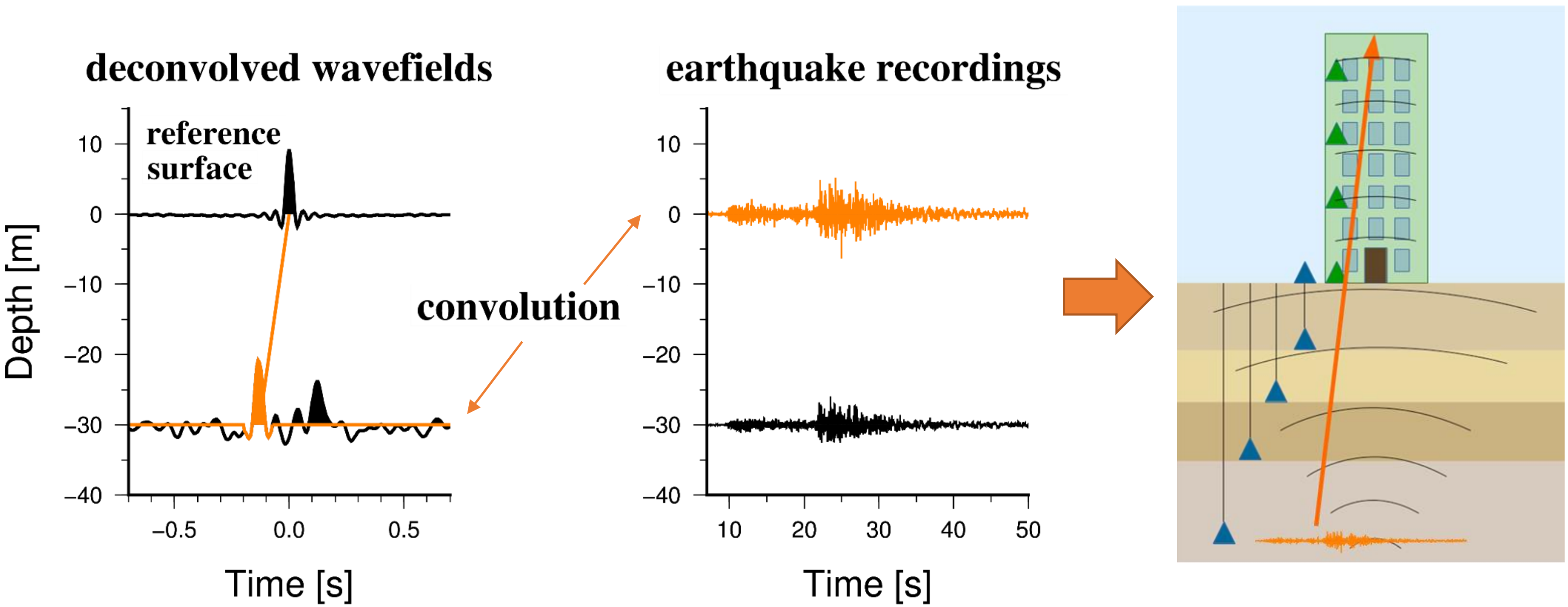

based on constrained deconvolution [Bindi et al., 2010]

[Petrovic and Parolai, 2016]

Methodology: Estimation of wavefield being radiated back from the building to soil

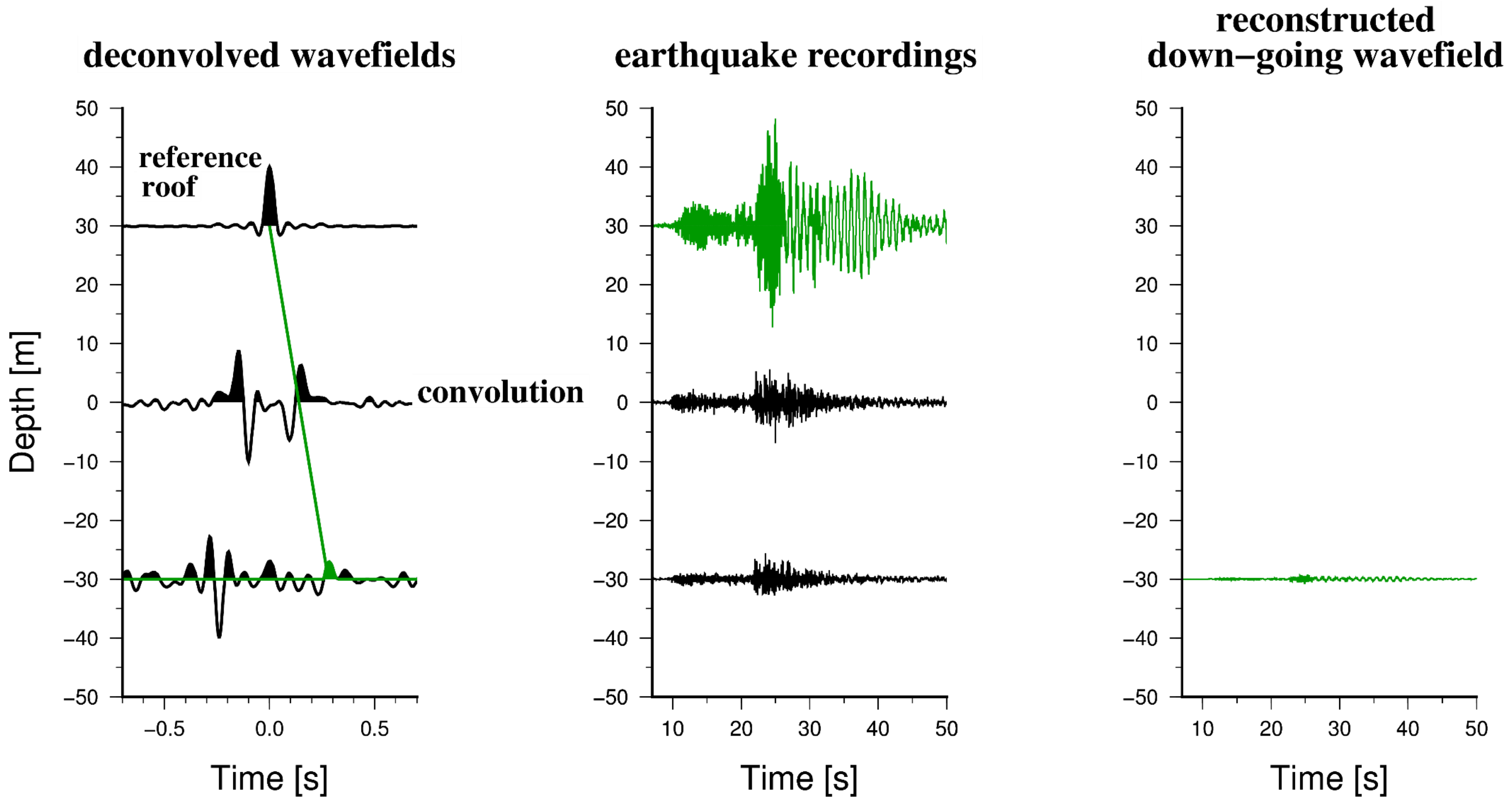

[Petrovic and Parolai, 2016]

Methodology: Estimation of wavefield being radiated back from the building to soil

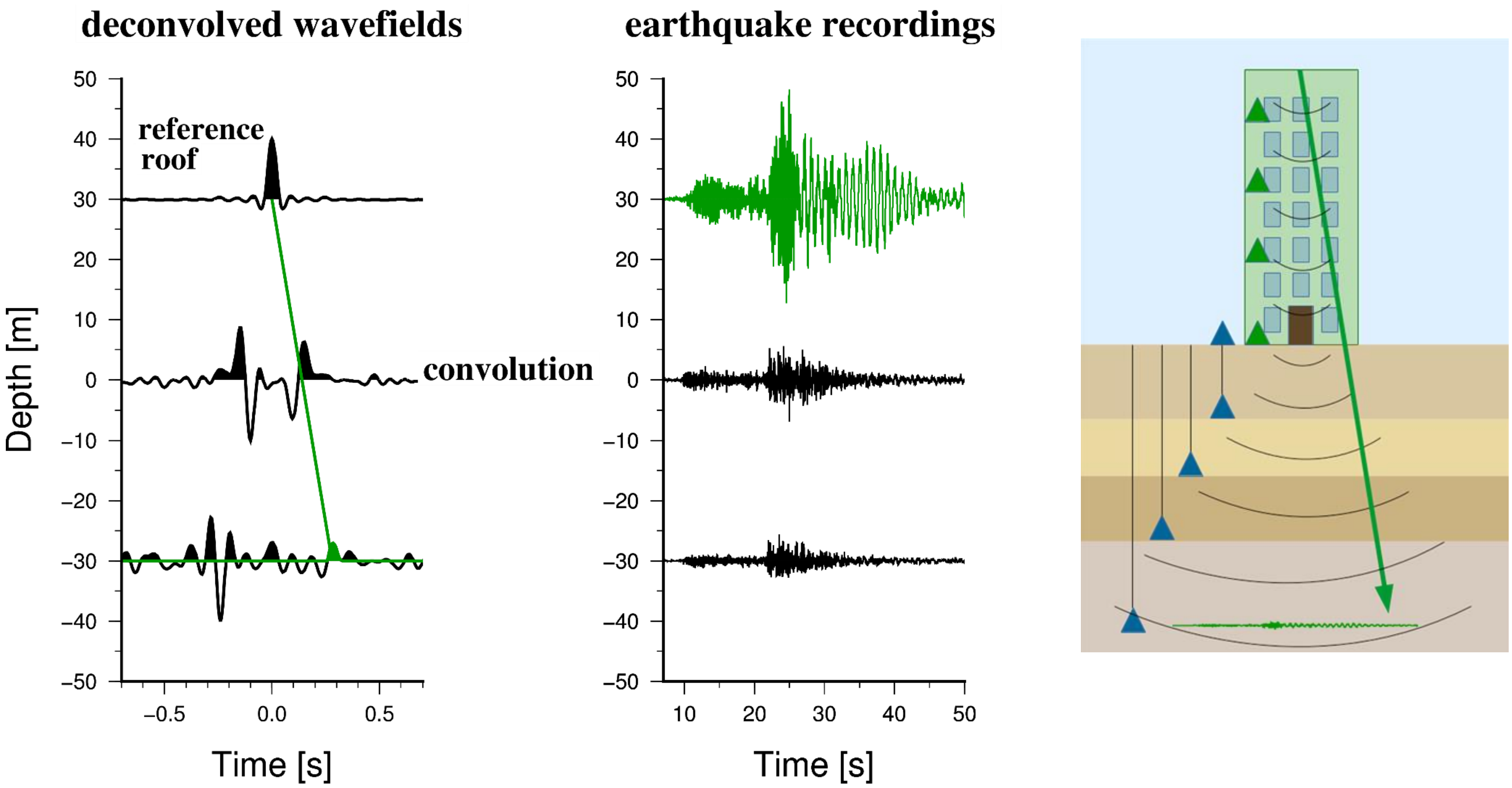

[Petrovic and Parolai, 2016]

Methodology: Estimation of spectral energy

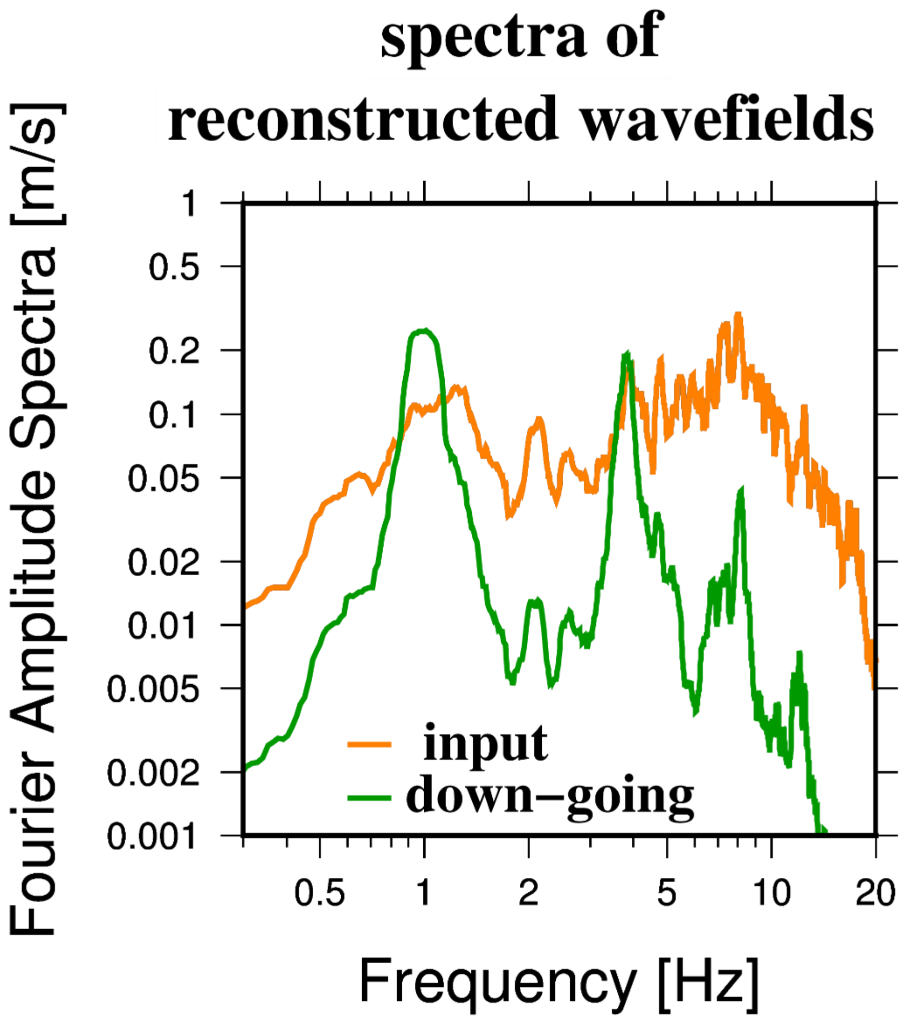

[Petrovic and Parolai, 2016]

Methodology: Estimation of spectral energy

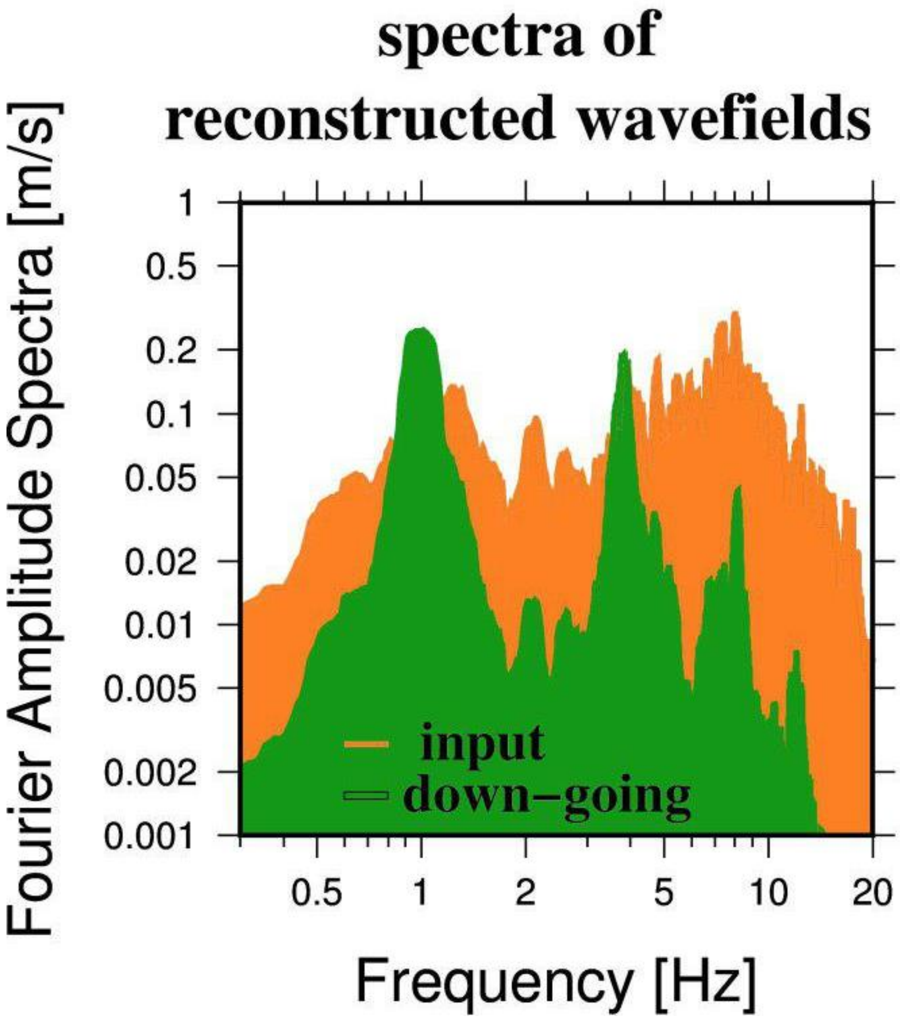

integration of velocity spectra

[Petrovic and Parolai, 2016]

Methodology: Estimation of spectral energy

spectra of reconstructed wavefields

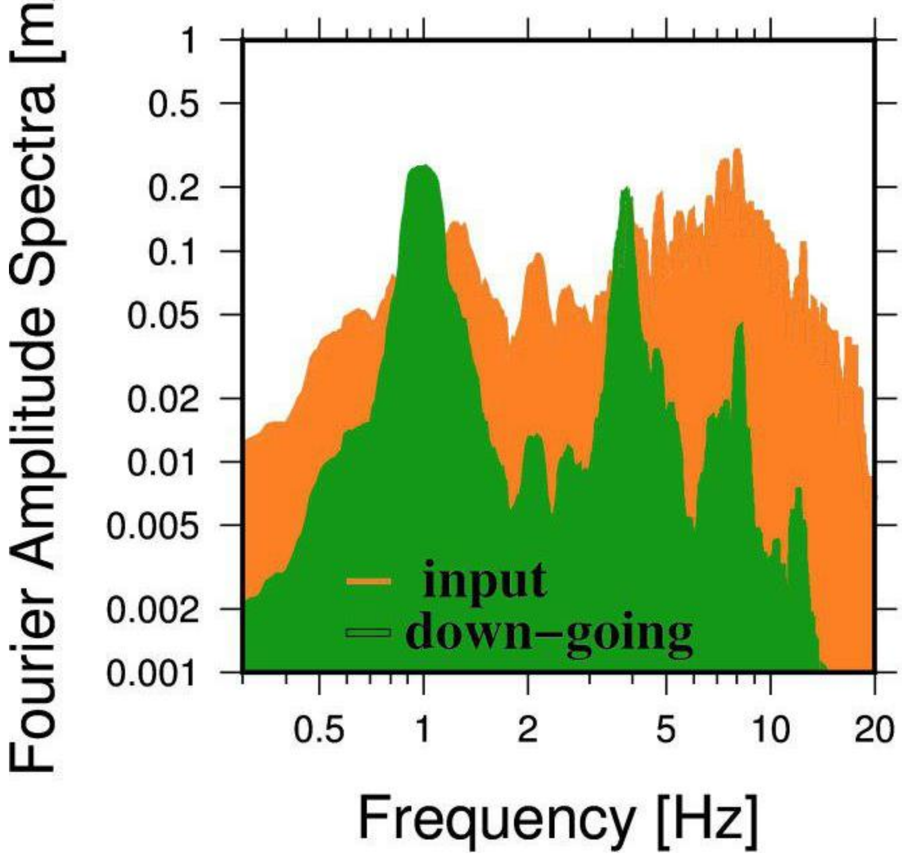

integration of velocity spectra

→

spectral energy

[Petrovic and Parolai, 2016]

The three test cases
The Bishkek (Kyrgyzstan) vertical array

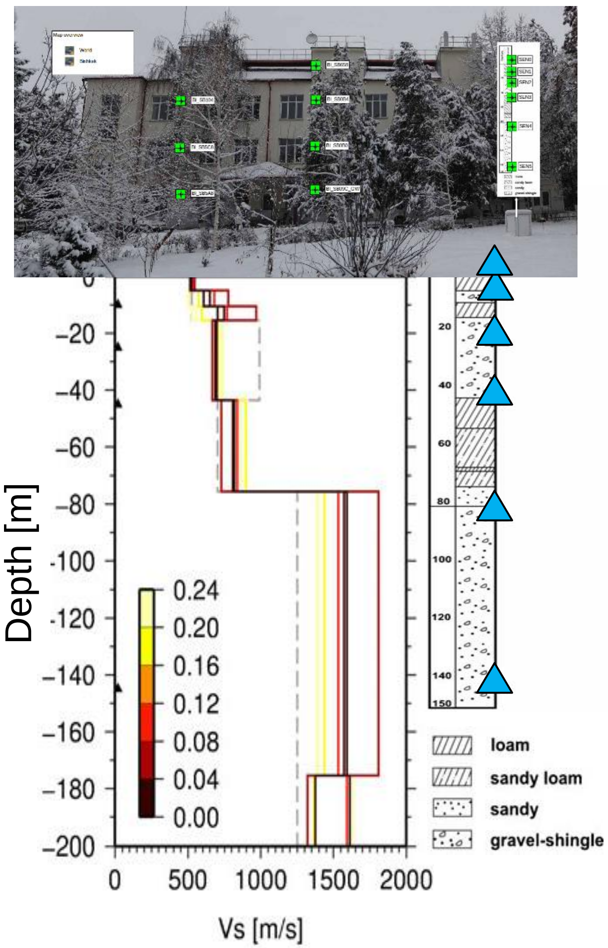

Installation

150m deep borehole equipped with six 3-component borehole accelerometers at depths of 0m, 10m, 25m, 45m, 85m and 145m.

3-story building of the CAIAG institute monitored by 7 SOSEWIN low-cost accelerometers.

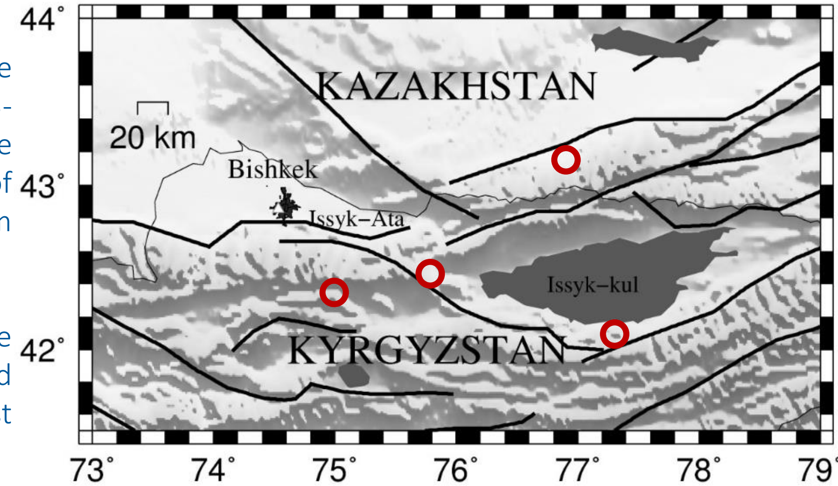

	date	M_w	epicenter	depth	Distance to epicenter
1	23.11.2013	4.9	75.77°E 42.46°N	10km	110 km
2	14.11.2014	5.2	77.31°E 42.10°N	45km	350 km
3	22.01.2015	4.9	77.99°E 42.34°N	0km	280 km
4	15.03.2015	4.8	76.90°E 43.15°N	10km	190 km

[Petrovic and Parolai, 2016]

The three test cases
The Ataköy, Istanbul (Turkey) vertical array

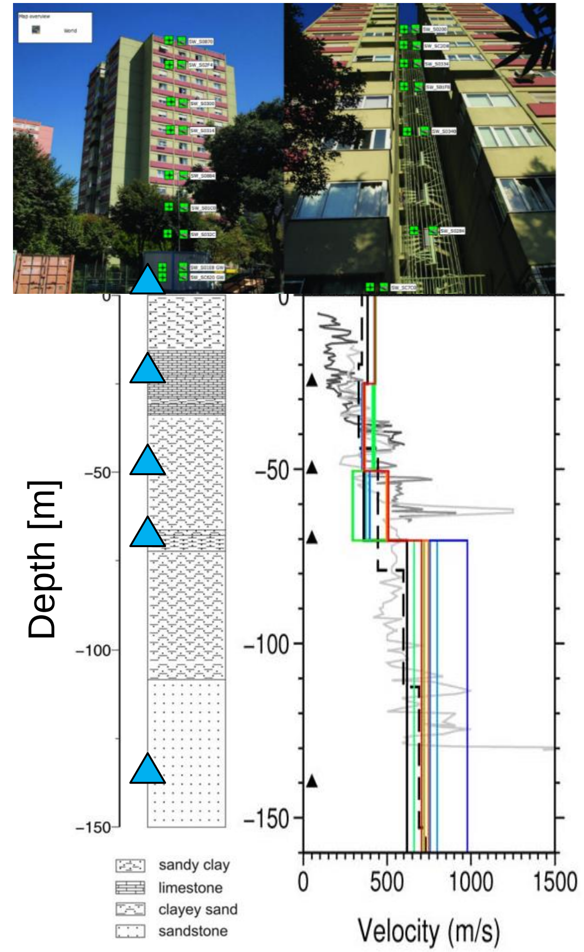

[Petrovic et al. 2017b]

Installation

4 boreholes instrumented with 3 shallow borehole accelerometers (-25, -50 and -70m) and a downhole accelerometer at -140 m

16-story residential tunnel formwork building monitored by 15 SOSEWINs low-cost accelerometers

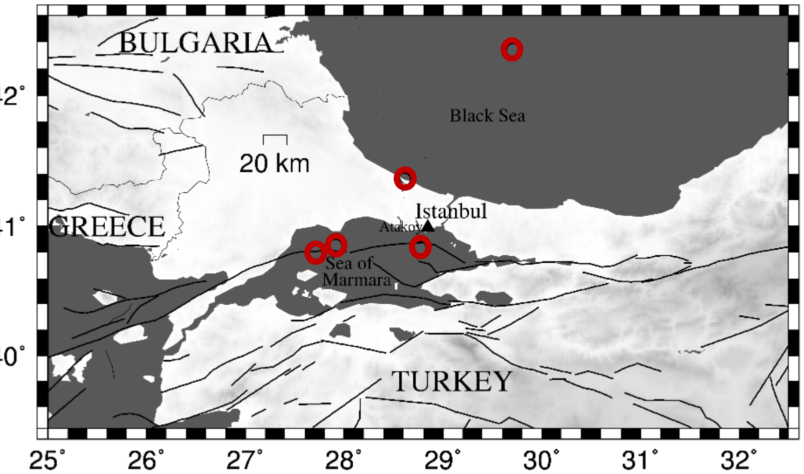

ID	date	M_w	epicenter	Depth	Distance to epicenter
1	27.11.13	4.8	27.92°E 40.85°N	9km	80km
2	27.11.13	4.0	27.91°E 40.85°N	7km	80km
3	05.02.14	3.7	28.61°E 41.36°N	12km	45km
4	28.10.15	4.6	27.72°E 40.80°N	16km	100km
5	16.11.15	4.3	28.76°E 40.83°N	8km	20km
6	15.12.15	4.1	29.71°E 42.34°N	30km	165km

The three test cases
The Mexico City (Mexico) vertical array

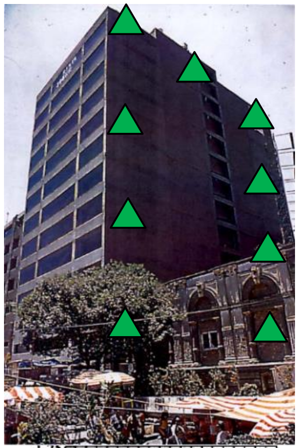

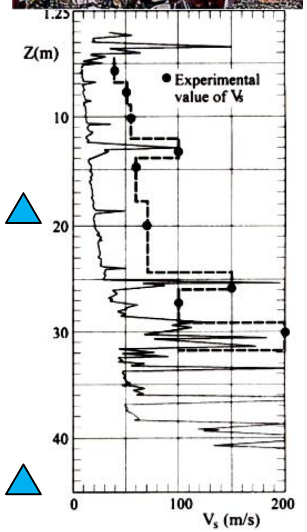

[Petrovic et al. 2017b]

Installation

2 tri-directional solid state digital accelerographs installed in boreholes at 20 m and 45 m depth

14-story reinforced concrete building instrumented with 11 instruments located at different locations on 4 floors (basement, 6th and 11th floor and the roof).

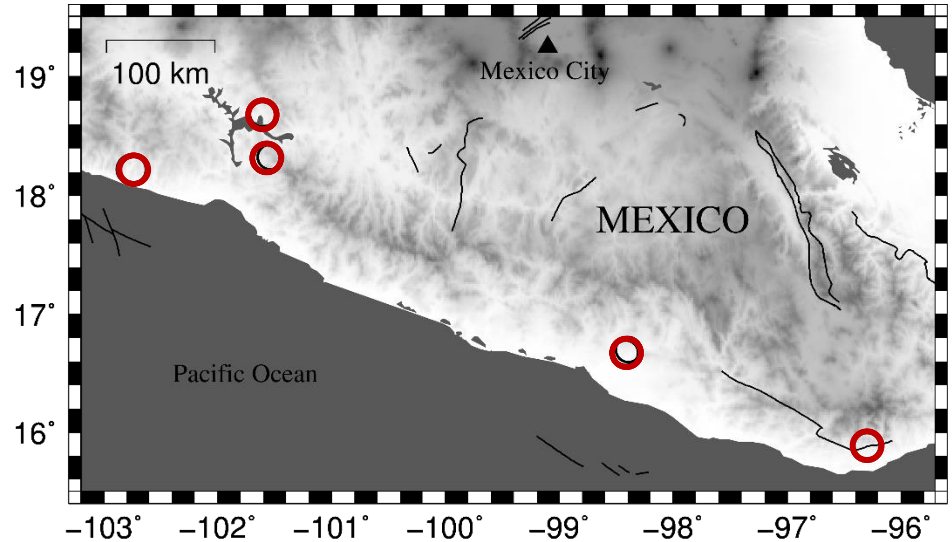

damage + retrofit

damage

ID	date	M_w	epicenter	depth	Distance to epicenter
1	15.05.93	6.0	98.42°W 16.67°N	19.7 km	318 km
2	15.05.93	6.1	98.40°W 16.70°N	20.8 km	315 km
3	11.01.97	7.2	102°W 18.22°N	33 km	330 km
4	22.05.97	6.5	101.60°W 18.68°N	70 km	270 km
5	03.02.98	6.3	96.42°W 16.67°N	33 km	420 km
6	21.06.99	6.2	101.54°W18.32°N	68.7 km	285 km

Joint deconvolution

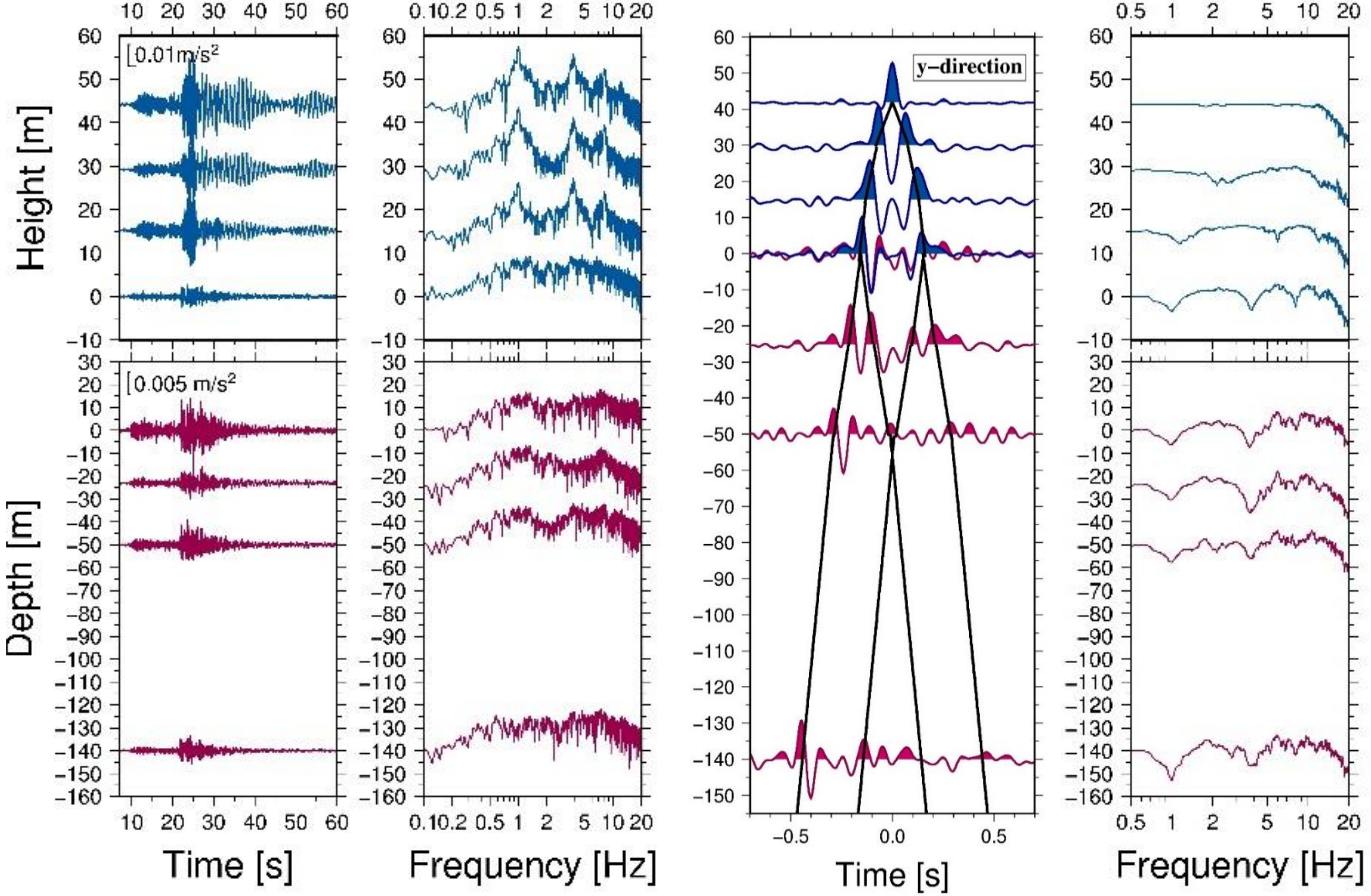

[Petrovic et al. 2017b]

Joint deconvolution

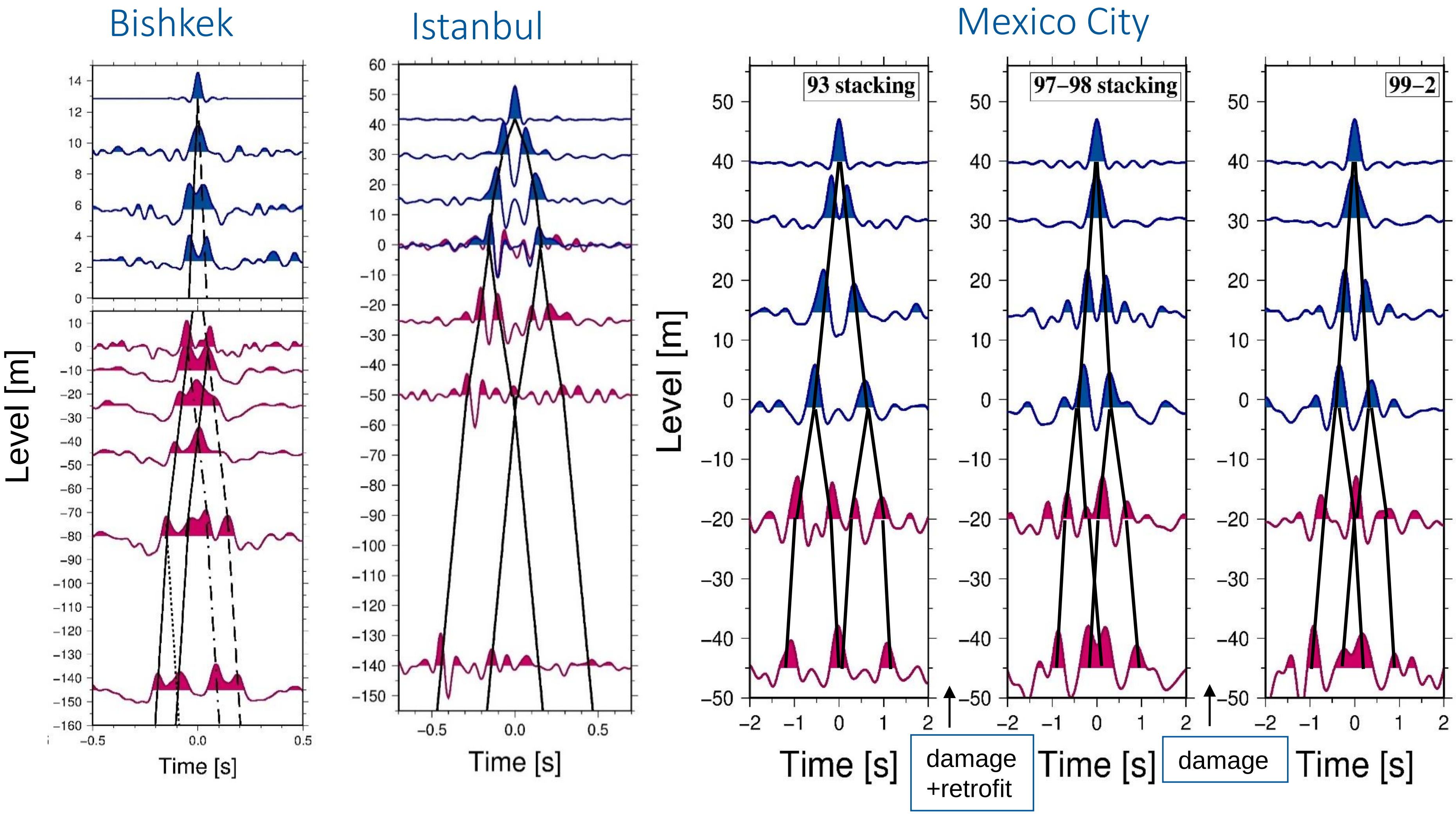

Deconvolved wavefield after stacking the results of several earthquakes for one horizontal component for the three test cases.

Joint deconvolution

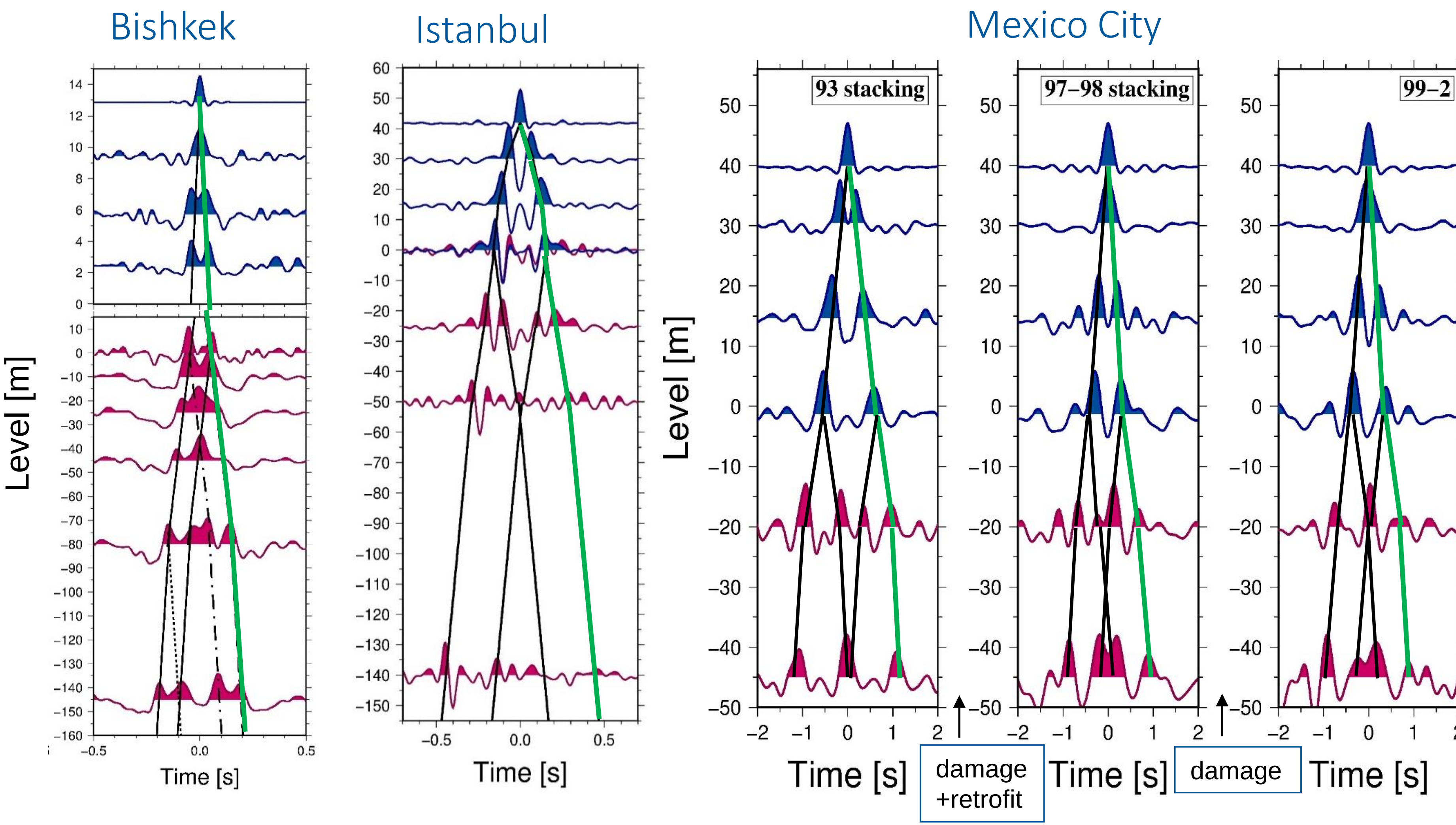

Deconvolved wavefield after stacking the results of several earthquakes for one horizontal component for the three test cases.

Reconstricting different wavefields

Real seismic input

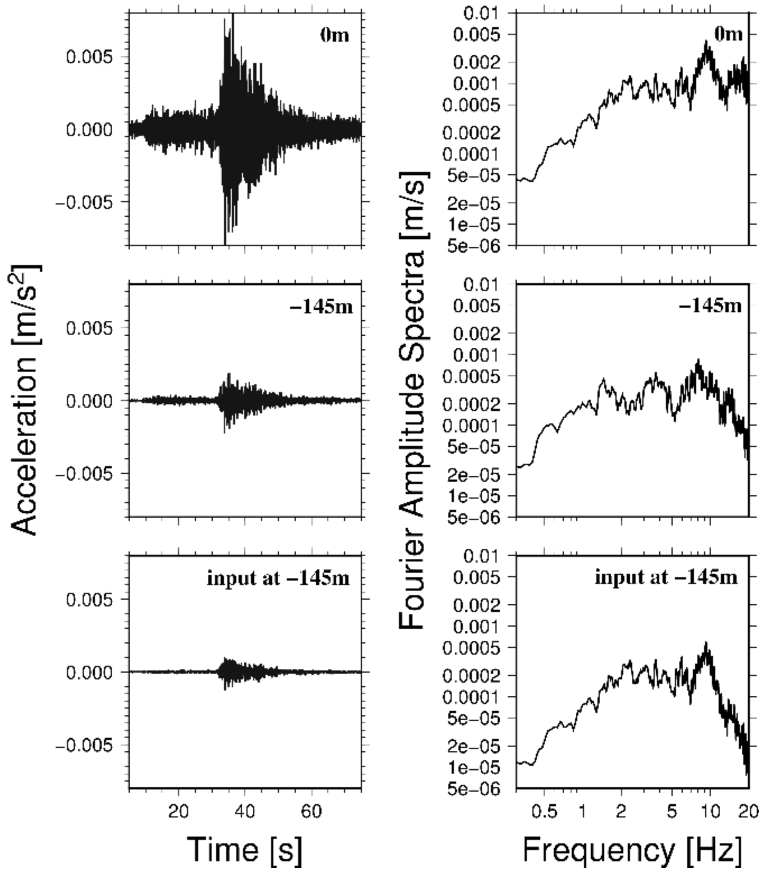

Downgoing waves

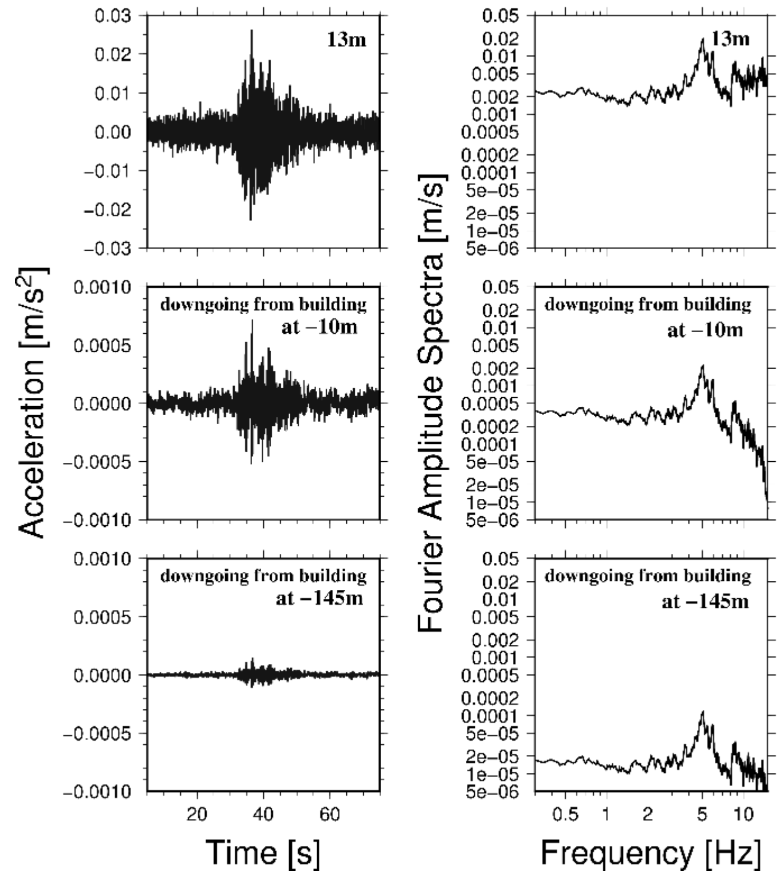

[Petrovic and Parolai 2016]

Estimation of energy being radiated back from the building to the soil

- At **-145m**: **10-15%** of estimated real input energy at -145m.
- At **-10m**: **40-50%** of estimated real input energy at -145m.

Bishkek

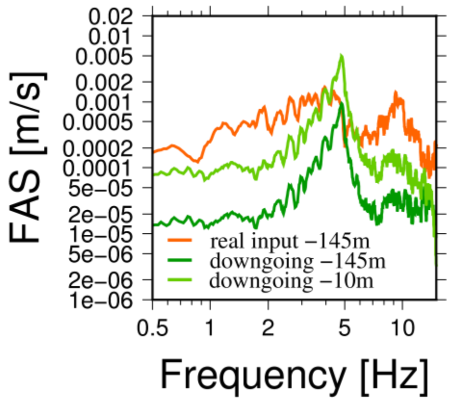

Istanbul

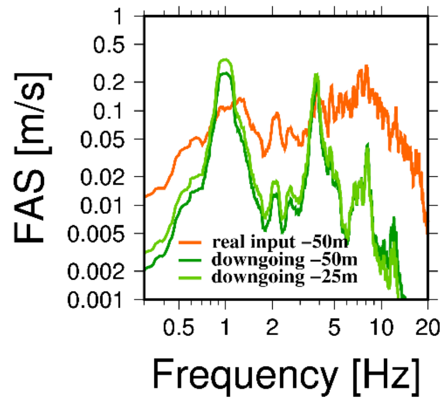

- At **-50m**: **10-15%** of the estimated real input energy at -50m.
- At **-25m**: **10-15%** of the estimated real input energy at -50m.

Mexico City

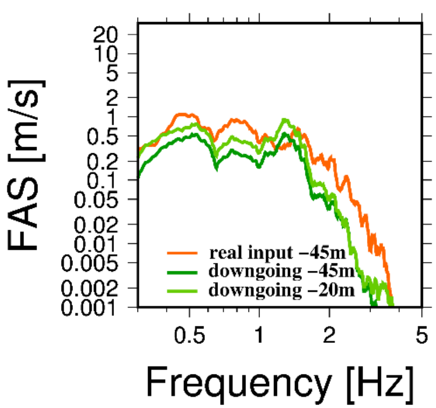

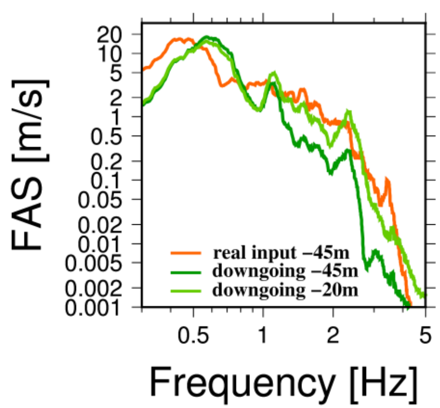

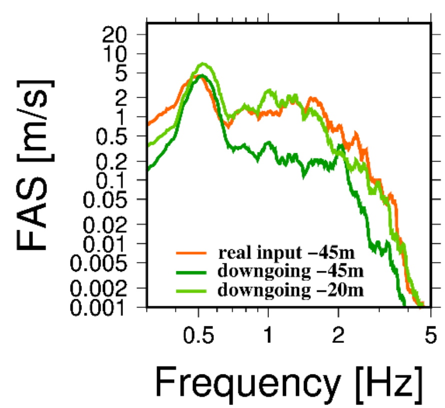

- At **-45m**: **25-65%** of the estimated real input energy at -45m.
- at **-20m**: **70-90%** of the estimated real input energy at -45m.

Conclusions

- A combined analysis of the **wave propagation** through the building-soil structure leads to univocal identification of the **different phases** contributing to the deconvolved wavefield.

- Even in a rather heterogeneous medium, the estimation of ground motion associated with the **real seismic input** (after downward propagating waves have been removed) is feasible.

- The **wavefield radiated back from the building to the soil** can be estimated, as well as **its corresponding energy.**

- For all three different test cases (different building types, velocity profiles of the soil, distances between borehole and building installations) **energy radiated back** from the buildings to the soil was estimated and is **not negligible**

Outlook: Studying site-city interaction effects

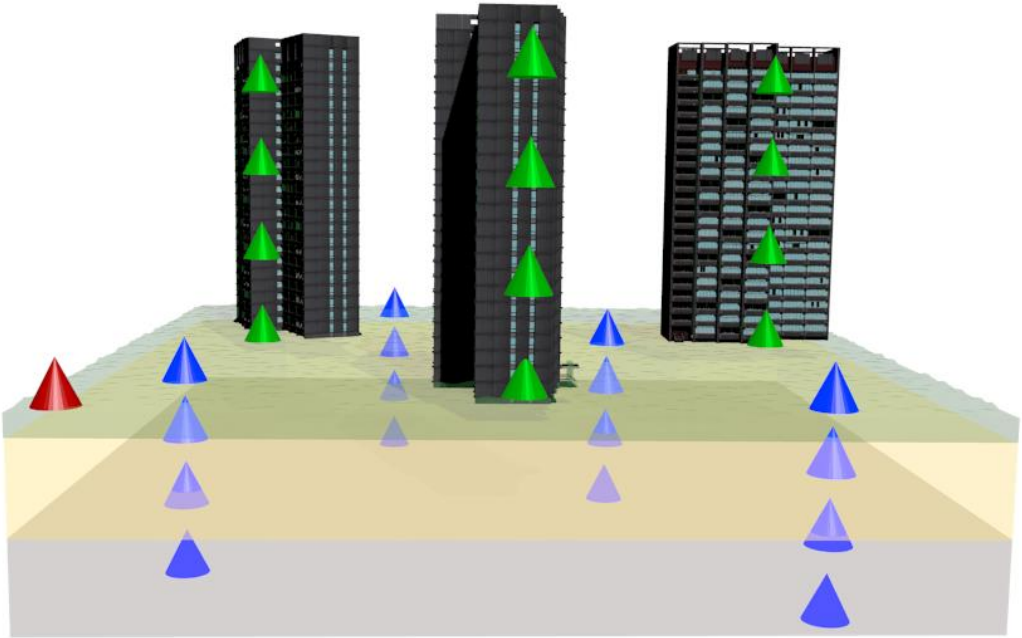

Quantification of energy being radiated back contributes to a better comprehension of interactions taking place between buildings and soil

- ⇨ Better understanding of already existing urban areas, identification of regions of higher seismic risk
- ⇨ Improvement of the building design and planning of urban areas
- ⇨ Improvements in seismic risk assessment and mitigation by taking these interactions into account

Studying soil-structure and building-building interaction effects

Studying soil-structure and building-building interaction effects

Studying soil-structure and building-building interaction effects

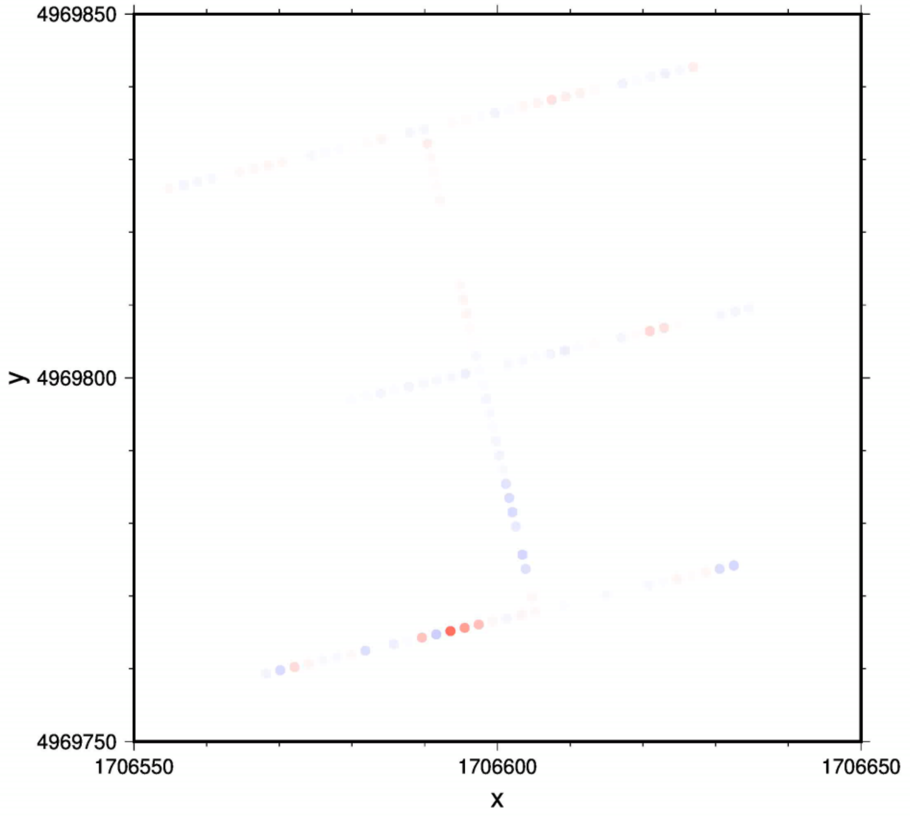

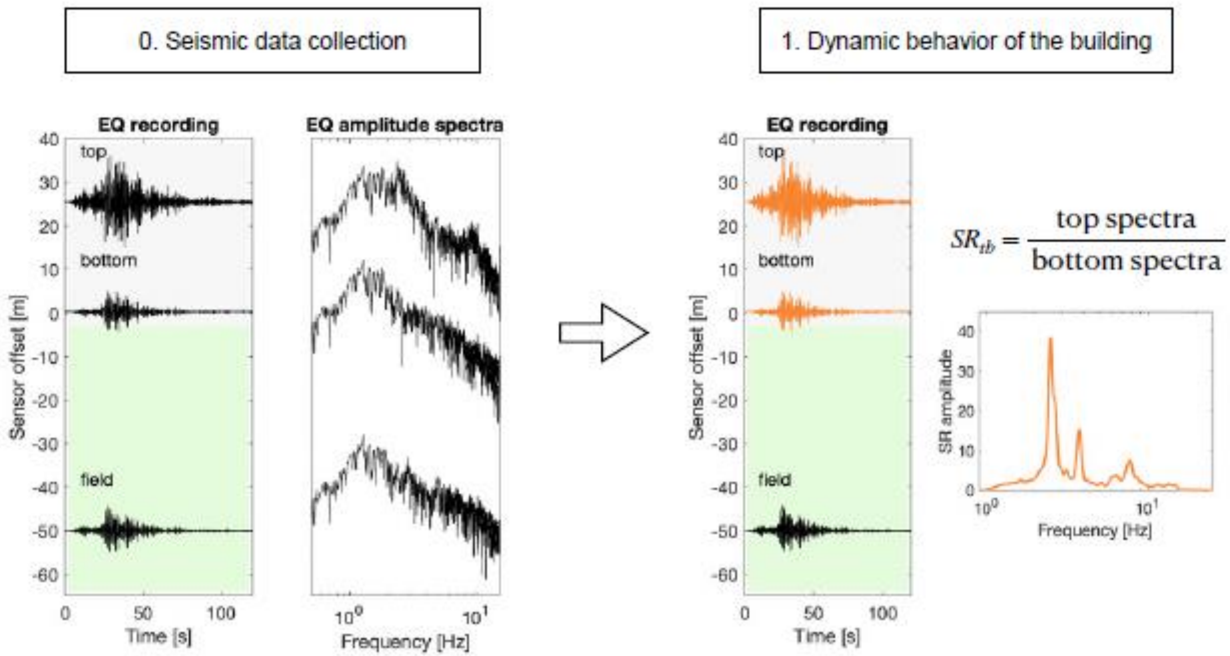

0. Seismic data collection
1. Dynamic behavior of the building
EQ recording
EQ amplitude spectra
top
bottom
field
Sensor offset [m]
Time [s]
Frequency [Hz]
$SR_{tb} = \frac{\text{top spectra}}{\text{bottom spectra}}$
SR amplitude

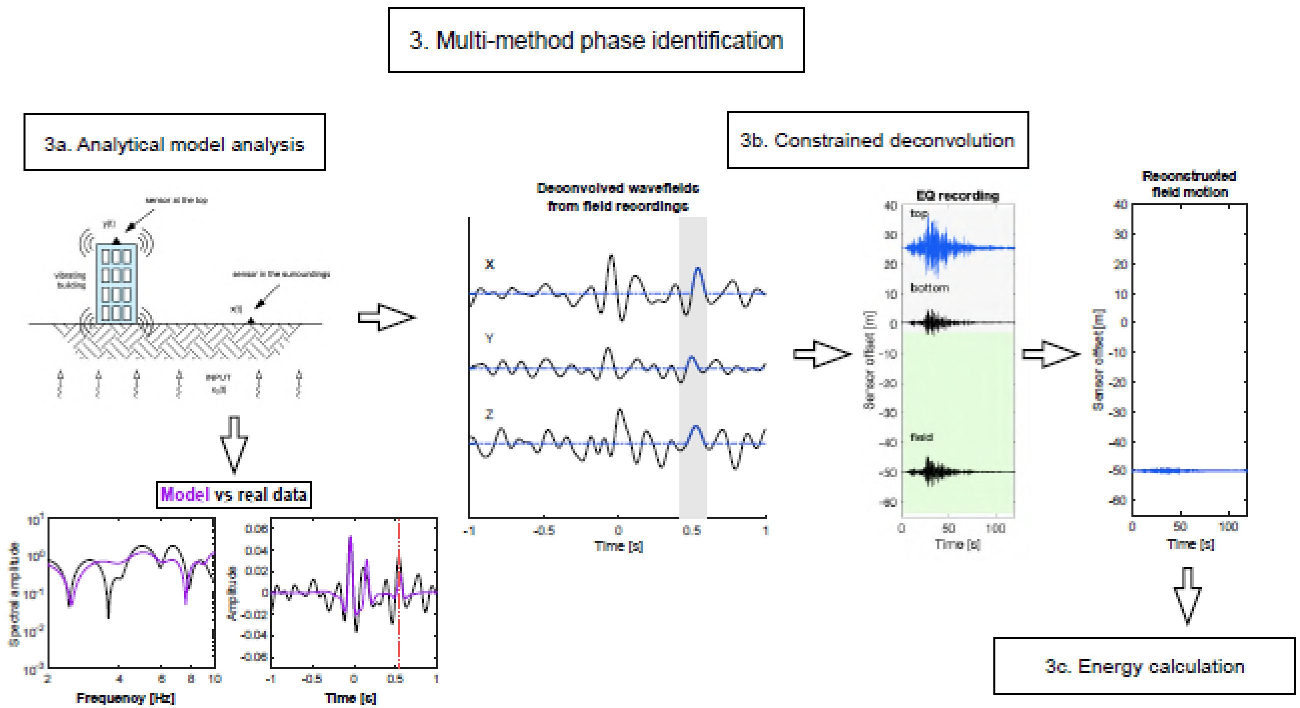
3. Multi-method phase identification
3a. Analytical model analysis
3b. Constrained deconvolution
3c. Energy calculation
Model vs real data
Spectral amplitude
Frequency [Hz]
Amplitude
Time [s]
Deconvolved wavefields
from field recordings
X
Y
Z
Time [s]
EQ recording
top
bottom
field
Sensor offset [m]
Time [s]
Reconstructed
field motion
Sensor offset [m]
Time [s]

The input ground motion at depth is reconstructed from that at the surface without requiring the knowledge of the borehole velocity structure

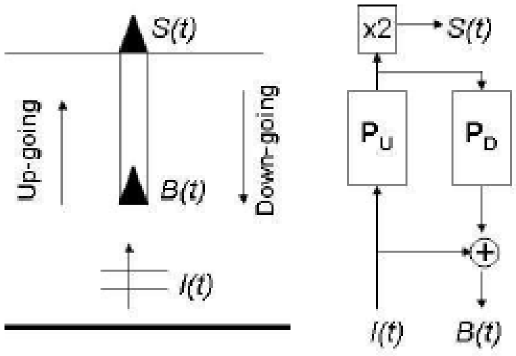

$$S_n(\omega) = W_n(\omega)\frac{u(z1,\omega)}{u(z2,\omega)}$$

where

$$W_n(\omega) = 1-(1-\tau\,|\,u(z2,\omega)\,|^2)^n$$

is the Landweber filter

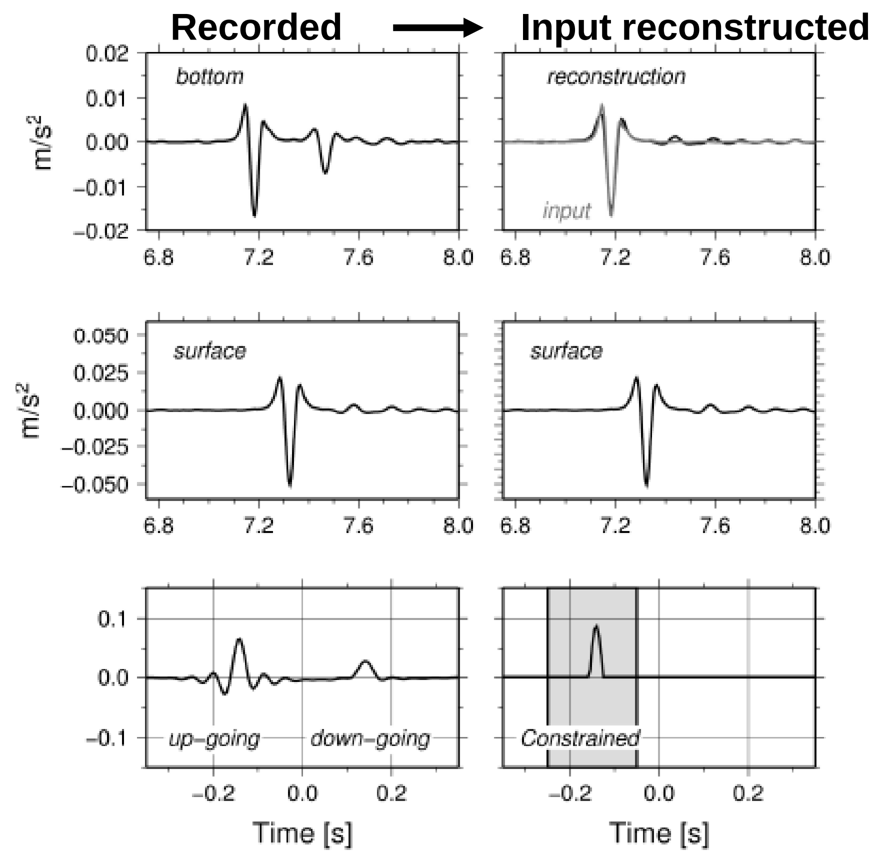

Bindi et al., 2010

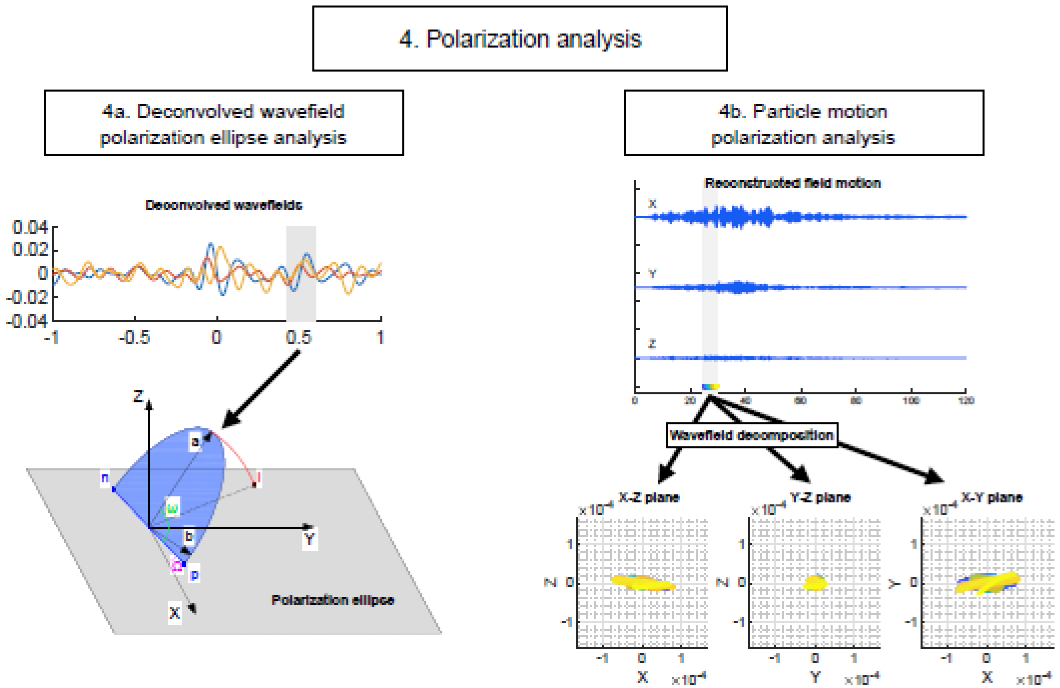

4. Polarization analysis
4a. Deconvolved wavefield polarization ellipse analysis
4b. Particle motion polarization analysis
Deconvolved wavefields
Polarization ellipse
Reconstructed field motion
Wavefield decomposition
X-Z plane
Y-Z plane
X-Y plane

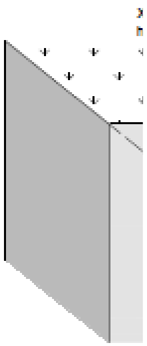

Figure 4.1: (a) Location of Matera test site (blue square) and the epicenter of the M4.6 Catanzaro earthquake on 25.10.2019 (red star). (b) Satellite view of Matera test site. Athletic field instrumentation deployment is indicated with red triangles (three-component sensors) and black dots (vertical geophones).

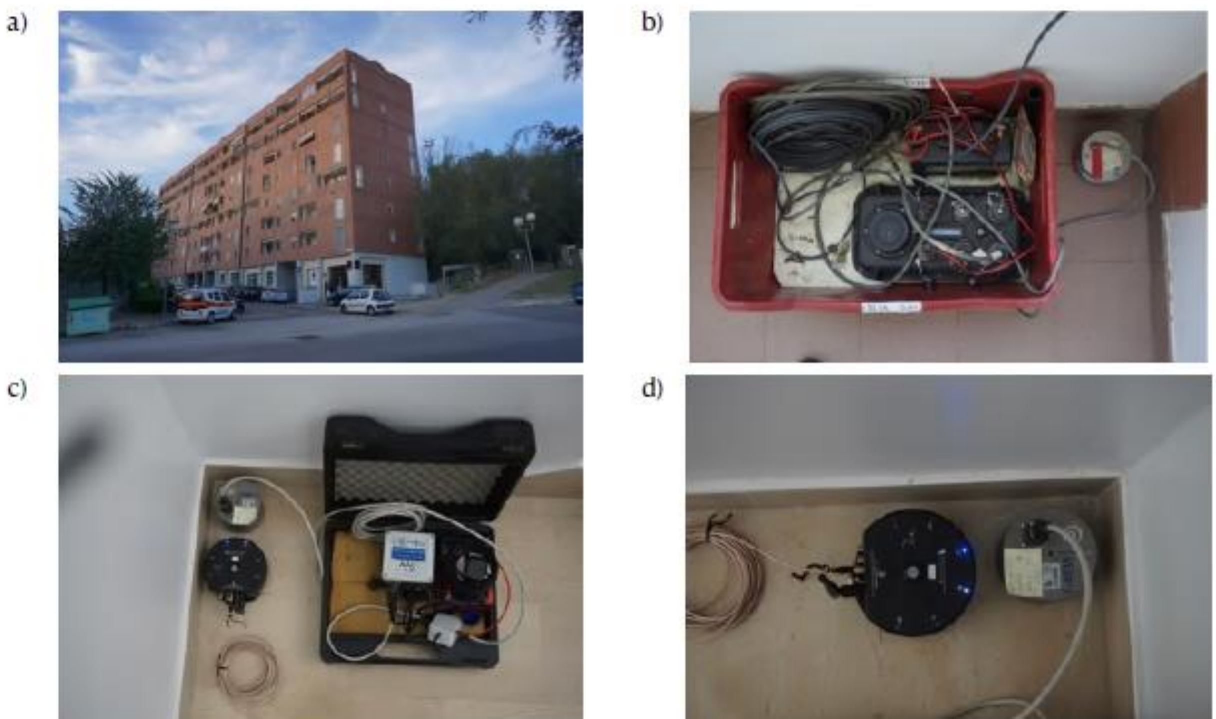

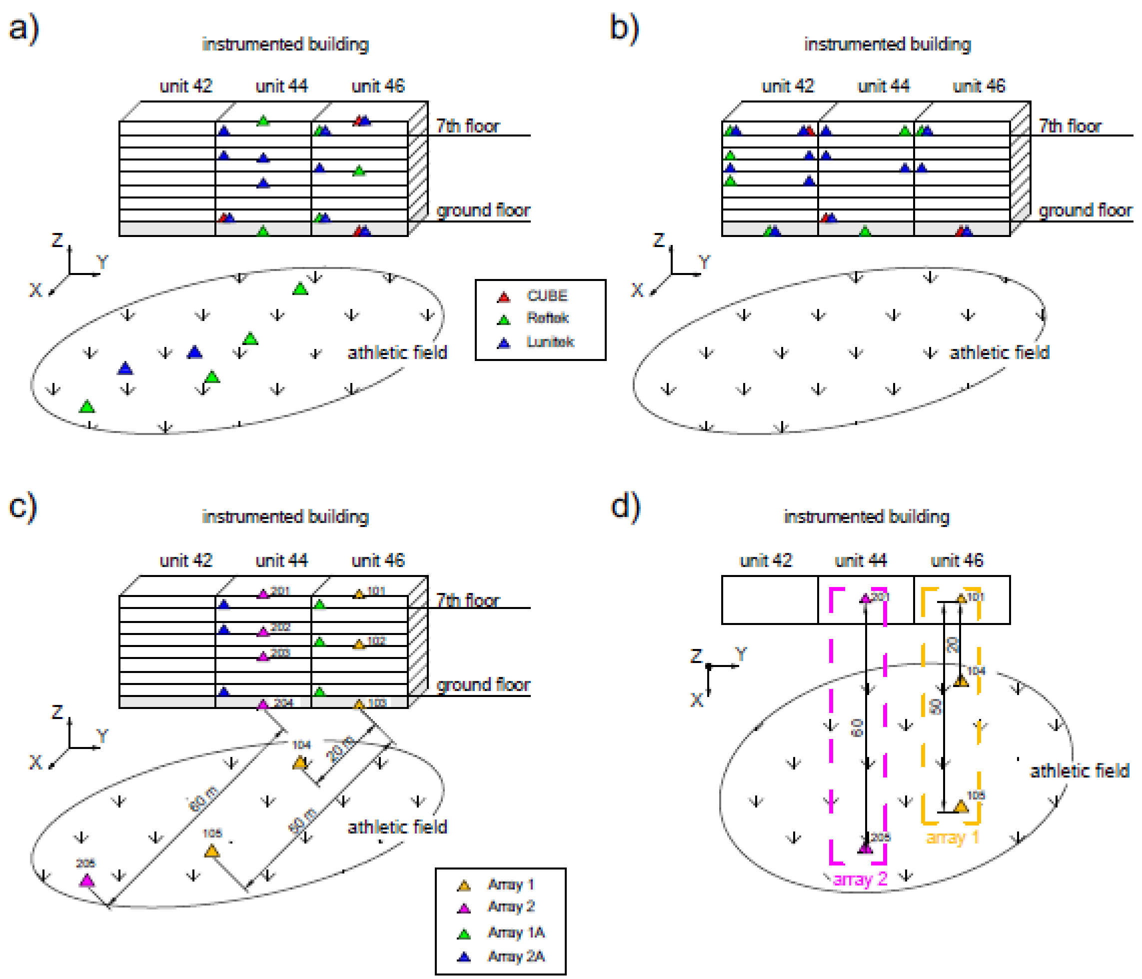

a)
instrumented building
unit 42
unit 44
unit 46
7th floor
ground floor
Z
Y
X
athletic field
CUBE
Reftek
Lunitek
b)
instrumented building
unit 42
unit 44
unit 46
7th floor
ground floor
athletic field
c)
instrumented building
unit 42
unit 44
unit 46
7th floor
ground floor
athletic field
60 m
20 m
Array 1
Array 2
Array 1A
Array 2A
d)
instrumented building
unit 42
unit 44
unit 46
athletic field
array 1
array 2

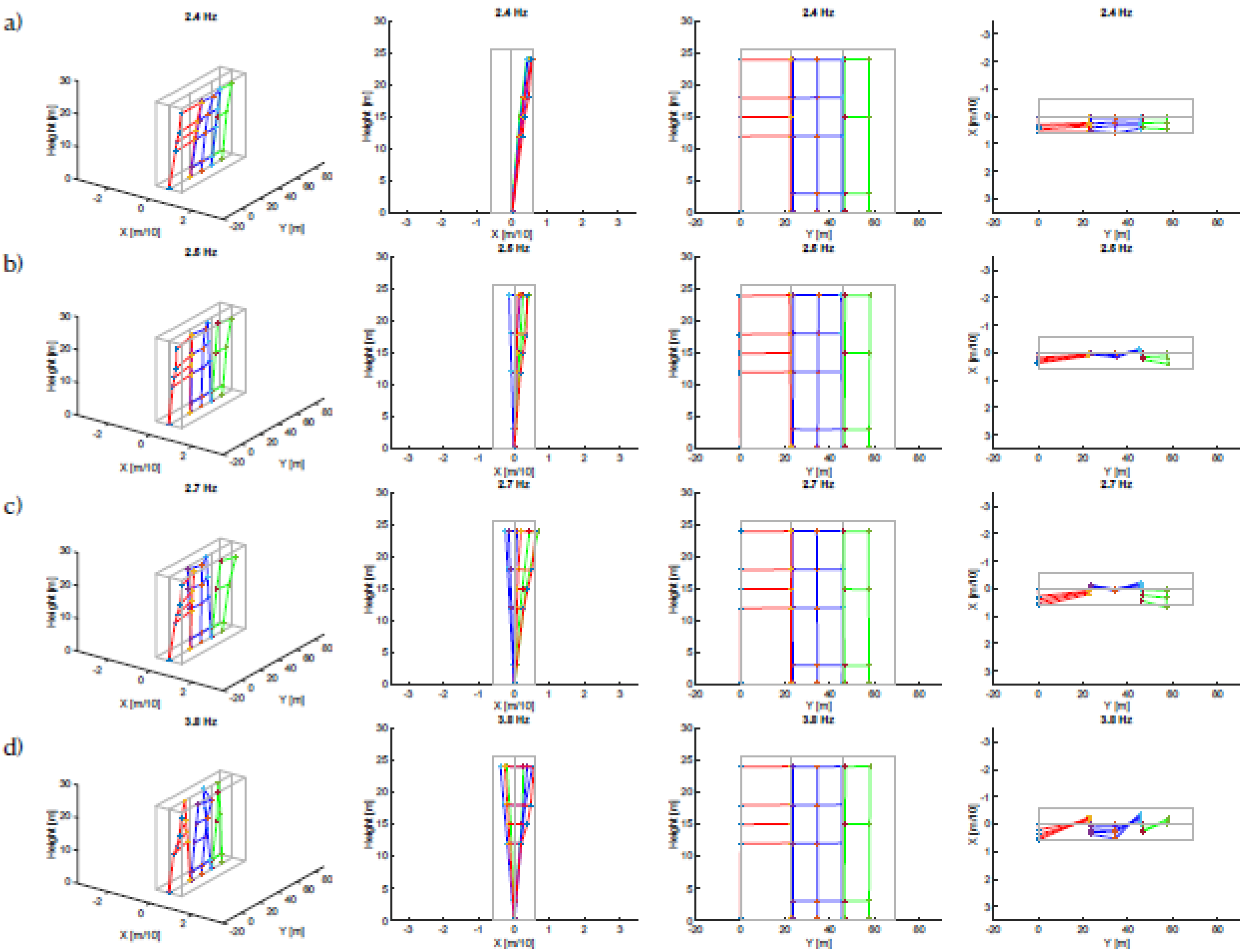
a)
b)
c)
d)
2.4 Hz
2.6 Hz
2.7 Hz
3.8 Hz
Height [m]
X [m/10]
Y [m]

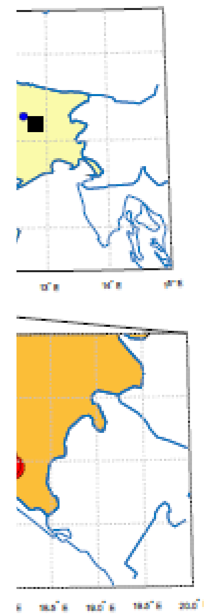

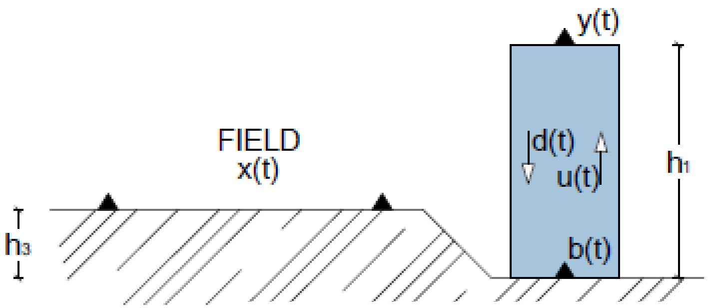

$$X(f) = Y(f)\frac{1}{1+r}[e^{-i2\pi f(-\tau_1} + re^{-i2\pi f\tau_1}] + (1-r)Y(f)e^{-i2\pi f(\tau_1+\tau_2+\tau_3)}$$

$$\frac{X(f)}{Y(f)} = P_1 + P_2 + P_3$$

$$P_1 = \frac{1}{1+r}e^{-i2\pi f(-\tau_1+\tau_3)},$$

$$P_2 = \frac{r}{1+r}e^{-i2\pi f(\tau_1+\tau_3)},$$

$$P_3 = \frac{(1-r)}{2}e^{-i2\pi f(\tau_1+\tau_2+\tau_3)}.$$

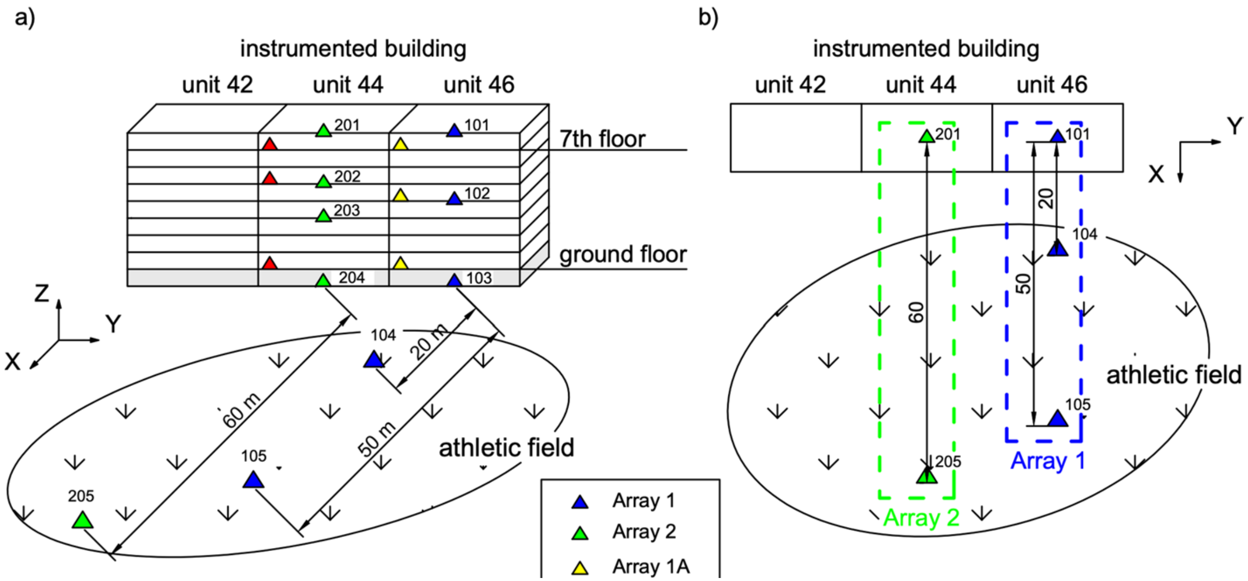
a)
instrumented building
unit 42
unit 44
unit 46
7th floor
ground floor
201
202
203
204
101
102
103
104
105
205
20 m
60 m
50 m
Z
Y
X
athletic field
Array 1
Array 2
Array 1A
b)
instrumented building
unit 42
unit 44
unit 46
201
101
104
105
205
20
60
50
Y
X
athletic field
Array 1
Array 2

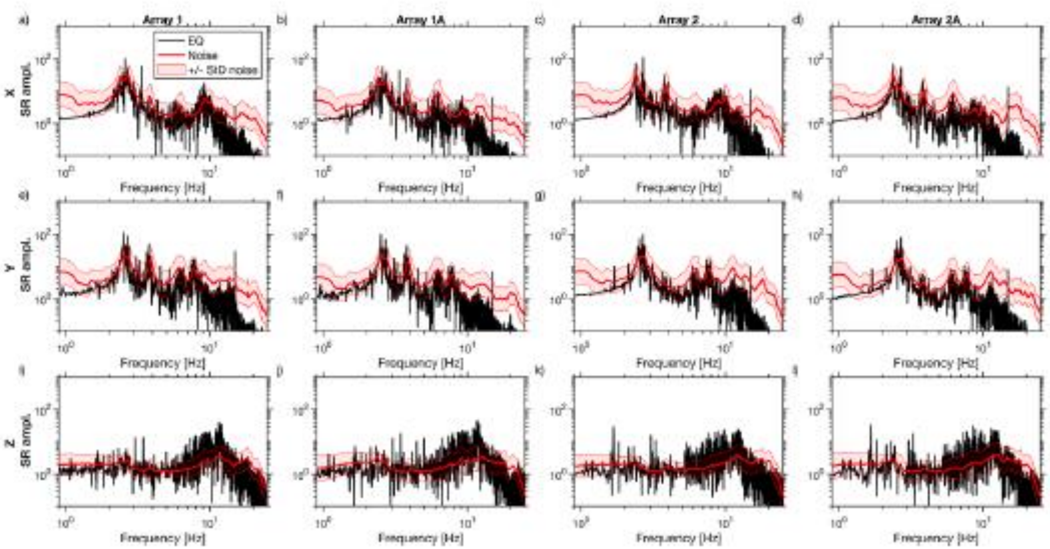
Array 1
Array 1A
Array 2
Array 2A
EQ
Noise
+/- StD noise
X
Y
Z
SR ampl.
Frequency [Hz]

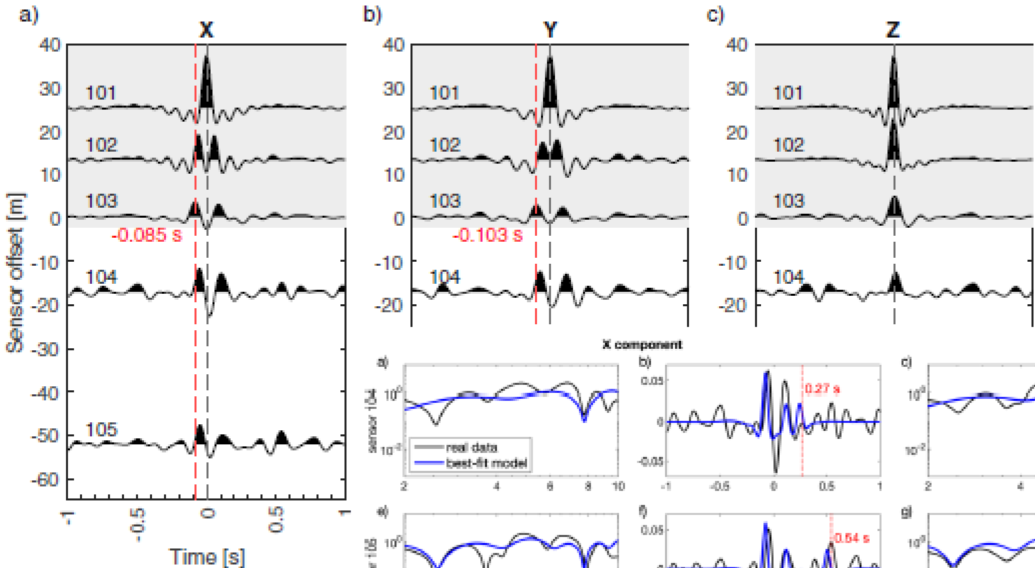
a)
X
b)
Y
c)
Z
101
102
103
104
105
-0.085 s
-0.103 s
Sensor offset [m]
Time [s]

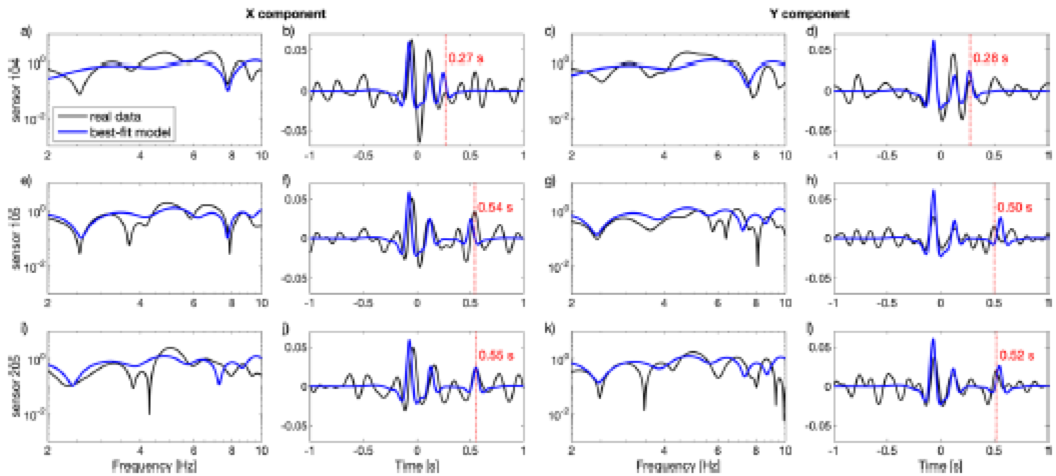
X component
Y component
real data
best-fit model
sensor 104
sensor 105
sensor 205
0.27 s
0.28 s
0.54 s
0.50 s
0.55 s
0.52 s
Frequency [Hz]
Time [s]

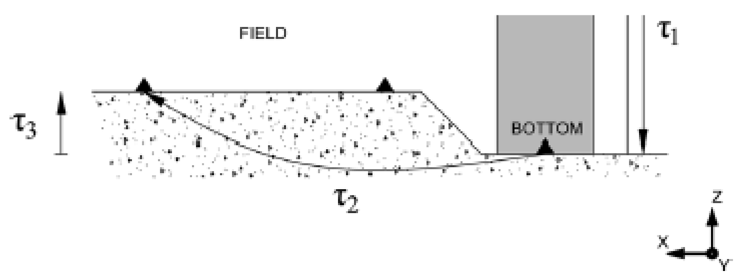
FIELD
BOTTOM
τ_1
τ_2
τ_3
Z
X
Y

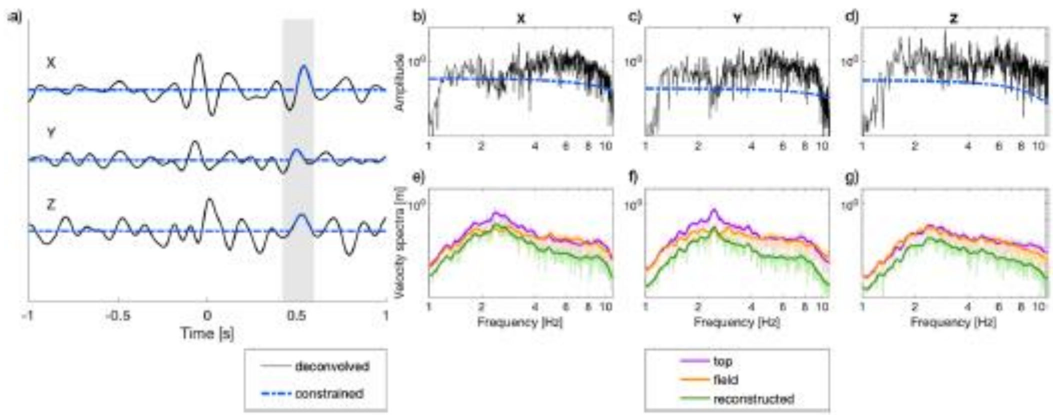

a)
X
Y
Z
-1
-0.5
0
0.5
1
Time [s]
deconvolved
constrained
b)
X
c)
Y
d)
Z
Amplitude
e)
f)
g)
Velocity spectra [m]
Frequency [Hz]
Frequency [Hz]
Frequency [Hz]
top
field
reconstructed

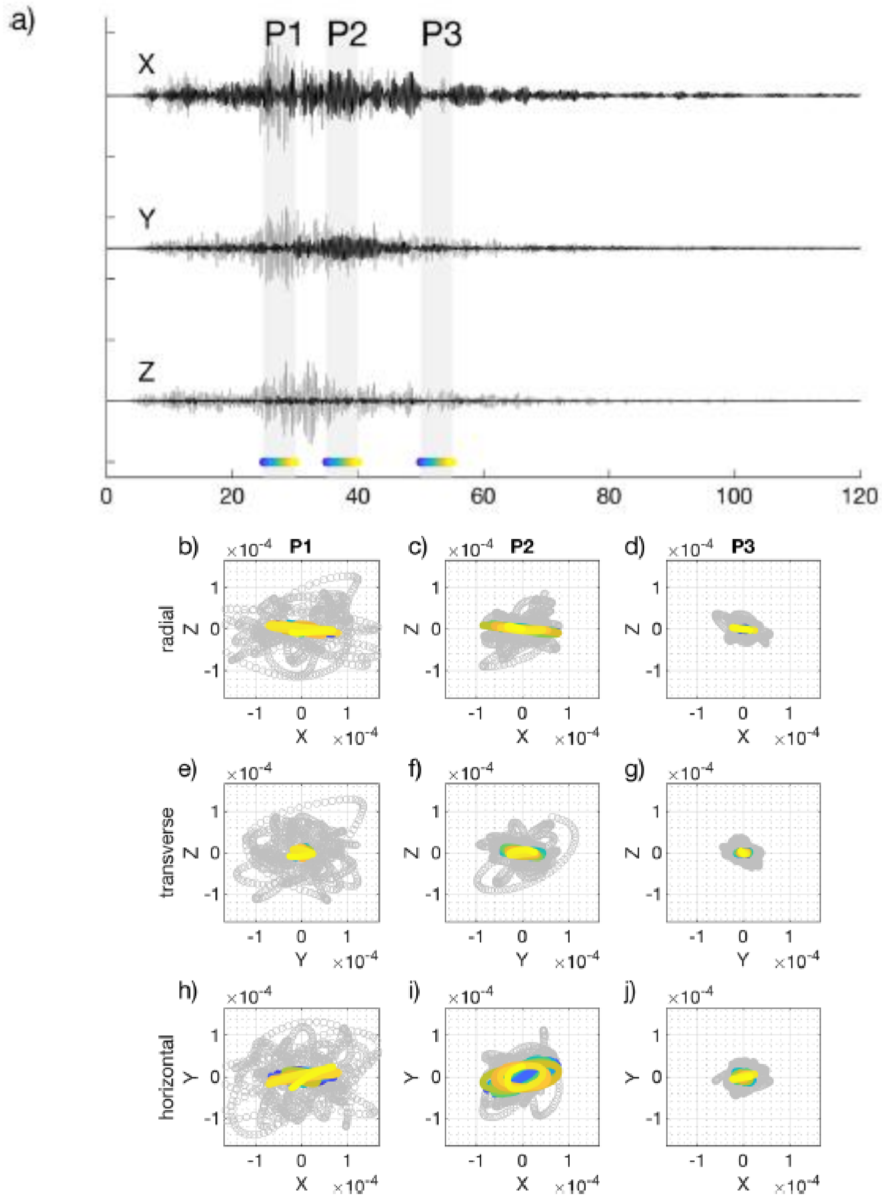
a)
P1 P2 P3
X
Y
Z
0 20 40 60 80 100 120
b) P1
c) P2
d) P3
e)
f)
g)
h)
i)
j)
radial
transverse
horizontal
×10^-4

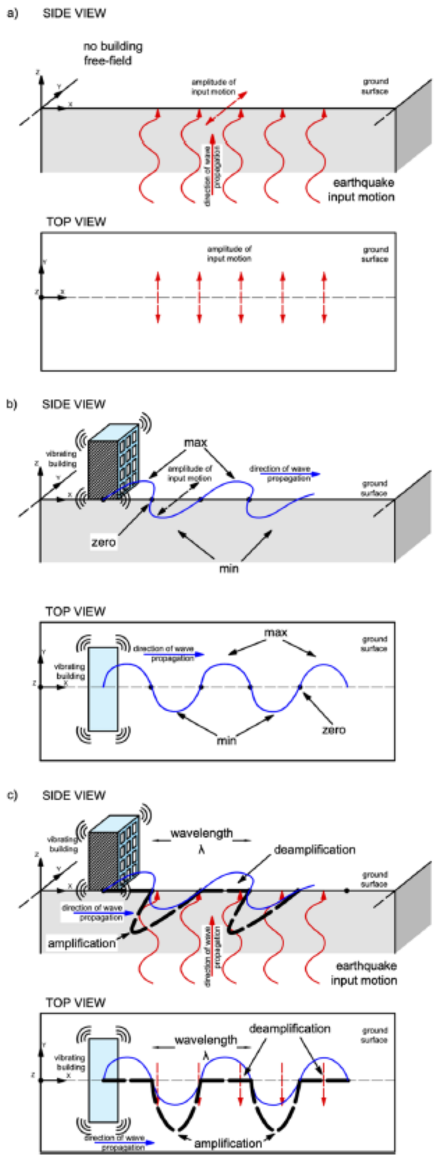

a) SIDE VIEW
no building
free-field
amplitude of input motion
ground surface
direction of wave propagation
earthquake input motion
TOP VIEW
amplitude of input motion
ground surface
b) SIDE VIEW
vibrating building
max
amplitude of input motion
direction of wave propagation
ground surface
zero
min
TOP VIEW
direction of wave propagation
max
ground surface
vibrating building
min
zero
c) SIDE VIEW
vibrating building
wavelength
λ
deamplification
ground surface
direction of wave propagation
amplification
direction of wave propagation
earthquake input motion
TOP VIEW
wavelength
λ
deamplification
ground surface
vibrating building
direction of wave propagation
amplification

THE AREA OF INTEREST

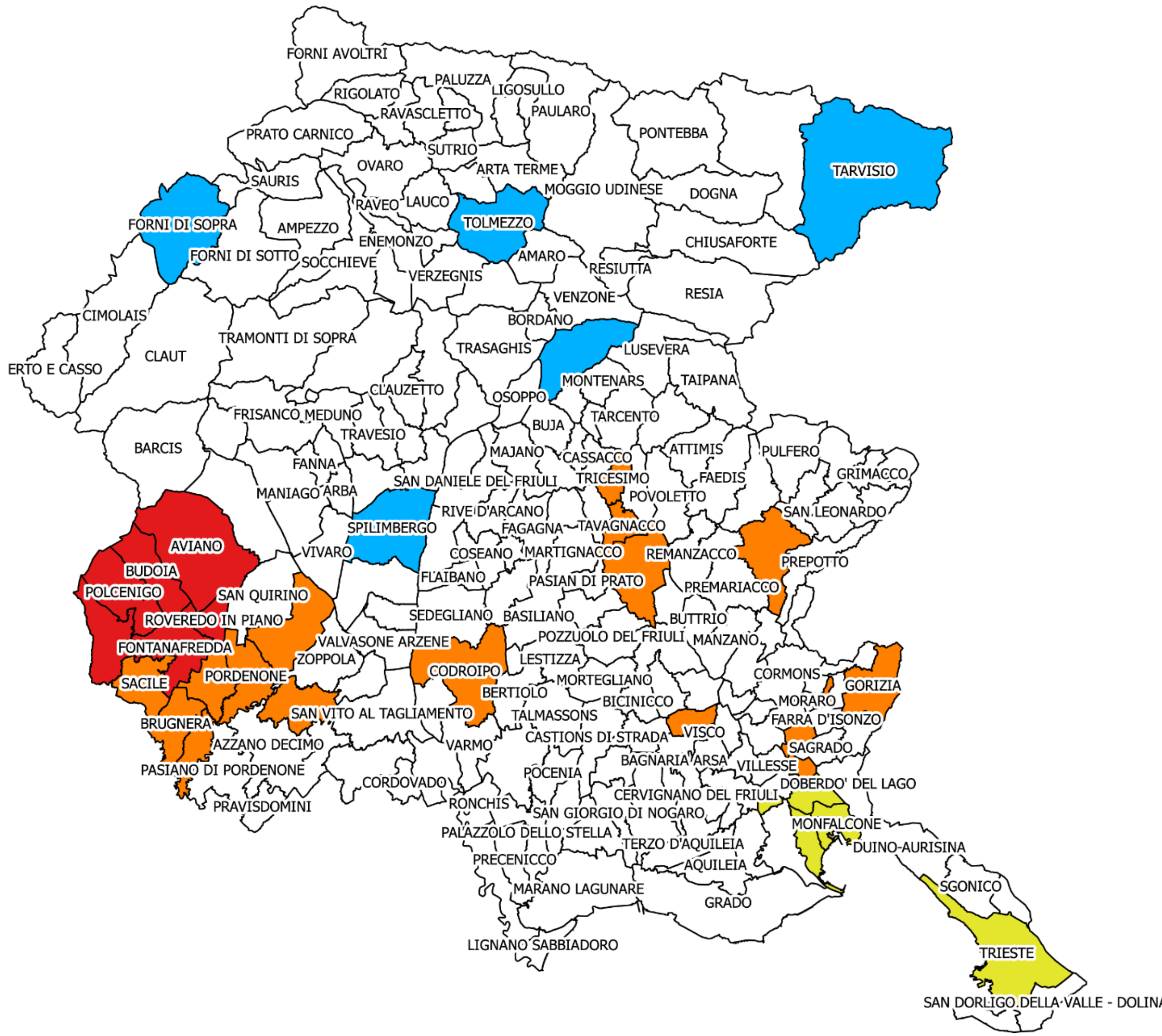

CHARACTERIZATION

Example: CANEVA – Civil Protection

At each of the selected sites a characterization of the site and the building is performed. Ambient vibration measure-ments give us information on the site response and the building' dynamic behavior.

Site characterization

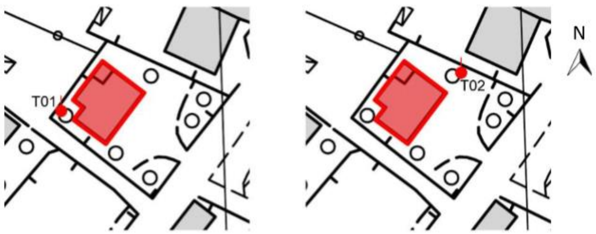

Building characterization

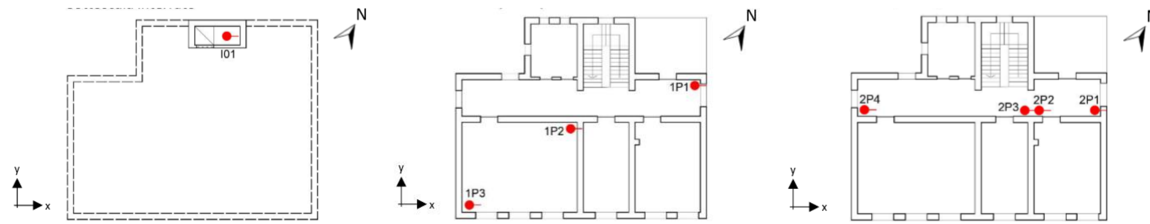

basement

1st floor

2nd floor

Dynamic behavior of the building

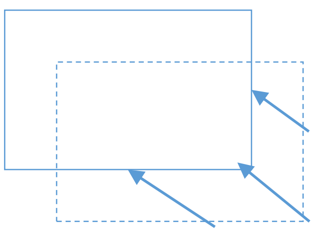

Translational mode,
f=6.3 Hz

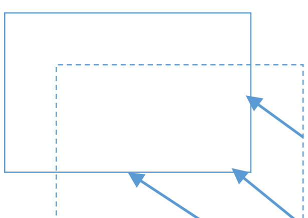

Translational mode,
f=6.6 Hz

Recommendation for installation

Area suggested for installation

Ideal position

Power supply

Internet connection

INSTALLATION

Example: TRICESIMO – Municipality

Based on the characterization of the buildings and the site by ambient vibration measurements, and the given possibilities, the position of the sensors is defined and the sensors are installed.

Installation at the roof


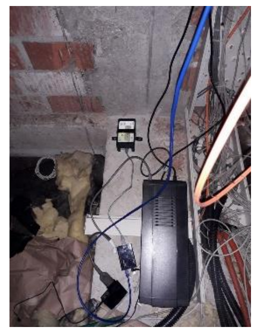
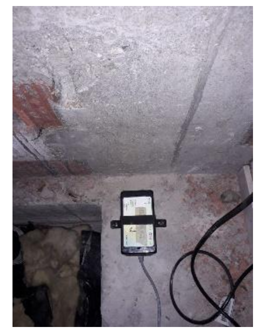

Installation on the ground floor

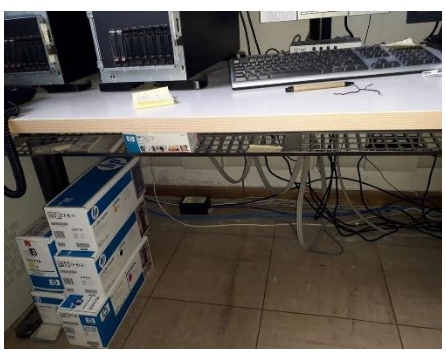

MONITORING DATA

Example: The Cavazzo M_L 3.9 earthquake

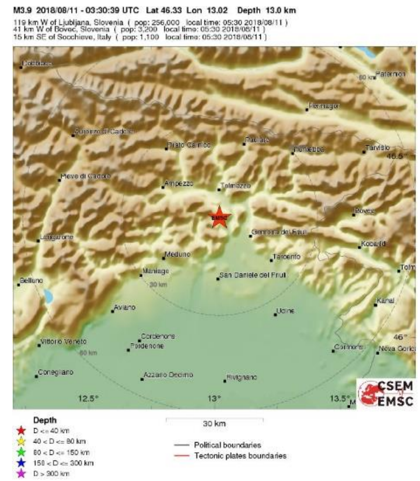

Recording at the roof in the municipality of Tolmezzo

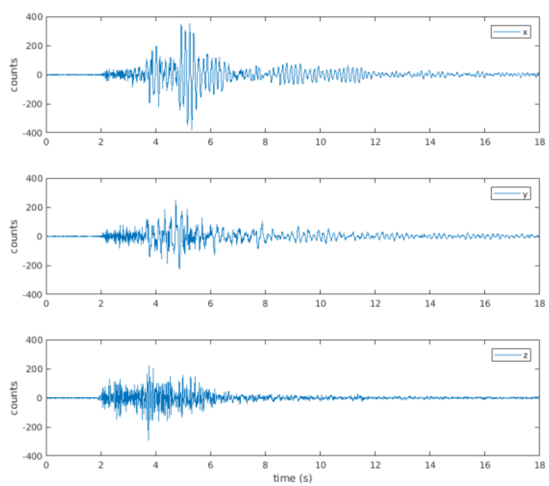

Recording at the roof in the municipality of Tricesimo

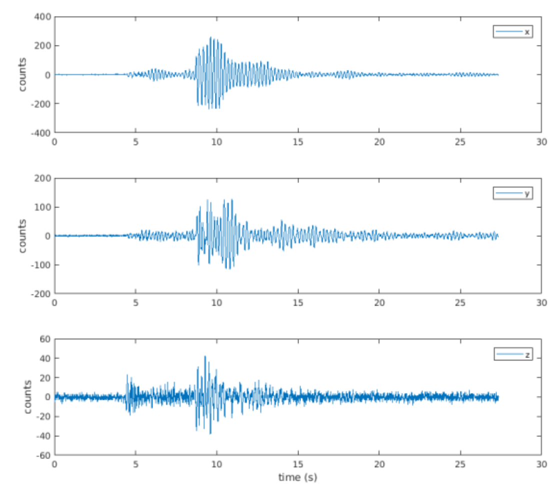

Towards the integration of shake maps and real-time shaking measurements

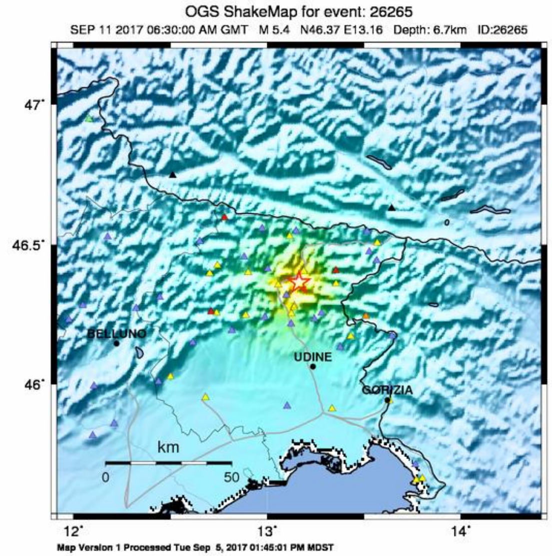

PERCEIVED SHAKING	Not felt	Weak	Light	Moderate	Strong	Very strong	Severe	Violent	Extreme
POTENTIAL DAMAGE	none	none	none	Very light	Light	Moderate	Mod./Heavy	Heavy	Very Heavy
PEAK ACC.(%g)	<0.05	0.3	2.8	6.2	12	22	40	75	>139
PEAK VEL.(cm/s)	*<0.02*	*0.1*	*1.4*	*4.7*	*9.6*	*20*	*41*	*86*	*>178*
INSTRUMENTAL INTENSITY	I	II–III	IV	V	VI	VII	VIII	IX	X+

Scale based upon Worden et al. (2011)

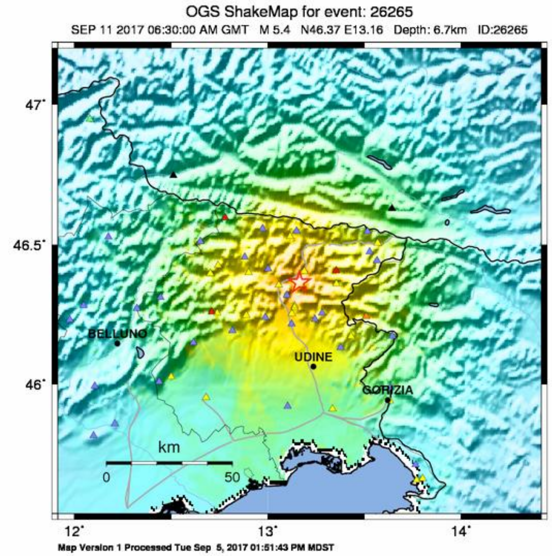

PERCEIVED SHAKING	Not felt	Weak	Light	Moderate	Strong	Very strong	Severe	Violent	Extreme
POTENTIAL DAMAGE	none	none	none	Very light	Light	Moderate	Mod./Heavy	Heavy	Very Heavy
PEAK ACC.(%g)	<0.06	0.2	0.8	2.0	4.8	12	29	70	>171
PEAK VEL.(cm/s)	*<0.02*	*0.08*	*0.3*	*0.9*	*2.4*	*6.4*	*17*	*45*	*>120*
INSTRUMENTAL INTENSITY	I	II–III	IV	V	VI	VII	VIII	IX	X+

Scale based upon Faenza and Michelini, 2010

Integration of seismic recordings with observations provided by Civil Protection Volunteers

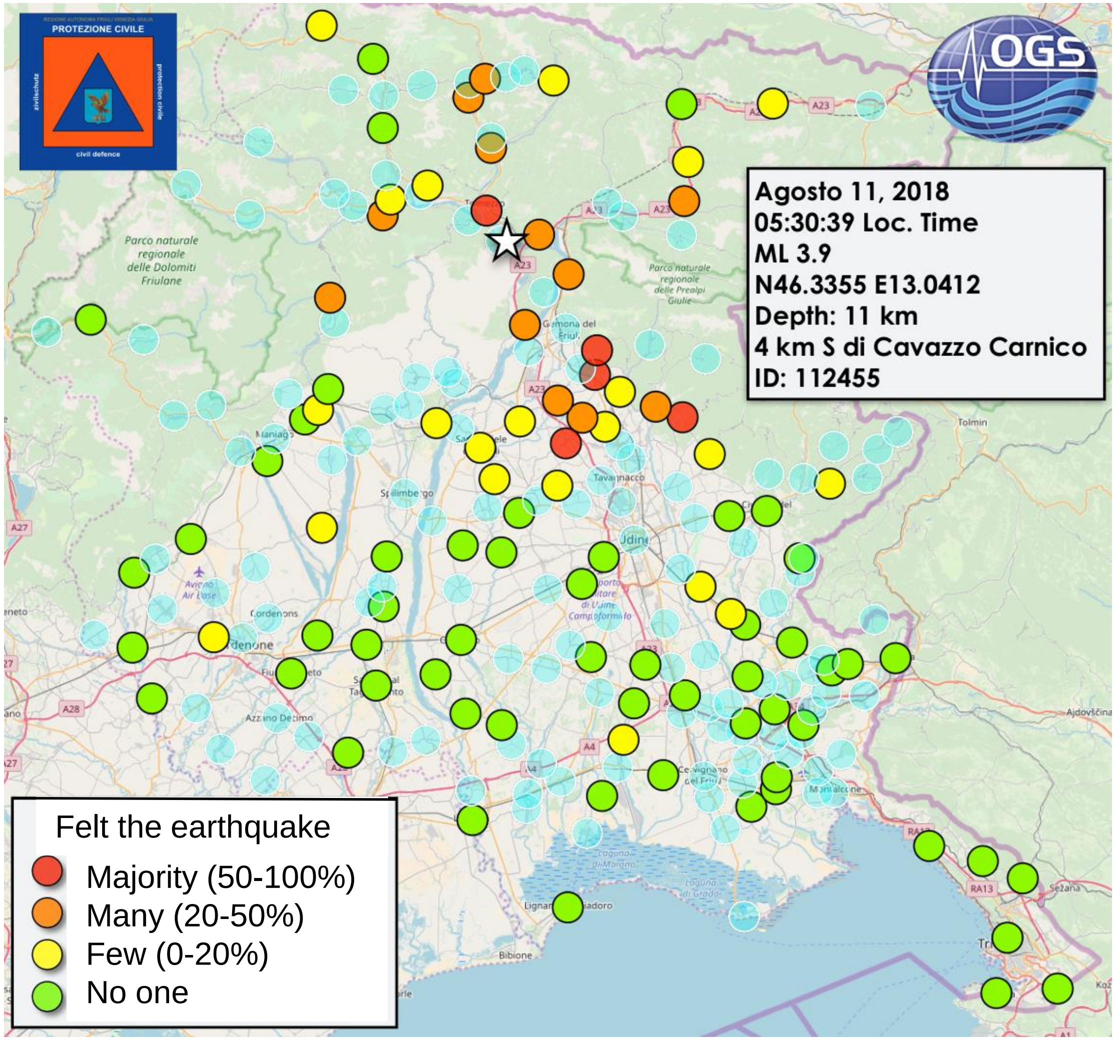

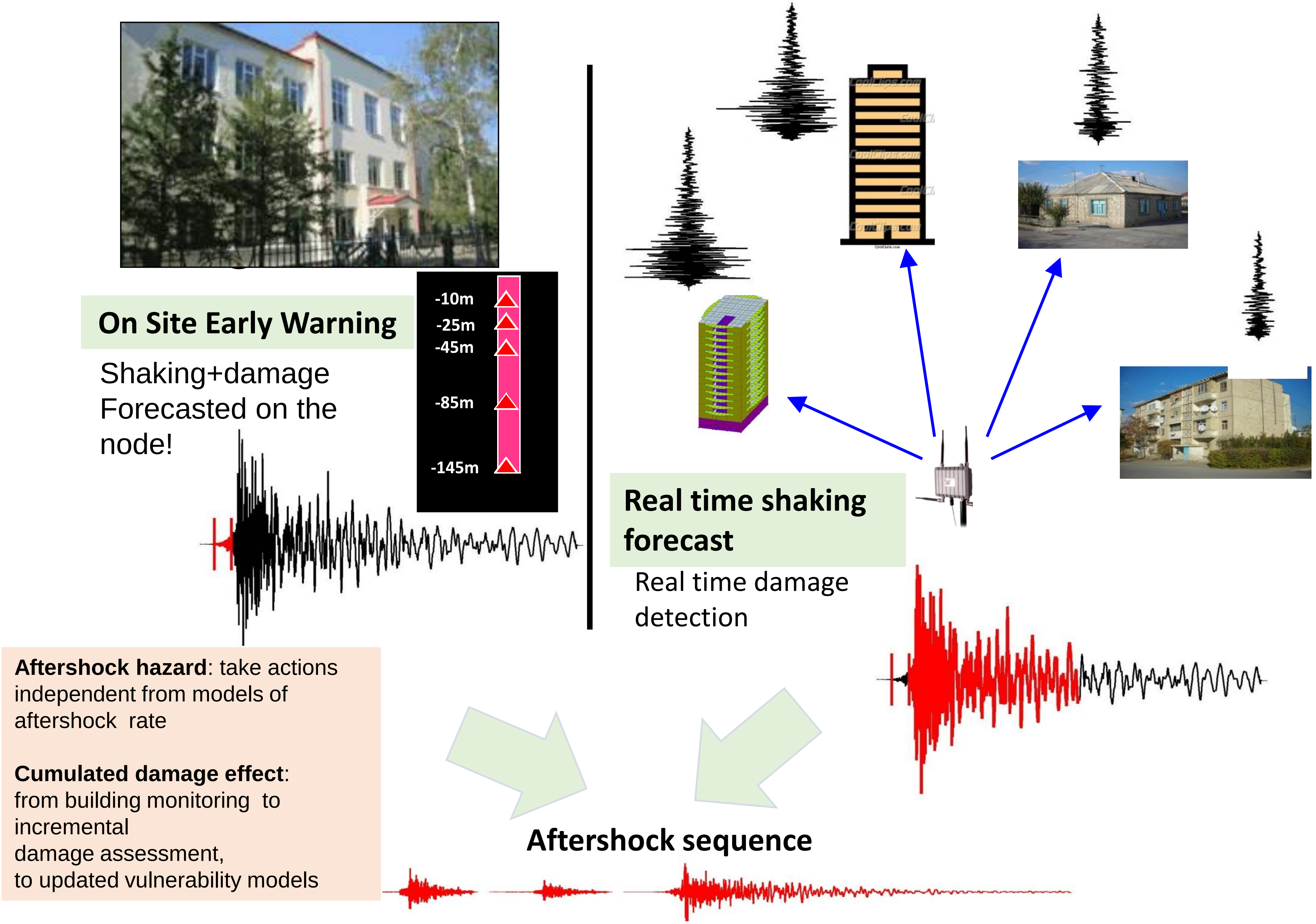
On Site Early Warning
Shaking+damage Forecasted on the node!
-10m
-25m
-45m
-85m
-145m
Real time shaking forecast
Real time damage detection
Aftershock hazard: take actions independent from models of aftershock rate
Cumulated damage effect: from building monitoring to incremental damage assessment, to updated vulnerability models
Aftershock sequence

Real-time shaking forecast

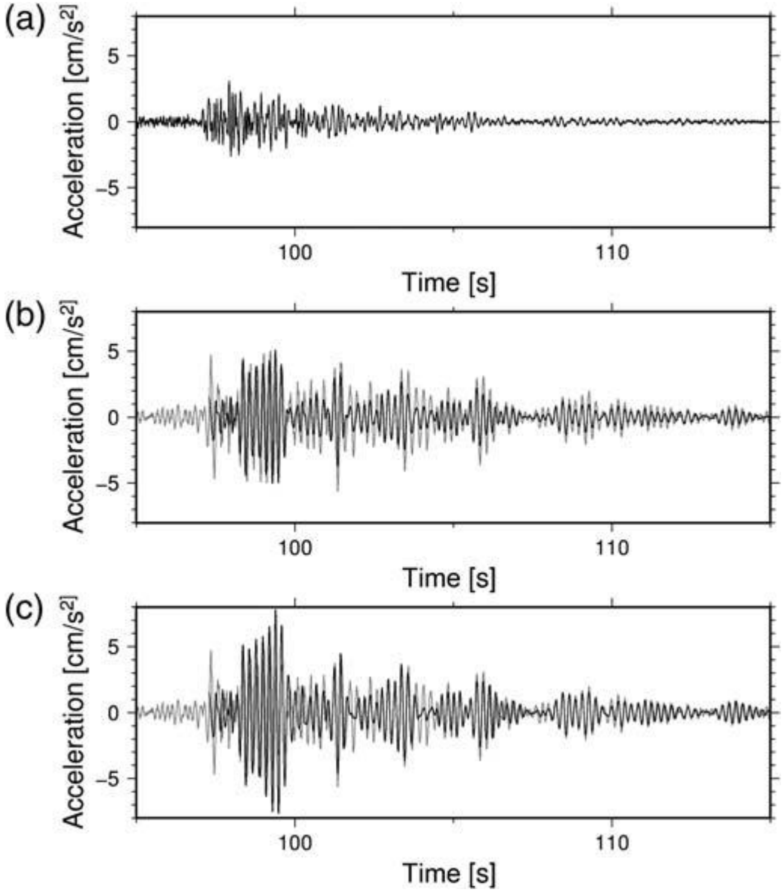

(a) The north–south recording of the 9 April 2009 ML 5.1 aftershock of the L'Aquila earthquake at the SOSEWIN station installed outside the City Hall of Navelli. b) The observed (gray) and simulated (black) recordings at the top floor of the building. (c) The same as (b), but simulating the recording with a lower damping value.

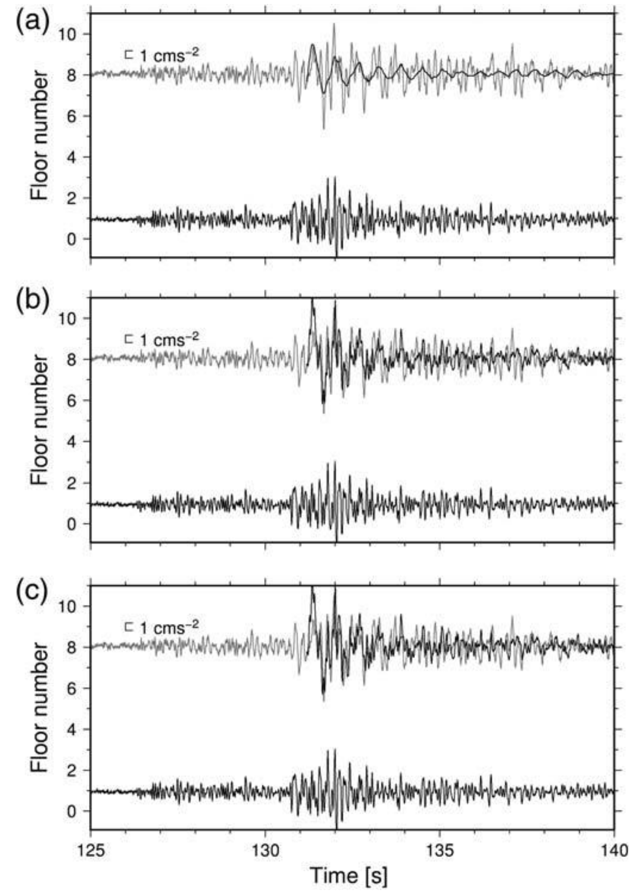

(a) The recording on the top floor of the AHEPA hospital (gray line) and its simulation (black line) using the first-mode frequency only of the 11 October 2013 ML 4.2 earthquake which occurred close to Thessaloniki. The lower trace (black line) is the recording at the first floor used as input. The lower panels show the same, but for the simulation carried out considering also (b) the second and (c) third modes, respectively.

Census data (Istat)

Buildings classification:
- Material
- Age
- Storey

Advantages:
- National coverage
- Simple and general building characteristics

Disadvantages:
- Uncertainty (especially about the material)
- Obsolescence (last census in 2011)
- Cannot grasp local building characteristics

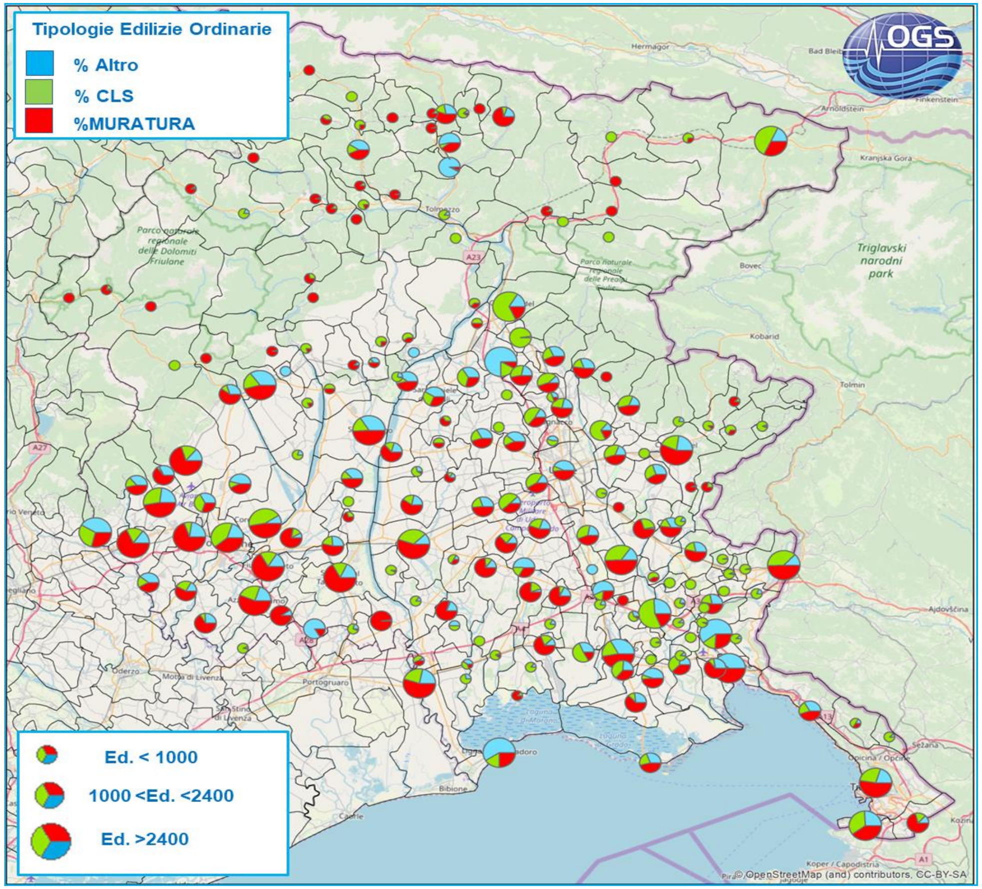

Local data

Integration Istat Census with local data:

- Technical building documentation, available at the municipalities archives.

- Buildings inspections

- Interviews to technicians and practitioners

- Documentation related to the reconstruction performed in Friuli Venezia Giulia after the 1976 earthquake, containing information on damages, reparations and costs.

- Ambient noise measurements to identify the frequency of the first mode (and, statistically, of the building typology)

Example: Aviano (PN)

Test municipality: Aviano (PN)

Included in the Sentinella/Armonia project (seismic monitoring of strategic buildings)

Buildings of different typologies (historical stone masonry, masonry from the ‘60s-’70s, reinforced concrete buildings).

Building stock representative of the Friulian foothill region

Few buildings have suffered damages during the recent earthquakes of 1936 and 1976.

Noise measurements

Instruments: 2 Tromino

Measures: higher/lower storey

30’ acquisition

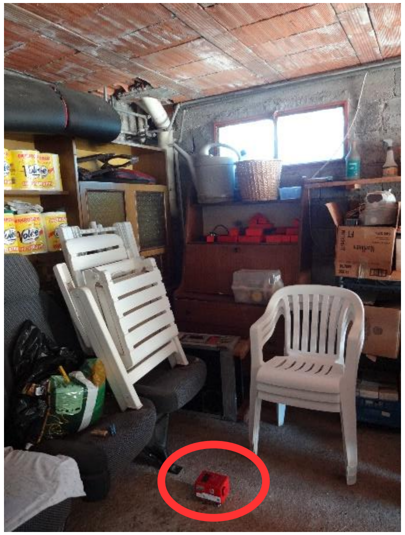

Data available

Integration of data sources

- Noise measures

- CARTIS Forms

- Building data

- CLE

- Microzonation

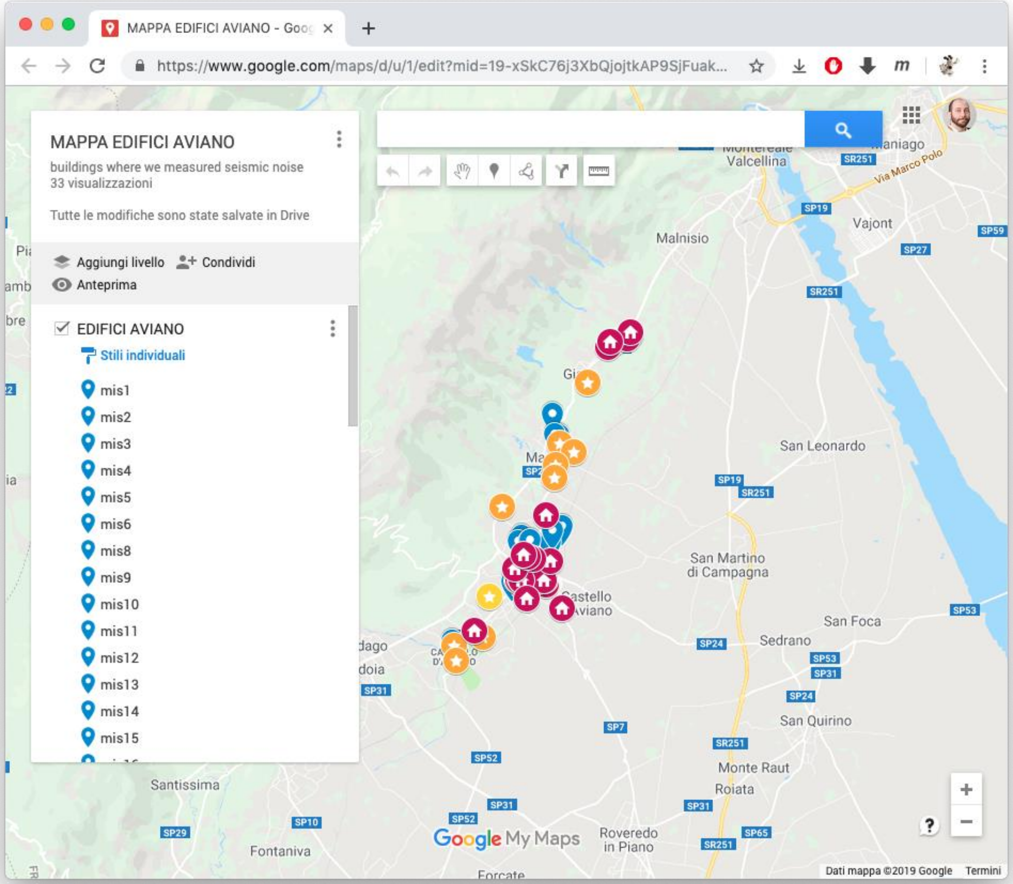

Damage assessment

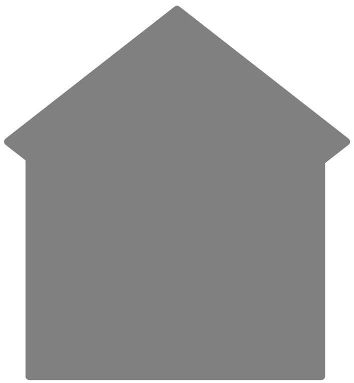

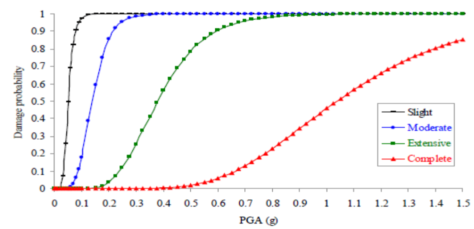

Figure 4: Typical SPSW fragility curves.

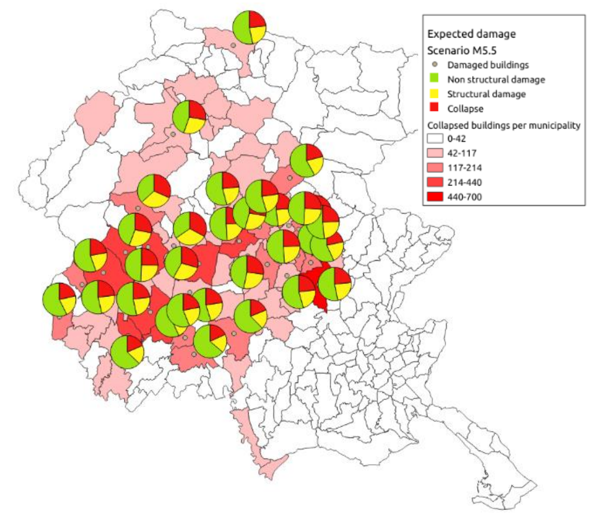

Building typologies (taxonomy to grasp specific characteristics)

Fragility curves for different damage states. Curves based on building characteristics

Number of buildings with complete, extensive, moderate and slight damage

Damage maps

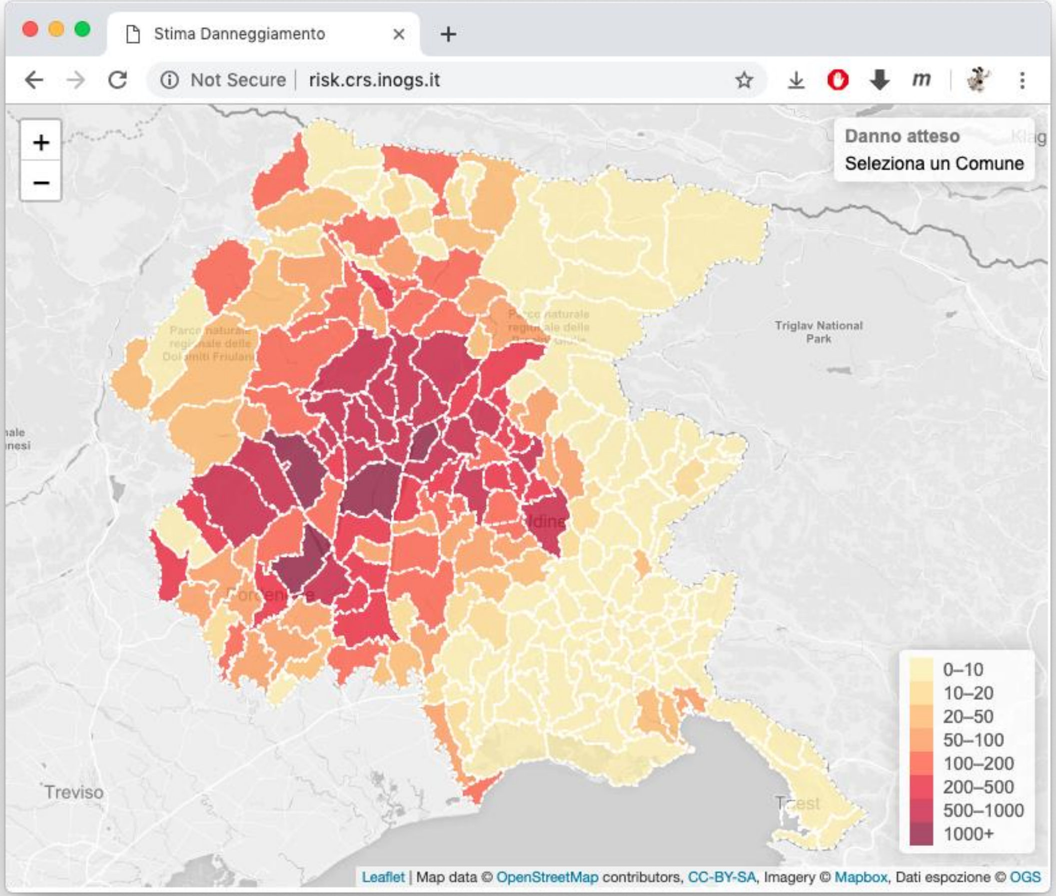

Damage calculation performed by Openquake, based on Shakemaps produced at CRS.

Features:

- Multiple layers (ground motion, intensity, damage, casualties, population..)
- Different scales and granularity (municipality, census units)
- Archive of past events simulations

Acknowledgment:
Thanks to Bojana Petrovic for some of the figures